Ultra-High Field MR Diffusion Tensor Imaging Characterization of Rabbit Tendons and Ligaments

BY

AMAN GUPTA
B.S., Panjab University, Chandigarh, India, 2006

THESIS

Submitted as partial fulfillment of the requirements
for the degree of Doctor of Philosophy in Bioengineering
in the Graduate College of the
University of Illinois at Chicago, 2012

Chicago, Illinois

Defense Committee:

Dr. Vincent M. Wang, Advisor
Dr. Richard L. Magin, Chair
Dr. Glenn T. Stebbins, Rush University
Dr. Thomas J. Royston
Dr. Belinda S. Akpa, Chemical Engineering
Dr. Anthony M. Zelazny, Rush University

ACKNOWLEDGEMENTS

I would like to acknowledge many individuals who played a vital role in bringing this dissertation together. First and foremost, thanks to my advisor, Dr. Vincent M. Wang, for providing me with opportunity and guidance throughout my time at UIC and Rush. Your constant encouragement, support and critique at every stage helped me look deeper into the problems with new perspectives and aim higher. I have the utmost respect for your knowledge, enthusiasm and discipline in the pursuit of good science.

Thanks to Dr. Richard L. Magin, my co-advisor for providing your valuable insights and MR expertise without which this dissertation wouldn't have been possible. I want to thank you for your constant encouragement and guidance. I value your willingness to listen and candid feedback. I will always count on you for a kind word and honest encouragement.

Thanks to Dr. Glenn T. Stebbins, my co-advisor for your invaluable contributions to this dissertation. I want to thank you for providing your MR and statistical expertise and your hands-on participation on the project. I am indebted to your mentoring and enormous patience throughout my time at Rush.

I would like to thank my dissertation committee members, Dr Thomas Royston, Dr Belinda Akpa and Dr. Anthony Zelazny for their guidance and assistance.

I wish to express my deep gratitude to Dr. Weiguo Li, without your insight and hands-on assistance this project wouldn't have been possible. Your intellectual and technical help greatly enriched my journey. I also want to thank Dr. Robert Kleps for his assistance with training on the 11.7 T magnet.

Besides the knowledge base that this experience has provided me, I am grateful to my fellow graduate students and colleagues in the Biomechanics and Diagnostic Imaging labs that have come and gone over the years for your great camaraderie and friendships. Many thanks to Elizabeth Shewman, Rebecca Bell, Justin Dishkin, Fanchia Wang, Mauli Pandya, Dr. Xu Feng, Dr. Mrignayani Kotecha, Ziying Yin and Benjamin Schwartz. You all helped make this possible.

Last but not the least; I dedicate this work to my parents who have instilled in me wholesome values and perseverance and raised me till I have become an independent person.

TABLE OF CONTENTS

LIST OF TABLES

LIST OF FIGURES

LIST OF ABBREVIATIONS

2D	Two-dimensional
3D	Three-dimensional
AD	Axial Diffusivity
ADC	Apparent Diffusion Coefficient
AF	Annulus Fibrosis
DTI	Diffusion Tensor Imaging
DWI	Diffusion-weighted Imaging
IVD	Intervertebral Disc
MR	Magnetic Resonance
MRI	Magnetic Resonance Imaging
FA	Fractional Anisotropy
FDI	Fiber Density Index
FOV	Field of View
MCL	Medial Collateral Ligament
MD	Mean Diffusivity
NEX	Number of Excitations
PG	Proteoglycan
RD	Radial Diffusivity
ROI	Region of Interest
RF	Radiofrequency
SemiT	Semitendinosus Tendon
SNR	Signal-to-noise Ratio

TR	Repetition Time
TE	Echo Time
UTE	Ultra-short Echo Time

SUMMARY

Tendons and ligaments are dense, fibrous connective tissues that facilitate transmission of loads from muscle to bone (tendon) or from bone to bone (ligament). These tissues are subjected to wear and tear from day-to-day mechanical usage leading to sprains, tendinopathies, or ruptures, each of which is a major source of musculoskeletal disability. Clinically, the diagnosis of tendon and ligament injury is based on a clinical examination as well as magnetic resonance imaging (MRI) of the relevant tissues. MRI is a reliable, non-invasive tool for detecting large and complete tears; however, conventional T1 and T2-weighted grayscale images exhibit poor contrast and a low signal-to-noise ratio which makes identification of low-grade injuries more challenging to delineate. Therefore, there exists a need for reliable, *quantitative* and more robust imaging approaches to assess tendon and ligament microstructure and integrity.

One of these MR approaches is diffusion tensor imaging (DTI), an advanced MRI technique primarily used in neuroimaging applications. DTI assesses tissue microstructural organization by quantifying the 3D diffusion of water molecules within tissues. It relies on the basic diffusion principle that water molecules diffuse more readily along (i.e., parallel to), rather than across physical barriers (e.g., collagen fibers). Diffusion of water molecules can be quantified by the diffusion tensor in each voxel, whereby the magnitude and orientation of water diffusion can be computed throughout the tissue, thus revealing the fiber microstructure. The primary aims of the proposed studies are to demonstrate applicability and reliability of the DTI technique for tendons

and ligaments, and determine the sensitivity of b-values to DTI derived parameters of tissue integrity.

The proposed studies will investigate the applicability and sensitivity of DTI to intact tendons and ligaments. The long term goal of these initial studies is to provide in depth quantitative as well as qualitative characterization of these tissues which can significantly advance our ability to accurately image intact, damaged, and healing tissues, further our understanding of the microstructural mechanisms of microtrauma and repair, and potentially improve clinical management of injuries.

1. Introduction

1.1 Overview

The intrinsic magnetic properties of atomic nuclei form the basis of magnetic resonance. The most abundant atom in biological tissue is hydrogen (1H), therefore, it has been the most studied magnetic resonance phenomena. The concept of Nuclear Magnetic Resonance (NMR) is based on the interaction between the spins and magnetic fields. Three kinds of magnetic fields are involved that interact with the spins, namely, static magnetic field (B0), radiofrequency field (B1) and gradient field [1] .

Without any static magnetic field, spins have random orientation and the sum of magnetic moments (magnetization) averages to zero. By placing a proton in a static magnetic field B0, it precesses around the axis of the magnetic field at a frequency proportional to the strength of the magnetic field, known as Larmor frequency governed by

$$\omega_0 = \gamma B_0 \tag{1.1}$$

where γ is the gyromagnetic ratio, a constant number unique for different types of atoms. The gyromagnetic ratio of a hydrogen atom is 42.58 MHz/Tesla. Once all the spins are aligned in the direction of the static magnetic field, they accumulate with a magnitude M0 along the direction z. The stable condition of the alignment of spins can be perturbed by applying a RF pulse, B1, which is tuned to the Larmor frequency of the spins. This causes to flip the magnetization vector out of equilibrium into the transverse plane. After the RF pulse, the tipped spins start to precess in the transverse plane at the Larmor frequency. Magnetization returns to the equilibrium state by two kinds of relaxation processess. The first one is the returning of spins from xy plane to the z axis, which is the

spin-lattice relaxation and is characterized by the time constant T1. The other is the decaying mechanism of spins in the xy plane, known as spin-spin relaxation and is characterized by the time constant T2.

While MRI provides excellent soft tissue contrast and high spatial resolution, there remains uncertainty regarding its ability to resolve and delineate low grade tendon and ligament injuries (e.g., sprains). Specifically, elevated MRI signal intensity is suggestive of tissue-level alterations which may include increased water content, elevated vascularity, inflammation, degeneration, or partial matrix disruption [2, 3]. Hence, elucidating these potential abnormalities using a qualitative measure such as signal intensity (a standard means of conventional MR assessment) is challenging. Currently, there exist very few published MRI approaches to quantify the structural and functional integrity of tendons and ligaments.

Conventional MRI studies have shown the potential of T1, T2 and proton density weighted sequences for the detection of large and complete ligament and tendon tears (e.g., rotator cuff, knee ligaments); this pathology is manifested by increased signal intensity at the injury site [4-6]. However, these techniques have considerably lower sensitivity and specificity for the detection of more subtle forms of tendon and ligament pathology such as sprains, inflammation, partial tears or chronic injuries and clinically reported accuracies of conventional MRI are as low as 65% [7, 8]. Furthermore, postoperative MRI appearance of these tissues reconstructed with autografts or allografts are often variable on proton density and T1/T2 weighted images [9]. With multiple ligament injuries, the diagnostic specificity of MR imaging for ligament tears decreases[6]. Interestingly, imaging results *from conventional MRI* often are not

consistent with clinical diagnosis and symptoms, for e.g., foci of increased signal intensity at proximal attachment of the patellar tendon and thickening of the patellar tendon (symptoms of patellar tendinosis) were observed in conventional MR images in otherwise asymptomatic collegiate basketball players [10-12].

Normal tendons and ligaments are challenging to image on MR as they provide low signal intensity and exhibit short T2 relaxation times. These structures also are subject to strong magic angle effects if imaged at parallel to B0, the static magnetic field[13-15].Different techniques have been applied to increase the signal from these tissues, including orienting the tendon fibers at the magic angle (~55° to B0) to increase the T2 relaxation times of these tissues. However, clinical imaging at the magic angle may be impractical and challenging. Use of ultrashort TE (UTE) pulse sequence which have TE's approximately 100-1000 times shorter than those of conventional sequences represents another method that can be used to increase the MR signal of tendons and ligaments[16, 17].

MRI-based investigations of tendons have characterized T1 and T2 relaxation times and the apparent diffusion coefficient (ADC) of isolated tissues under conditions of static and repeated mechanical loads [18-22]. Navon and colleagues have utilized proton double quantum filtered MRI to investigate the anisotropy of collagen fibril orientation in tendon [23, 24] as well as fiber orientation during tendon healing [25, 26]. The study of water transport to/from and within ligament and tendon is of fundamental importance as this mechanism is thought to play an important role in tissue nutrition, mechanotransduction and mechanical function of the tissue [27, 28]. However, the extent to which matrix damage alters water diffusion in either tendon or ligament is largely unknown. This

chapter discusses the MR imaging methods that have been used to image tendons and ligaments such as UTE MRI and diffusion-weighted imaging and adds diffusion tensor imaging currently being studied by our group which provides more quantitative information about the microstructure of these tissues.

1.2 Ultra-short TE (UTE) MRI

Ultrashort echo time (UTE) pulse sequences can be used to enhance the MR signal from tissues with short T2 relaxation times, in our case, tendons and ligaments. UTE sequences image the restricted protons directly to produce images weighted by the actual size of the bound proton and its relaxation rate. UTE pulse sequences have TEs that are 100–1,000 times shorter than those used in conventional spin-echo sequences for imaging tendons and ligaments and can detect signal from these tissues before the signal has significantly decayed. Bydder et al have published extensively on the use of UTE pulse sequences to image not just tendons and ligaments but also other short T2 musculoskeletal tissues and their components such as entheses, deep layers of articular cartilage, meniscus, cortical bone, components of intervertebral disc and muscle. Using TE's of 8 microseconds and shorter Bydder et al was able to show clear collagenous fascicular structure from T2 weighted MR images of cadaveric Human Achilles tendons (Figure 1.1) rarely possible previously through conventional spin-echo sequences. Through short TE's the investigators were also able to identify the anatomical details of the entheses of the Achilles tendon and the three different fibrocartilage components of the "entheses organ" (which serves to dissipate the stress concentration away from the tendon-bone junction) not possible through conventional pulse sequences. UTE sequences are also beneficial in

imaging tendon collagen degeneration proximal to the insertion site, i.e. where the tendon is most vulnerable to degenerative change and rupture, 2–6 cm above its enthesis and where it is surrounded by a paratenon.

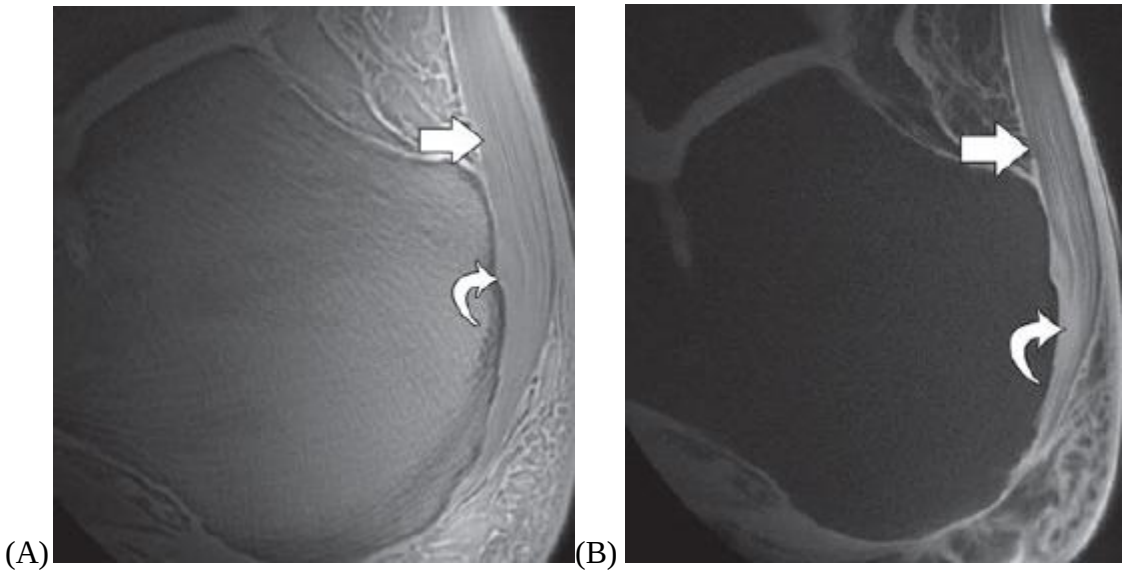

Figure 1.1: Appearance of Achilles tendon from a cadaveric specimen with ultrashort-TE (UTE) MR sequence. A and B, Sagittal UTE MR images obtained without (A) and with (B) fat suppression show normal striated appearance of Achilles tendon in mid tensile region (straight arrow). Adapted from Filho et al [16].

Several studies [17, 29, 30] have shown that bulk T2 in tendon is multi-exponential, therefore the ability to quantify the signal from each individual pool could enable the examination of sub-tissue populations such as collagen, proteoglycans and ground substance and provide a better understanding of early tissue degeneration by monitoring changes in T2 relaxation times of “bound water” associated with these microstructures. Conventionally, clinicians have used only mono-exponential fitting of T2 relaxation, assessing relaxation from only “free” water molecules, leaving out any relaxation information from the “bound” water molecules. Use of UTE pulse sequences can provide

information from faster relaxing pools of “bound water” bound with collagen fibers, proteoglycans and other ground substance through multi-exponential fitting of the relaxation not possible with conventional MR pulse sequences, and can give a better understanding of the overall tissue microstrucutre.

1.3 Diffusion Weighted and Diffusion Tensor Imaging

Water content is the primary factor governing MR differences between tissues, where the relaxation time is generally a linear function of the solute concentration. These MR parameters have the potential to be used to evaluate water distribution within tissues and thus visualize the disease progression or tissue regeneration. Diffusion of water is an indication of the morphological and biochemical integrity of tissues. In the region where cells swell or cell membranes rupture due to diseases, for example, the water diffusion is faster because there are fewer physical barriers. Diffusion weighted imaging (DWI) is an MR technique based on the measurement of the random Brownian motion of water molecules, which is sensitive to the physiological and anatomical environment of tissues. In isotropic tissues, where the apparent diffusivity is independent of the orientation of the tissue, it is usually sufficient to characterize the diffusion characteristics with a single scalar apparent diffusion coefficient (ADC). In anisotropic tissues, MRI can characterize molecular diffusion through a second-order tensor called “diffusion tensor imaging”. DWI and DTI have potentials for investigating fluid movement within regenerating tissues. Sotak et al [18-22] have studied the diffusion behavior in intact rabbit Achilles tendons along with changes in ADC after tensile loading of the tissues in vitro. The

investigators showed that ADC was significantly greater in the direction parallel to the long axis of the tendon than in the perpendicular direction for unloaded tendons for both freshly isolated and PBS stored tendons. Following tensile loading of 5N, significant increase in ADC in the "rim" region (periphery) of the tendon was found compared to the "core" of the tissue indicating extrusion of the water along the radial direction of the tendon. The transient response of the ADC to a 5-N tensile load was also studied. The absolute ADC in both directions increased with loading and recovered to baseline upon unloading.

The DTI technique combines magnetic resonance diffusion-weighted pulse sequences with tensor mathematics to measure molecular diffusion in three dimensions, thereby providing a non-invasive proxy measure of microstructural integrity [31]. The diffusion of water molecules within fibrous tissues (e.g., ligament) is not equal in all directions, as molecular restriction is greater *across* than *along* the major fiber axis. Hence, it is presumed that intact tendons and ligaments promote anisotropic diffusion, whereas damaged tissue promotes isotropic diffusion (Figure 1.2).

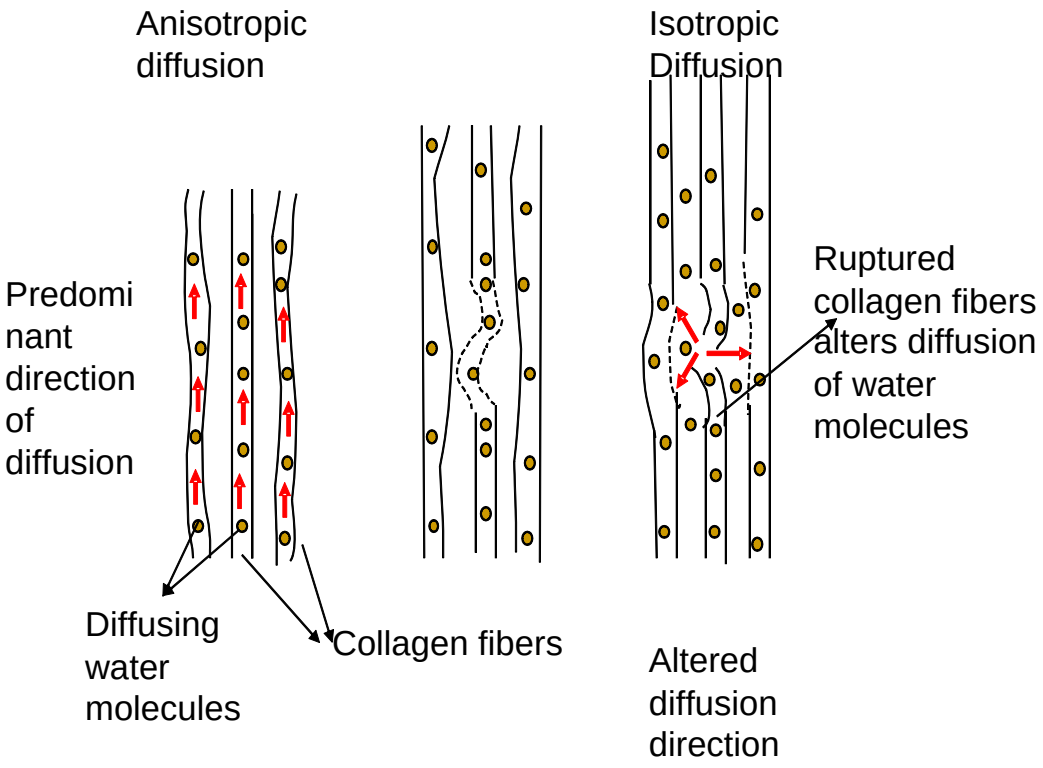

Figure 1.2: Schematic diagram illustrating effects of matrix disruption on water diffusion. In normal tendon or ligament, water molecules (brown circles) preferentially diffuse in a direction parallel to the collagen fibers. Matrix disruption promotes isotropic diffusion whereby there is no longer a predominant

In each voxel a diffusion tensor **D** expresses a diffusion coefficient in the direction given by the subscript as shown below:

$$\mathbf{D} = \begin{bmatrix} D_{xx} & D_{xy} & D_{xz} \\ D_{yx} & D_{yy} & D_{yz} \\ D_{zx} & D_{zy} & D_{zz} \end{bmatrix}$$

The principal diffusion direction is described by the eigenvector of **D** corresponding to the largest eigenvalue. Fractional anisotropy (FA) is a commonly reported DTI metric; it is rotationally invariant and can be calculated as

$$FA = \sqrt{3\{(\lambda_1 - <\lambda>)^2 + (\lambda_2 - <\lambda>)^2 + (\lambda_3 - <\lambda>)^2\}} / \sqrt{2(\lambda_1^2 + \lambda_3^{\,2} + \lambda_3^{\,2})}$$

where $<\lambda> = (\lambda_1 + \lambda_2 + \lambda_3)/3$ is the mean diffusivity (MD)

Water diffusion can be characterized by the tensor in each voxel, along with DTI indices (e.g., FA and MD) describing the magnitude and orientation of water diffusion (cellular integrity). To date, the vast majority of published studies have used DTI to investigate changes in the brain. Whole-brain and regional alterations in DTI indices have been associated with normal aging[32-34], as well as a number of neurologic and psychiatric disorders, including Parkinson's disease,[35] mild cognitive impairment/Alzheimer's disease[36-38], stroke,[39] multiple sclerosis[40], and schizophrenia[41, 42]. For example, decrease in fractional anisotropy has been reported with normal aging; and increase in mean diffusivity and a decrease in fractional anisotropy has been reported in patients with diseases such as Alzheimer's, multiple sclerosis and schizophrenia. Fiber tractography is another DTI visualization tool which has been used to visualize the microstructural organization and integrity of white matter tracts in these studies.

Recently, *ex vivo* [43, 44] and *in vivo* [45-49] characterization of articular cartilage, anulus fibrosus, and skeletal muscle has demonstrated the ability of DTI to provide

reliable, accurate collagen fiber architecture data in normal and damaged musculoskeletal tissues. For example, in one of the studies de Visser et al demonstrated the application of diffusion tensor imaging to observe adaptations of collagen fibers to mechanical compression in bovine articular cartilage. Spin-echo DTI sequence was used to acquire images on a 7.0T vertical bore research magnet. Ex-vivo bovine cartilage plugs were scanned before and after application of a 30% compression strain. Compression resulted in a decrease in mean diffusivity, particularly in the superficial and transitional zones. In the transitional zone, the average orientation of the principal eigenvectors with respect to the normal to the articular surface increased by up to 40°, indicating that the collagen fiber bundles were oriented more parallel to the surface when compressed.

Hsu et al studied the application of diffusion tensor imaging to characterize the architecture of porcine intervertebral disc annulus fibrosis. DTI scans were performed on ex-vivo intervertebral disc segments from porcine lumbar spine on 7.1T horizontal bore magnet using a diffusion-weighted spin-echo pulse sequence. The investigators found the diffusion in the annulus fibrosis to be anisotropic. The orientations of anisotropy exhibited a layered morphology that agreed with light micrographs of the corresponding samples, and the behavior of the orientation angles was consistent with the known characteristics of collagen lamellar structure of the annulus fibrosis.

Zaraiskaya et al explored the capability of diffusion tensor imaging for evaluation of human skeletal muscle injury on patients with gastrocnemius and soleus muscles injuries. Diffusion- weighted spin-echo sequence was used to acquire images from the patients on a 3 T clinical scanner. FA values reduced by more than 50% for the patients compared to the healthy controls and ADC was consistently higher for the patients compared to the

controls. 2D projection maps revealed muscle fiber disorder in injured calves, while in healthy controls the 2D projection maps showed a well organized fiber structure.

Many of the above studies have used high magnetic field strengths (greater than 3T) for scanning the tissues. Using this high field strength has its advantages and disadvantages. The advantage is that one can achieve a high enough resolution which is desirable for the small size of the animal tissues being studied and can provide an improved signal to noise ratio. On the other hand signal averaging needs to be increased to reduce the noise which increases the scan time. High field MRI also exhibits imaging artifacts such as B0 and gradient field inhomogeneties and susceptibility artifacts. Also, high field strengths greater then 7T are highly unlikely to be used for human use because of the higher specific absorption rate (SAR) which causes heating of the tissue.

1.4 Summary

Specifically, Diffusion tensor imaging (DTI) can quantify differences in water diffusion resulting from damage to the matrix of tendons or ligaments. The technique combines magnetic resonance diffusion-weighted pulse sequences with tensor mathematics to measure molecular diffusion in three dimensions, thereby providing a non-invasive proxy measure of microstructural tissue integrity.

2. Background and Significance

2.1 Tendon and Ligament Structure and Function

Tendons and ligaments are dense, fibrous connective tissues composed primarily of type I collagen (85% of dry weight) and water (~55% of wet weight), along with other collagens (e.g. type II, III, V, IX, XI), proteoglycans, and cells [50, 51]. The primary function of these tissues is to facilitate transmission of uniaxial tensile loads from muscle to bone (in the case of tendon) or from bone to bone (ligament). Accordingly, the hierarchical, composite extracellular matrix structure of tendons and ligaments (Figure 2.1) is characterized by a predominantly parallel arrangement of collagen fibers [50, 52, 53].

Tendon and ligament biomechanical properties, like their fibrous structure, are highly anisotropic (i.e., direction-dependent). The tensile modulus (i.e., material stiffness) in the longitudinal (fiber-aligned) direction is one to two orders of magnitude larger than that measured in the transverse direction [54-57]. This contrasts the structure and function of, for example, dermal tissue[48] and joint capsule [58], whose collagen fibers are arranged in a "basket-weave" or random pattern in order to resist loads in multiple anatomic directions.

Comparing tendons and ligaments specifically, material properties for the tendons including linear modulus, maximum stress and energy density to maximum stress are generally higher than the ligaments[59] Ligaments have a higher crimping pattern/ organization than tendons representing a longer toe-region for ligaments on the stress-

strain curves. With regards to the biochemical composition, ligaments are more metabolically active than tendons, have higher DNA content, and the presence of more type III collagen, as compared with tendons. Ligaments also contain slightly less total collagen than tendons and more glycosaminoglycans [60]. As shown in figure 2.1, fascicular collagen structure of these tissues can be observed by using scanning electron microscopy (SEM), and fibril and sub-fibrillar structures can be observed using X-ray diffraction techniques, conventional MRI can go down to as low as the scale of fascicles using high resolution scanners (3T or higher) using ultra-short TE (UTE) sequences.

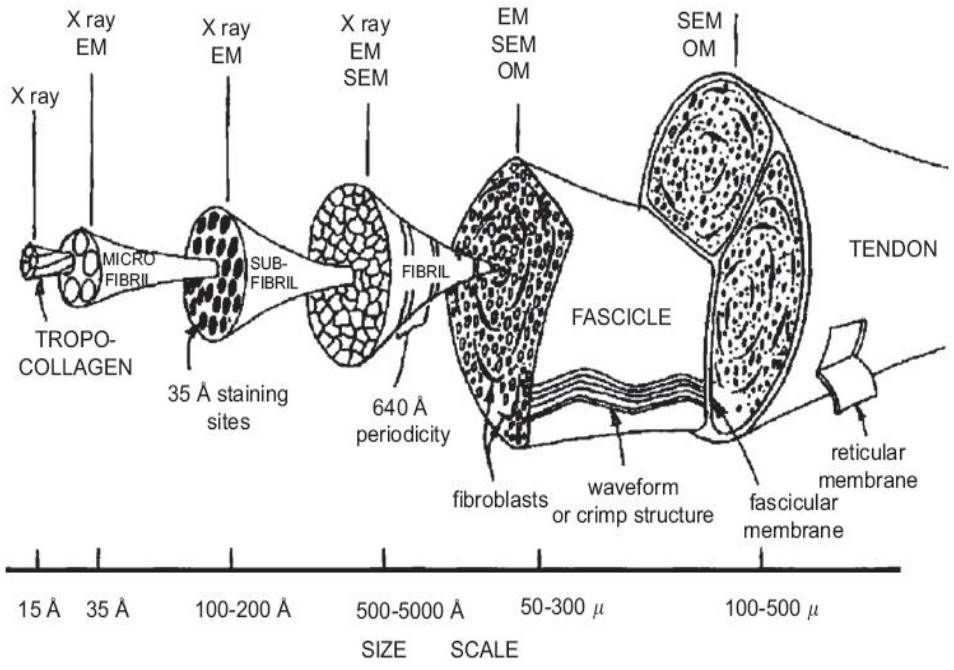

Figure 2.1: Hierarchical structural model of tendon (adapted from Kastelic et al.[53])

2.2Tendon and Ligament Injury and Repair

Like all skeletal tissues, tendons and ligaments are subjected to wear and tear from mechanical usage. Tendon and ligament injuries are major clinical problems which restrict athletic participation, impair motion and daily functions, and disable patients in the workplace. Studies have revealed that in healthy middle-aged and older individuals, non-ruptured tendons showed histological evidence of degenerative changes and cellular response to microscopic injuries, indicating that extensive matrix remodeling had occurred in these tendons[61].

Broadly, tendon and ligament injuries are classified as acute or chronic. Acute injuries are the result of "macrotrauma" (e.g. direct lacerations, sprains due to sudden tensile overload) while chronic injuries are widely believed to result from repetitive overuse (cumulative microtrauma) [62], as likely occurs in high-demand sports such as professional football. However, many apparently acute injuries occur in a tendon or ligament weakened by prior accumulated fatigue damage and degeneration; it has been argued that some form of degeneration must generally be present prior to complete rupture of the tendon [63].

The microstructural bases for microtrauma in tendon and ligament are postulated to included collagen fiber/fibril tearing and delaminations between fiber bundles [61, 64]. Ex vivo studies have established that significant matrix damage and degradation of tendon/ligament material properties can be produced by single (e.g., ramp to high subfailure deformation level) or multiple loading events (i.e., fatigue) [65-71]. Correlative biomechanical and histologic studies by Wang et al have shown that tendon

elongation during cyclic loading is a reliable index of subrupture matrix-level damage [72, 73].

Animal studies of tendon and ligament healing have demonstrated a strong correlation between the functional quality of the repaired tissue and its collagenous organization; namely, a remodeled tendon/ligament with well-arranged, parallel collagen bundles (resembling the native, intact structure) generally translates to superior biomechanical properties of the repaired construct [74]. Hence, restoration of fiber orientation is critical to successful tissue repair.

2.3 MRI studies of Tendon & Ligament

Numerous studies have reported high levels of diagnostic accuracy of MRI for detecting large and complete tears in ligaments and tendons [75, 76]. While conventional MRI provides excellent soft tissue contrast and high spatial resolution, for example, resolution as high as 500 μm have been reported for imaging ACL's [77] on a 3T clinical magnet and even higher for imaging the whole knee, there remains uncertainty regarding its ability to resolve and delineate more subtle forms of tendon and ligament pathology such as sprains and tendinosis/tendinitis. Specifically, elevated MRI signal intensity is suggestive of tissue-level alterations which may include increased water content, elevated vascularity, inflammation, degeneration, or partial matrix disruption [2, 3]. Hence, elucidating these potential abnormalities using a qualitative measure such as signal intensity is challenging. Furthermore, imaging appearance often is not consistent with clinical diagnosis and symptoms (e.g., for patellar tendinosis)[10-12] Currently, there

exist very few (if any) MRI approaches to quantify the structural integrity of tendons and ligaments as discussed in chapter 1 of this thesis.

Water content is the primary factor governing MR differences between tissues. Quantitative MR parameters describing diffusion can be used to evaluate water distribution within tissues and thus visualize disease progression or tissue regeneration. Quantification of water is an indication of the morphological and biochemical integrity of tissues. Diffusion weighted imaging (DWI) is an MR technique based on the measurement of the random (Brownian) motion of water molecules, which is sensitive to the physiological and anatomical environment of tissues [78]. In isotropic tissues, where the apparent diffusivity is independent of the orientation of the tissue, it is usually sufficient to characterize the diffusion characteristics with a single scalar apparent diffusion coefficient (ADC). In anisotropic tissues, MRI diffusion tensor imaging can characterize three-dimensional molecular diffusion [79].

2.4 Diffusion Tensor Imaging.

Diffusion tensor imaging (DTI) is an emerging technique that can quantify differences in water diffusion resulting from damage to the matrix of tendons or ligaments. The diffusion of water molecules within tissue is not equal in all directions, as molecular restriction is greater across fibrous material such as tendons and ligaments, than along the major axis of these tissue types. Hence, intact tendons and ligaments promote anisotropic diffusion, whereas damaged tissue promotes isotropic diffusion. The diffusion of water molecules can be characterized by the tensor in each voxel, and the corresponding eigenvalues (λ_1, λ_2 and λ_3) can be used to calculate a number of quantitative indices

reflecting the magnitude and orientation of water diffusion (cellular integrity). The most common of these indices include fractional anisotropy (FA), the ratio of anisotropic to isotropic diffusion at the voxel level, mean diffusivity (MD), an estimate of the overall free diffusion of water, axial diffusivity (AD), representing diffusion of water along the long axes of the fibers, and radial diffusivity (RD), representing diffusion perpendicular to the long axes of the fibers. These indices derived from the eigenvalues can be described using the following equations [78, 79]:

$$\mathrm{MD} = \langle \lambda \rangle = \frac{\lambda_1 + \lambda_2 + \lambda_3}{3}$$

$$\mathrm{AD} = \lambda_1$$

$$\mathrm{RD} = \frac{\lambda_2 + \lambda_3}{2}$$

$$\mathrm{FA} = \sqrt{\frac{3}{2}} \sqrt{\frac{(\lambda_1 - \langle \lambda \rangle)^2 + (\lambda_2 - \langle \lambda \rangle)^2 + (\lambda_3 - \langle \lambda \rangle)^2}{\lambda_1^2 + \lambda_2^2 + \lambda_3^2}} \tag{2.1}$$

The aim of these diffusion-weighted sequences is to obtain images whose contrast is influenced by the differences in water molecule mobility. This is done by adding diffusion gradients during the preparatory phase of an imaging sequence. The diffusion gradients are strong and symmetrical in relation to the 180° rephasing pulse.

For a Stejskal-Tanner gradient pulse pair each of duration δ, amplitude G and separation by interval Δ, the classical equation of the transverse magnetization in the rotating frame is

$$\frac{M}{M_o} = \exp(-(\gamma\delta G)^2 D\Delta) = exp(-bD) \tag{2.2}$$

To date, the vast majority of published studies have used DTI to investigate changes in the brain. Whole-brain and regional alterations in DTI indices have been associated with normal aging[32-34], as well as a number of neurologic and psychiatric disorders, including Parkinson's disease,[35] mild cognitive impairment/Alzheimer's disease[36-38], stroke,[39] multiple sclerosis[40], and schizophrenia[41, 42]. Recently, *ex vivo*[43, 44] and *in vivo*[45-49] characterization of articular cartilage, anulus fibrosus, and skeletal muscle has demonstrated the ability of DTI to provide reliable, accurate collagen fiber architecture data in normal and damaged musculoskeletal tissues. Intuitively, the highly anisotropic organization of collagen fibers in ligaments and tendons may also be well suited for DTI analyses.

2.5 Hypothesis and Specific Aims

The central hypothesis to be tested in this work is that results obtained from Diffusion Tensor Imaging (DTI) of tendons and ligaments at ultra-high magnetic field (B0) confirm and relate with the microstructural organization and integrity of these tissues and DTI metrics provide complimentary information to conventional MR imaging techniques for imaging of these tissues.

Within the above hypothesis, another sub-hypothesis that will be tested is whether tendons are different from ligaments.

The hypothesis will be tested with three specific aims:

Specific Aim 1: Refinement Aim

To assess the applicability and refine the technique of Diffusion Tensor Imaging for tissue type and orientation, scanning media, image acquisition parameters, and slice orientation.

Sub-aims:

1. To assess rabbit Patellar and Semitendinosus tendons for feasibility for DTI scans.
2. To study the effect of different scanning media and comparison of 2-Dimensional and 3-Dimensional DTI scans.
3. To study the effect of tissue orientation comparing vertical, horizontal and magic angle orientations feasibility to the main magnetic field.
4. To refine various resolutions including scanning tissues at 50 and 100 μm resolution and acquisition plane refinement for coronal and axial scans.

Specific Aim 2: Assessment Aim

To quantify and compare the regional structural organization of rabbit medial collateral ligaments and semitendinosus tendons using high field MRI.

Sub-aims:

1. To determine Fractional Anisotropy (FA), Mean diffusivity (MD), Axial Diffusivity (AD), Radial Diffusivity (RD), T1 and T2-relaxation times for intact rabbit SemiTs and MCLs.
2. To perform tractographic analysis of the tendon and ligament microstructure and histologic evaluation and its correlation with tractography.
3. To assess water content and mechanical properties for both MCLs and SemiTs.
4. To assess regional variation and determine inter and intra-slice variability (voxel-wise assessment) for FA, MD and the three eigenvalues for the two tissue types.

Specific Aim 3: Optimization aim

To determine sensitivity of b-value on diffusion tensor metrics and optimize these parameters for rabbit semitendinosus tendons.

Sub-aims:

1. To determine sensitivity of b-values and optimize it for Mean diffusivity and Fractional Anisotropy.
2. To determine Fiber Density index (FDI) for different b-values for determination of the optimum b-value.

3. To assess the applicability and refine the technique of Diffusion Tensor Imaging for tissue type and orientation, scanning media, image acquisition parameters, and slice orientation

3.1 Invivo human and exvivo rabbit patellar and semitendinosus tendon DTI scans for feasibility.

Initial pilot studies consisted of assessing the applicability of DTI for *in vivo* analyses of the human anterior cruciate ligament (ACL) and patellar tendon (PT). Knees of five healthy, asymptomatic volunteers (mean age 25±5 y.o.) were imaged on a 1.5 Tesla scanner equipped with high speed gradients. All knees were positioned in full extension for scanning and each subject received one imaging protocol. Two high-resolution structural protocols and three high-resolution DTI protocols were examined for utility. The best imaging results were obtained from the two subjects receiving (a) structural protocol featuring a fast spin echo (FSE) proton density (PD) weighted pulse sequence (60 contiguous sagittal plane images, 1.6 mm sections, matrix = 256x256, repetition time (TR)/echo time (TE) = 2000/15 ms, echo train length = 4) and (b) DTI protocol consisting of diffusion weighted single shot spin echo, echo planar images acquired in the sagittal plane, TR/TE = 12100/97ms, FOV =16 cm, matrix =128x128, 30 3 mm gapless slices, 6 repetitions, and application of high-order shimming. In all DTI parameters, two diffusion weights were used: b = 0 and 800 s/mm^2. An additional set of inversion

recovery images was acquired and used to un-warp the eddy current effect of the diffusion gradients. Mean Diffusivity and Fractional Anisotropy were computed for ACL and patellar tendon and the results are presented in Table 3.1 with a comparison with other musculoskeletal tissues.

Tissue	**Subject #**	**Mean Diffusivity ($x10^{-6}mm^2/s$)**	**Fractional Anisotropy**
Anterior Cruciate Ligament*	1	359.5 ± 251.7	0.487 ± 0.296
	2	469.3 ± 191.0	0.455 ± 0.345
Patellar Tendon*	1	576.3 ± 667.0	0.645 ± 0.378
	2	466.1± 135.2	0.589 ± 0.405
Anulus fibrosus		1200	0.13
Skeletal muscle		1450-1720	0.19-0.37
Articular Cartilage		1070-1900	0.04-0.38

Table 3.1: Comparison of ACL and PT mean diffusivity and fractional anisotropy among musculoskeletal soft tissues

Despite their relatively high variability, FA and MD are, respectively, higher and lower than those reported for articular cartilage, intervertebral disc, and skeletal muscle. The aforementioned comparisons are consistent with the microstructural organization of the fibrous matrix of the respective tissues.

However, limitations with the clinical scanner such as low field strength, low SNR, low resolution, high scanning costs and no histological validation with in-vivo scans prompted us to move to high field ex-vivo scans on a 11.7T vertical bore research magnet. This magnet has previously validated applications such as high field imaging of human articular cartilage, engineered cartilage and bone[80, 81]. High field imaging allows high resolution and histological validation is possible with ex-vivo scans. Also, it is less expensive and we can try a variety of protocol parameters with no time limitations. Our initial experiments on the 11.7T scanner focused on refining the scan acquisition parameters for DTI using mouse flexor digitorum longus tendons (FDLs), rabbit patellar tendon, semitendinosus tendon and medial collateral ligaments. In particular, effect of different media for scanning including perflourinated (PFPE) oil and saline were examined, differences in DTI metrics when comparing 2-dimensional and 3-dimensional scans was examined, tissue orientations of vertical, horizontal and at an angle of 55 degrees (called the magic angle) to the main magnetic field were studied, coronal and axial acquisition planes were compared, in-plane resolutions of 50 and 100 μm were examined, isotropic resolutions were examined both in the coronal and axial acquisition planes. Total scan time varied with the selection of different acquisition planes and in-plane resolutions, for example, 50 and 100 μm resolutions in coronal planes resulted in scan times of 16 and 8 hrs respectively whereas in-plane resolution of 50 μm in axial plane with a slice thickness of 3.2 mm resulted in a scan time of 2 hrs. Considering the long scan durations for examining each set of acquisition parameters, scanning efficiency and practicality were primary considerations to refine these parameters and get down to the best acquisition parameters. Mouse FDLs proved to be too small in size as we were

able to get less than 100 voxels for these tissues; and rabbit Patellar tendons proved to be too large for the 10 mm NMR tube and this made it difficult to place these tissues at the magic angle orientation; therefore we used semitendinosus tendons and medial collateral ligaments for our subsequent scans.

A custom designed tissue holder was used to secure the tissues in the NMR tube (Figure 3.1). The holder allowed two tissues to be scanned at the same time at an angle of 55° called the magic angle (discussed below) to the main magnetic field B0. All these scans were conducted at 11.74T (500 MHz for protons) in a 56mm vertical bore magnet using a Bruker DRX Avance spectrometer (Bruker BioSpin, Billerica, MA, USA). Images were acquired using a Bruker Micro 5 imaging probe with triple axis gradients (maximum strength 200 G/cm) and a 10 mm diameter RF saddle coil (Figure 3.2). [80, 81]

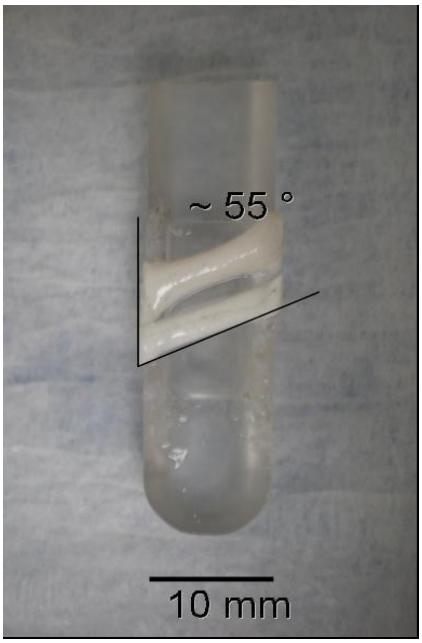

Figure 3.1:Custom designed tissue holder that allows two tissues (Rabbit SemiTs shown above) to be scanned simultaneously at the magic angle (55° to the main magnetic field, B0).The picture shows two semitendinosus tendons glued to the holder at magic angle.

Figure 3.2: Top: Bruker superconducting magnet with field strength of 11.74 T (500 MHz for protons) located at Research Resource Center at the University of Illinois at Chicago. The magnet stands on three shock absorbent legs stabilizing the magnet.

3.2 Effect of different scanning media and comparison of 2-Dimensional and 3-Dimensional DTI scan.

DTI scans were performed on two rabbit patellar tendons, one immersed in normal isotonic saline (Cardinal Health, IL, USA) and the other immersed in perfluoroalkylether (PFPE) oil (Krytox GPL-102 PFPE oil, DuPont, NJ, USA) to examine the effect of oil as the surrounding medium. DTI was performed using a 3D spin echo DTI sequence with TR = 1s, TE = 15 ms, δ/Δ = 2/8 ms, NEX = 1, FOV = 9.6 x 3.2 mm, six diffusion directions, b= 600 s/mm^2, in-plane resolution= 50 µm. Fractional Anisotropy was extracted from the experimental data using Bruker's Paravision software version 4.0. Table 3.2 represents the FA values obtained from these scans.

	Tissue	Medium	FA
1.	Rabbit Patellar Tendon	Saline	0.54 ± 0.26
2.	Rabbit Patellar Tendon	PFPE Oil	0.67± 0.23

Table 3.2: Comparison of saline and PFPE oil as scanning medium for DTI of a Rabbit patellar tendon.

Perfluorinated oil maintains the hydration state of the tendons as well as minimizes proton signals from the bathing medium[18-22]. Higher FA values were observed from the sample immersed in PFPE oil compared to the sample immersed in saline probably

because surrounding saline contributes to background noise decreasing the SNR for the tissue resulting in lower FA values[18-22][18, 20-22].

Another set of scans was done to determine the differences between a 2-dimensional and 3-dimensional DTI scan. 2D DTI scan was performed using a 2D spin echo DTI sequence with TR = 1s, TE = 15 ms, δ/Δ = 2/8 ms, NEX = 1, FOV = 9.6 x 3.2 mm, six diffusion directions, b= 600 s/mm^2, whereas the 3D DTI scan was performed using 3D spin echo DTI sequence with TR = 1s, TE = 15 ms, δ/Δ = 2/8 ms, NEX = 1, FOV = 9.6 x 3.2 mm, six diffusion directions, 200 µm thick axial slices, b= 600 s/mm^2, in-plane resolution= 50 µm on one rabbit patellar tendon for each type of scan. Table 3.3 summarizes the FA and MD values obtained from these two types of scans.

	Tissue	**Scan Type**	**FA**	**MD ($x10^{-6}$ mm^2/s)**
1.	Rabbit Patellar Tendon	2D	0.59 ± 0.27	875 ± 432
2.	Rabbit Patellar Tendon	3D	0.67± 0.23	891± 389

Table 3.3: Comparison of 2D to a 3D scan for DTI of a rabbit patellar tendon.

Lower FA values were observed for the 2D scan compared to the 3D scan probably because in a 2D scan (which represents the whole tissue volume as the slice thickness) the voxel size is large resulting in a lower fiber anisotropy whereas in a 3D scan, the slice thickness was 200 µm which reduced the voxel size to 50x50x200µm. Fascicles would appear to be more aligned and parallely organized in a smaller voxel compared to the whole tissue volume because over a large distance (slice thickness) crimping and inter-

weaving of the fascicles would be more pronounced which apparently would decrease anisotropy of molecular diffusion.

3.3 Effect of Tissue Orientation

Tissue orientation with respect to the main magnetic field can influence the T2 relaxation times of the tissues, therefore scans were done to determine the best orientation for the tissues. Rabbit SemiTs were scanned in horizontal, vertical and 55° (magic angle) orientations to the main magnetic field. Initially, T2-weighted scans were performed on the tissues to determine if high enough T2 relaxation times can be obtained for subsequent DTI scans which have inherently low SNRs. Two semiTs were scanned in horizontal position (perpendicular to the main magnetic field) since the custom made tissue holder allowed two tissues to be scanned at once for the available field of view, one semiT was scanned in the vertical position (parallel to the main magnetic field) and six semiTs were scanned at the magic angle. Table 3.4 summarizes the T2 relaxation times from these scans.

	Tissue	**Orientation**	**T2 (ms)**
1.	Rabbit Semitendinosus tendon	Vertical	9.1 ± 1.1
2.	Rabbit Semitendinosus tendon	Horizontal	23.9± 1.4
3.	Rabbit Semitendinosus tendon	55° to B_0 (Magic angle)	33 ± 2

Table 3.4: T2 relaxation times for rabbit semitendinosus tissues scanned in vertical, horizontal and magic angle orientations to the main magnetic field.

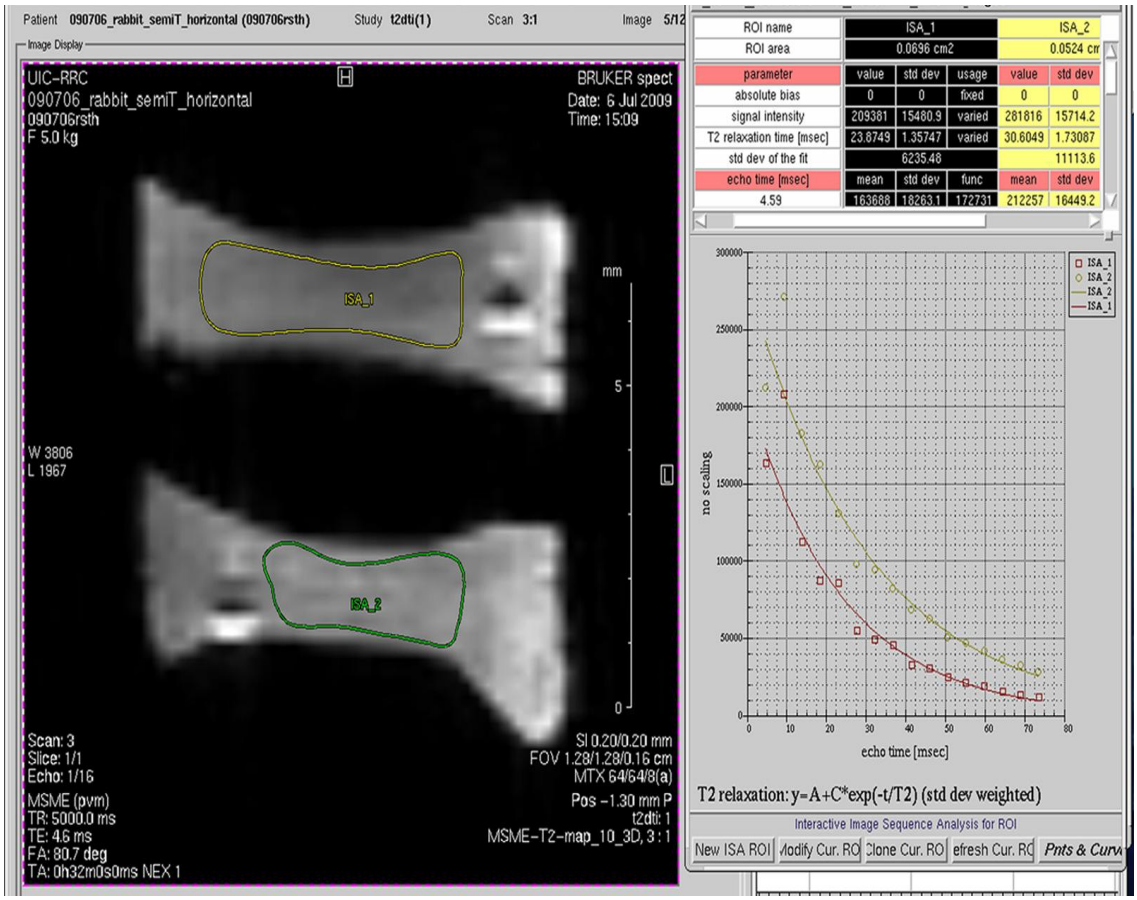

Figure 3.3: T2-weighted scans of two semitendinosus tendons scanned horizontally (i.e., perpendicular to the main magnetic field).

Magic angle orientation resulted in a higher T2 relaxation times compared to the vertical and horizontal orientations. Tissue orientation refers to the angle the tissue fibers make to static magnetic field B_0. When tissues themselves have oriented fibrous structures, two most important effects are angular dependence of T_2 and diffusional signal loss which can be tracked by DTI. Changes in T_2 with angle are the results of the so-called magic angle effect. Dipolar interactions between two spins are proportional to:

$3\cos^2\theta - 1$

where θ is the angle between the tissue fiber and B_0 .This interactions cause the magnetic field fluctuation responsible for T_2 relaxation. The rapid rotation of mobile spins quickly averages away these fluctuations. This average is eliminated for spins in crystalline solids for lack of motion, causing short T_2 in solid. However, the dipolar interaction goes to zero when the angle with B_0 is approximately 54.7° (the reason to rotate the samples at this angle in solid-state MR spectroscopy). When a tissue with highly ordered structure, such as tendon and ligament, is oriented at a 54.7° angle to B_0, dipole-dipole interactions go to zero, resulting in a prolongation of T2 relaxation time which leads to an increase in signal compared with orientations at other angles. This leads to bright regions in MR images in portions of curved tendons, ligaments. We used this tissue orientation for the subsequent DTI scans for SemiTs and MCLs. Figures 3.1 and 3.2 show T2-weighted scans of semitendinosus tendons done in horizontal and vertical directions to the main magnetic field respectively.

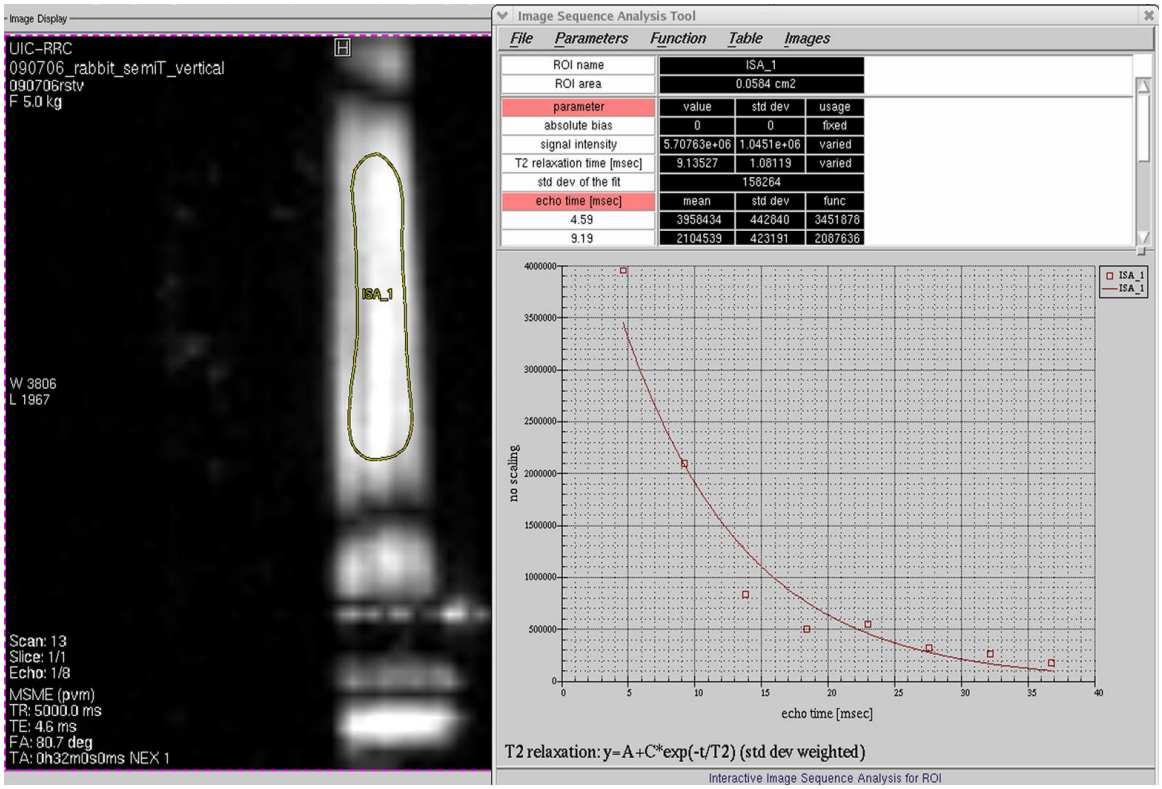

Figure 3.4: T2-weighted scan of a semitendinosus tendon scanned vertically (i.e., parallel to the main magnetic field).

3.4 Refinement of different resolutions for DTI scans.

Scans were conducted to determine the effect of different in-plane resolutions on the DTI parameters FA and MD. Two in-plane resolutions of 50 µm and 100 µm were studied with two specimens scanned at 50 µm and four specimens scanned at 100 µm resolutions as shown in Table 3.4. DTI was performed using a 3D spin echo DTI sequence (TR = 1 s, TE = 14 ms, δ/Δ = 1/9 ms, NEX = 2, FOV = 1.28 x 1.28 cm, six diffusion directions, 100 µm thick coronal slices, b= 600 s/mm2) at two in-plane resolutions of 50 µm (scan time= 16 hrs/sample, 2 samples) and 100 µm (scan time= 8 hrs/sample, 4 samples). Table 3.5 represents the FA and MD values for the two in-plane resolutions.

Specimen #	Diffusion Tensor Imaging results			
	50 µm resolution		100 µm resolution	
	FA	MD ($x10^{-6}$ mm^2/s)	FA	MD ($x10^{-6}$ mm^2/s)
1	N/A	N/A	0.45±0.09	1290±134
2	N/A	N/A	0.48± 0.1	1180±115
3	0.58±0.17	1230±234	0.48±0.09	1260±156
4	0.59±0.18	1210±283	0.48± 0.1	1290±166

Table 3.5: FA and MD ($x10^{-6}$ mm^2/s) values obtained from four rabbit medial collateral ligaments at two different in-plane resolutions.

Higher Anisotropy values were observed for the 50 µm resolution relative to 100 µm resolution because of the fact that fascicles would appear to be more aligned and parallely organized in a smaller voxel compared to a larger voxel because in a larger voxel crimping and inter-weaving of the fascicles would be more pronounced which apparently would decrease anisotropy of molecular diffusion.

3.5 Coronal and axial acquisition plane differences.

DTI was performed on an MCL and a semiT to examine the differences in the DTI metrics between the axial and coronal plane acquisitions with isotropic resolutions. For the axial plane acquisition, DTI scans were performed using a 3D spin echo DTI sequence with the following scan parameters: TR = 1s, TE = 15 ms, δ/Δ = 1/8 ms, NEX = 1, FOV = 9.6 x 3.2 mm, six diffusion directions, 100 µm thick axial slices, b= 600 s/mm^2, resolution= 100x100x100 µm, scan time= 6 hrs/sample, number of slices=96. Table 3.6 summarizes the DTI data from three axial slices from both the MCL and SemiT.

	MCL Ligament			**SemiT Tendon**		
Slice #	**# of Voxels**	**FA**	**MD (x10^{-6} mm^2/s)**	**# of Voxels**	**FA**	**MD (x10^{-6} mm^2/s)**
27	375	0.55±0.09	1500±184	234	0.55±0.08	1590±142
37	344	0.55±0.10	1480±190	247	0.55±0.07	1600±134
57	359	0.58±0.10	1460±189	266	0.52±0.07	1640±127

Table 3.6: Number of voxels, FA and MD values (mean ± SD) from one rabbit Medial Collateral Ligament and one SemiT tendon in axial acquisition plane.

For the coronal acquisition plane, DTI was performed using a 3D spin echo DTI sequence with the following scan parameters: TR = 1s, TE = 15 ms, δ/Δ = 1/8 ms, NEX = 1, FOV = 9.6 x 3.2 mm, six diffusion directions, 100 μm thick coronal slices, b= 600 s/mm^2, resolution= 100x100x100 μm, scan time= 8 hrs/sample, number of slices=24. Table 3.7 summarizes the DTI data from three central coronal slices from both the MCL and SemiT.

	MCL Ligament			**SemiT Tendon**		
Slice #	**# of Voxels**	**FA**	**MD ($x10^{-6}$ mm^2/s)**	**# of Voxels**	**FA**	**MD ($x10^{-6}$ mm^2/s)**
11	1188	0.45± 0.08	1300±119	901	0.44±0.09	1430±109
12	1578	0.45± 0.09	1310±127	1036	0.44±0.1	1400±129
13	2143	0.47± 0.1	1330±133	987	0.43± 0.09	1410±111

Table 3.7: Number of voxels, FA and MD values (mean ± SD) from one rabbit Medial Collateral Ligament and one SemiT tendon in coronal acquisition plane.

3.6 Discussion

Pilot in-vivo human DTI scans demonstrated the feasibility of investigating the DTI metrics using diffusion tensor imaging with a 1.5T clinical scanner. FA and MD obtained were, respectively, higher and lower than those reported for articular cartilage, intervertebral disc, and skeletal muscle. The aforementioned comparisons are consistent with the microstructural organization of the fibrous matrix of the respective tissues. However issues with low SNRs, low resolutions and high scanning costs prompted us to move our analysis to high field 11.7 T magnet. Examining these different tissues thoroughly in different ways such as with different scanning media, different tissue orientations, different acquisition planes and different scan parameters on 11.7 T magnetic field helped us to narrow down to the best scan acquisition conditions and parameters which were used for the subsequent DTI scans on larger number of rabbit SemiTs and MCLs to maintain consistency and obtain publishable quality results. For example, scanning a rabbit Patellar tendon we found that not only was it difficult to achieve a magic angle orientation with such a wide tissue for the 10 mm limit of the NMR tube width and field of view but also our scan sessions would be less efficient as we could only scan one tissue at a time. Also, mouse FDLs provided only a limited number of voxels for analysis. Use of semitendinosus tendons and medial collateral ligaments eliminated all of these limitations.

Another important decision to make was to choose between coronal and axial acquisition planes. For example, a 50x50 μm in-plane resolution in a coronal plane with a 100 μm thick slice led to acquisition times of as high as 16 hrs whereas a 50x50 μm resolution in

an axial plane with a 200 μm thick slice brought down the acquisition times to about 2 hrs. Considering scanning efficiency and practicality for these feasibility and the subsequent b-value optimization scans (chapter 5), we used axial acquisition plane for all of our scans. Use of a 3D acquisition sequence allowed us to divide the tissue in several 200 μm thick slices (as opposed to the whole tissue volume for a 2D scan) which made it possible to study the regional variation (inter-slice variability) in the DTI metrics along the length of the tissue for the subsequent DTI scans.

With regards to tissue orientation, the magic angle orientation of the tissues provided the highest T2 relaxation times compared to the vertical and horizontal configurations which is desirable for the DTI scans which inherently suffer from low SNRs.

All of these above preliminary set of experiments led us to narrow down to the best possible tissues, media, tissue orientation and scan acquisition parameters and we finalized the following parameters to be used for the subsequent DTI scans: TR = 1s, TE = 15 ms, δ/Δ = 2/8 ms, NEX = 1, FOV = 9.6 x 3.2 mm, six diffusion directions, 200 μm thick axial slices, b= 600 s/mm^2, in-plane resolution= 50 μm, scan time= 2 hrs/sample with tissues immersed in PFPE oil and scanned at the magic angle orientation.

4. Determination of DTI metrics for intact rabbit medial collateral ligaments and semitendinosus tendons.

4.1 Fractional Anisotropy (FA), Mean diffusivity (MD), Axial Diffusivity (AD), Radial Diffusivity (RD), T1 and T2-relaxation time measurements for intact rabbit SemiTs and MCLs.

A total of 3 male, skeletally mature New Zealand White rabbits (3 months old, 2.5 kg weight each) that had been sacrificed for other unrelated research (IACUC protocol number: 08-062) were utilized for these set of scans. Contralateral pairs of Semitendinosus tendons (SemiTs) and medial collateral ligaments (MCLs) were dissected out from each rabbit, for a total 6 MCLs and SemiTs, and stored at -20° C until the day of scans. A custom made tissue holder was used to secure the tissues inside the NMR tube (Figure 4.1a). The proximal and distal aspects of each tissue were glued to the specimen holder at an approximate angle of 55° to the direction of B0, the applied magnetic field, to increase signal intensity and achieve higher T2 relaxation times due to the magic angle effect. Tissues were glued on the specimen holder in a taut state with minimal tension applied to the tissues. The holder was then placed in a 10 mm diameter NMR tube containing perfluorinated oil (Krytox GPL-102 PFPE oil, DuPont, NJ, USA) (Figure 4.1b). Perfluorinated oil was used in order to maintain the hydration state of the tendons as well as to minimize proton signals from the bathing medium [19-22]The tube was then placed in a RF saddle coil and inserted into the bore of the magnet.

Scans were conducted at 11.74T in a 56mm vertical bore magnet using a Bruker DRX Avance spectrometer (Bruker BioSpin, Billerica, MA, USA). Images were acquired using a Bruker Micro 5 imaging probe with triple axis gradients (maximum strength 200 G/cm) and a 10 mm diameter RF saddle coil. Each specimen received T1, T2 and

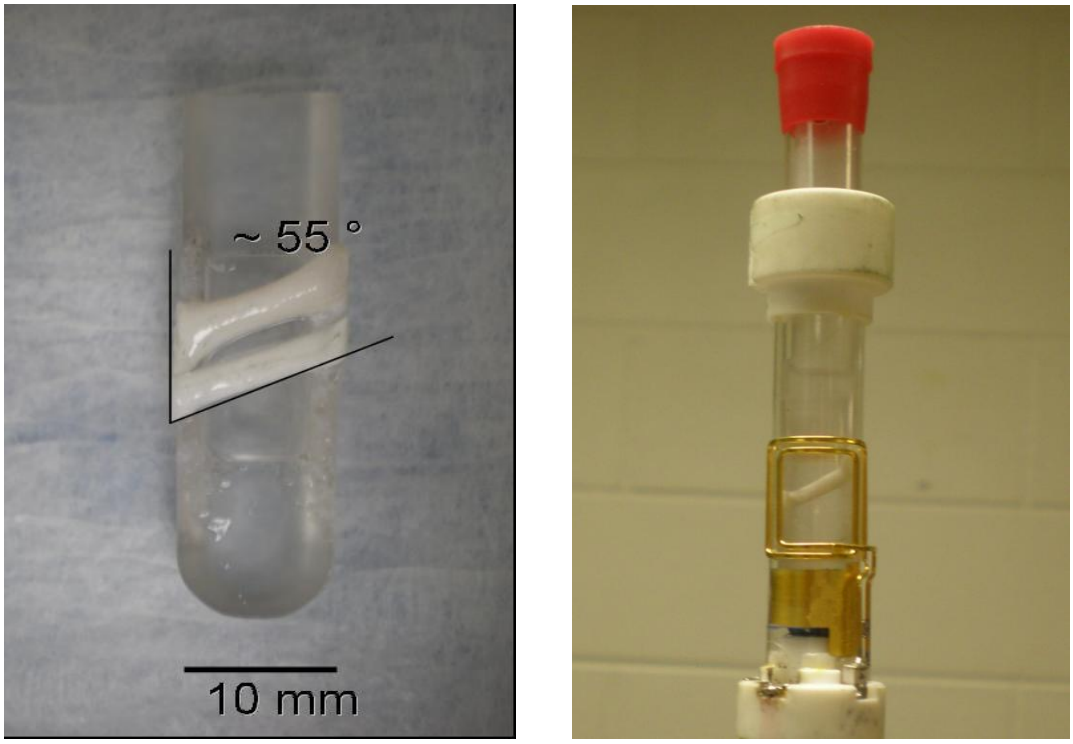

Figure 4.1: (a) Custom made tissue holder with two rabbit Semitendinous tendons superglued at an angle of 55° (magic angle) to B0 field. (b) Specimen holder with a tendon placed in the NMR tube which is placed in the 10 mm Micro5 imaging probe.

diffusion tensor weighted sequences. DTI was performed using a 3D spin echo DTI sequence (for both MCLs and SemiTs: TR = 1s, TE = 15 ms, δ/Δ = 2/8 ms, NEX = 1, FOV = 9.6 x 3.2 mm, six diffusion directions, 200 µm thick axial slices, b= 600 s/mm^2, in-plane resolution= 50 µm, scan time= 2 hrs/sample). T1 was measured using a saturation recovery spin echo sequence in 12 steps with TRs from 105 to 5000 ms (TE =

8 ms, slice thickness = 200 µm). T2 was measured using a CPMG spin echo sequence with 16 echoes and 5.3 ms echo spacing (TR = 3 s, slice thickness = 200 µm).

Fractional anisotropy (FA), mean diffusivity (MD), axial diffusivity (AD) and radial diffusivity (RD) results were obtained from the experimental data using custom written MAS software (Mareci Research Group, University of Florida, Gainesville, Florida) which are defined by the following equations:

$$MD = \langle \lambda \rangle = \frac{\lambda_1 + \lambda_2 + \lambda_3}{3}$$

$$AD = \lambda_1$$

$$RD = \frac{\lambda_2 + \lambda_3}{2}$$

$$FA = \sqrt{\frac{3}{2}} \sqrt{\frac{(\lambda_1 - \langle \lambda \rangle)^2 + (\lambda_2 - \langle \lambda \rangle)^2 + (\lambda_3 - \langle \lambda \rangle)^2}{\lambda_1^2 + \lambda_2^2 + \lambda_3^2}}$$

where λ_1, λ_2, λ_3 are the eigenvalues of the primary, secondary and tertiary eigenvectors generated from the diffusion weighted images. λ_1 corresponds to primary diffusion direction described by the primary eigenvector denoted as axial diffusivity. λ_2 and λ_3 represent the other two orthogonal diffusion directions perpendicular to the primary diffusion direction and their average is denoted by radial diffusivity. These values were computed from the ROIs drawn on the central slice of the image data acquisition set for each tissue. The signal-to-noise ratio (SNR) was calculated as the mean signal intensity of the ROIs (ROI 1) divided by the standard deviation (SD) of the background noise (ROI 2) as shown in Figure 4.2.

(a)

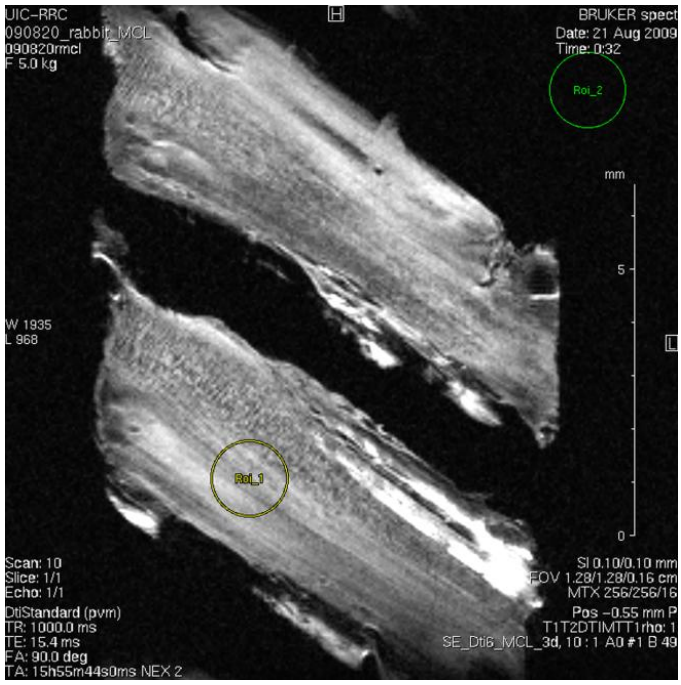

(b)

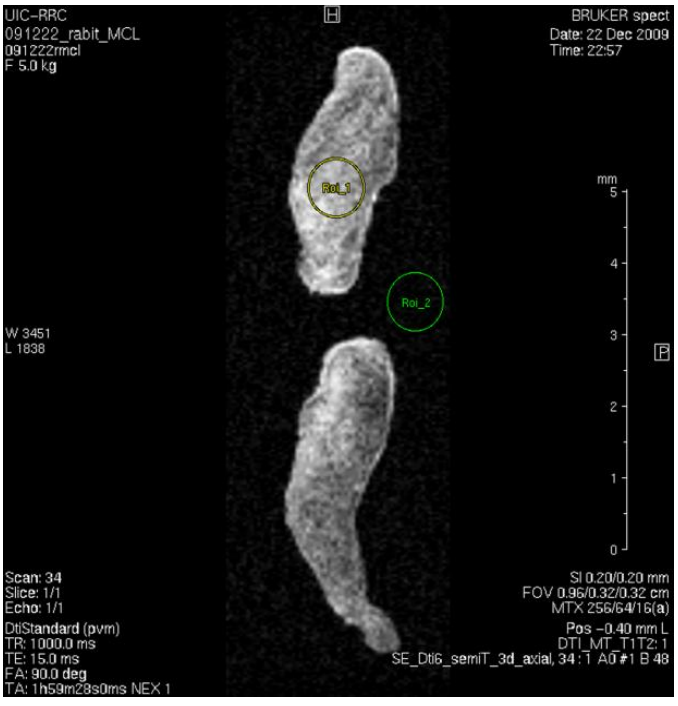

Figure 4.2: Coronal(a) and axial(b) view of Diffusion weighted images of two Rabbit Medial Collateral Ligaments showing ROIs for SNR calculation. SNR was caluclated as the mean of the signal divided by the standard deviation of the background noise.

FA is a scalar metric that describes the directionality of the diffusion tensor and has values ranging between 0 (isotropic) and 1 (anisotropic). MD is a non-directional measure of free translational diffusion and provides an index of general tissue integrity. Axial and Radial diffusivity represent the diffusive transport along the long axis and perpendicular to the long axes of the fiber respectively.

DTI-Studio version 3.0.1 (John Hopkins University, Baltimore, MD, USA) was used to generate collagen fiber tracts for both types of tissues using the Fiber Assignment by Continuous Tracking (FACT) algorithm.Tracking of fibers started when the fractional anisotropy (FA) threshold was above 0.15 and the fiber angulation exceeded 50°. Tractographic analysis of DTI data is based on the assumption that the primary eigenvector of the diffusion tensor coincides with the local fiber orientation.

The average T1 and T2 relaxation times for the six SemiT and six MCL samples studied are presented in Table 4.1. Figure 4.3 shows a T2 weighted image and a T2 map of an axial slice of two semitendinosus tendons.

Tissue	**T1 (ms)**	**T2 (ms)**
SemiT (n=6)	1350 ± 84	33 ± 2
MCL (n=6)	1259 ± 80	37 ± 6

Table 4.1: T1 and T2 relaxation times for the two types of tissues.

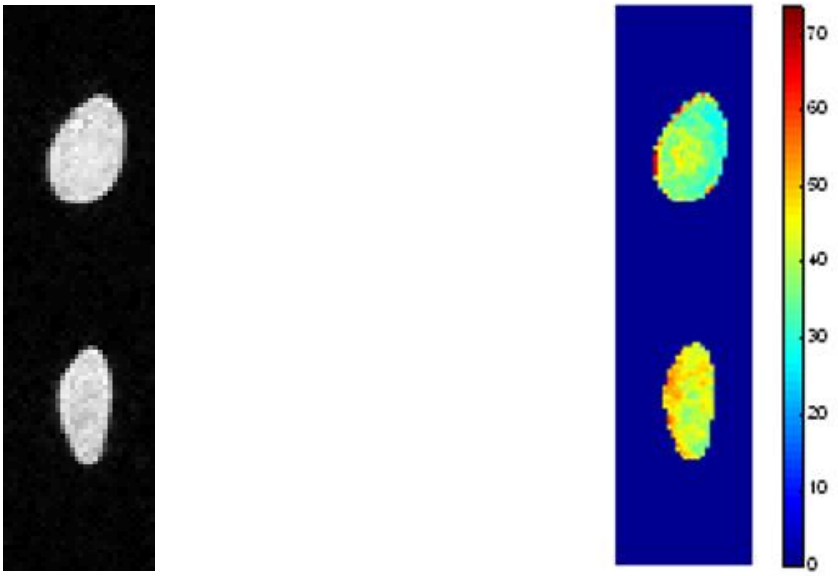

(a) **(b)**

Figure 4.3: Axial T2 weighted image of two Semitendinosus tendons (b) T2 map of the same slice of two Semitendinosus tendons.

Fractional Anisotropy, Mean Diffusivity, Axial diffusivity and Radial diffusivity results for the six semiTs and six MCLs are presented in Tables 4.2 and 4.3 respectively. Average FA and MD values for the six SemiTs were **0.67±0.18** and **1398.3±363.2 x10^{-6} mm^2/s** respectively, and corresponding values for the six MCLs were **0.66 ± 0.17** and **1423.3 ±378.3x10^{-6} mm^2/s** respectively. Average AD and RD values for the six SemiTs were **2623.3± 779.1 x10^{-6} mm^2/s** and **786±331.9 x10^{-6} mm^2/s** respectively and these values for six MCls were **2666.7±824.4 x10^{-6} mm^2/s and 800±333.4 x10^{-6} mm^2/s** respectively. ROIs drawn on the middle slice represented an average number of voxels of **609±84** for SemiTs and **898±250** for MCLs. Signal-to-noise ratio (SNR) for the diffusion weighted images was 20.

Color coded primary eigenvector maps of coronal and axial slices were obtained to determine the direction of the fibers. Combination of blue and red colors on the coronal

image and green on the axial image confirmed the predominant fiber orientations (Figure 4.4). Coronal slices of diffusion weighted images (Figure 4.5 a) of the ligaments show parallel collagen fiber bundles running along the major axis of the tissue. This is supported by the 3D tractography image showing the spatial distribution and orientation of individual fiber tracts in the tissue (similar in both SemiTs and MCLs) (Figure 4.5b). Histological evaluation of tissues was performed by processing a semitendinosus tendon for paraffin embedding, followed by sectioning it longitudinally and staining with Toluidine Blue. Figure 4.7 shows coronal histological sections of a Rabbit semitendinosus tendon taken after the DTI scan with a 100x magnification and a 200x magnification.

Another visualization tool to view the DTI metrics in a slice is though the use of glyphs. In a glyph visualization (Figure 4.6) each voxel is overlaid with a diffusion ellipsoid, the shape of which indicates the direction of primary eigenvector for each voxel, in other words gyphs show the general direction of diffusion in each voxel.

The above FA, MD, AD and RD results showed excellent repeatability among both types of tissues, and imaging results confirm the known microstructural organization of collagen bundles in tendons and ligaments.

Sample#	FA	MD ($x10^{-6}$ mm^2/s)	AD ($x10^{-6}$ mm^2/s)	RD ($x10^{-6}$ mm^2/s)
1	0.63±0.17	1490±339	2680±755	889±311
2	0.61±0.16	1540±343	2730±744	942±290
3	0.67±0.18	1370±342	2600±786	761±311
4	0.68±0.17	1290±336	2480±744	701±297
5	0.73±0.19	1320± 403	2610±849	670±368
6	0.68±0.17	1380±345	2640±768	753±320
Avg±SD	**0.67±0.18**	**1398.3±363.2**	**2623.3±779.1**	**786±331.9**

Table 4.2: FA, MD, AD and RD values (mean ± SD) from six rabbit Semitendinosus tendons. Average number of voxels were 690± 84.

Sample#	FA	MD ($x10^{-6}$ mm^2/s)	AD ($x10^{-6}$ mm^2/s)	RD ($x10^{-6}$ mm^2/s)
1	0.67±0.17	1370±329	2590±734	767±302
2	0.67±0.16	1550±383	2920±819	862±326
3	0.64±0.17	1360±326	2470±706	805±287
4	0.69±0.19	1510±464	2940±1030	789±396
5	0.62±0.15	1420±294	2550±665	847±270
6	0.67±0.18	1330±396	2530±807	730±381
Avg±SD	**0.66±0.17**	**1423.3 ± 378.3**	**2666.7±824.4**	**800±333.4**

Table 4.3: FA , MD, AD and RD values (mean ± SD) from six rabbit Medial Collateral Ligaments. Average number of voxels were 898± 250.

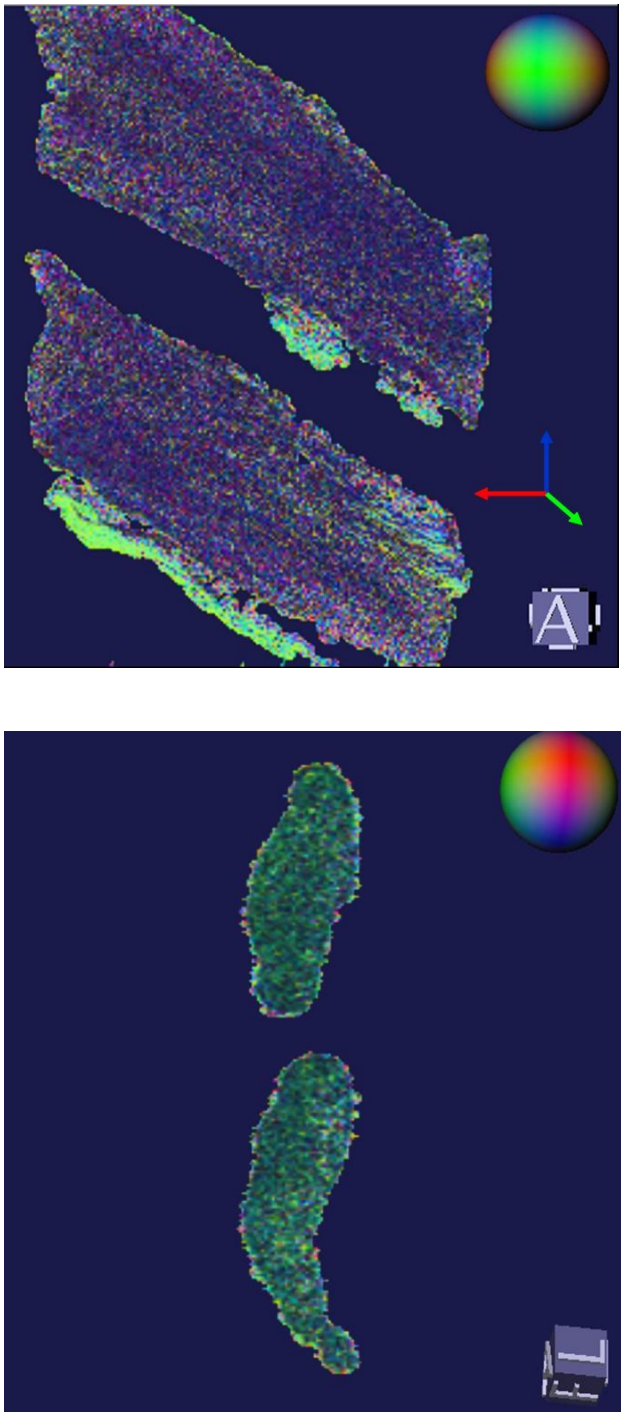

Figure 4.4: Color coded eigenvector map of a slice showing the direction of the fibers. (a) Combination of blue and red colors in the coronal view confirms the predominant fiber orientations. (b) Green color in the axial view shows the primary direction of the fibers to be out-of-the plane of paper.

(a)

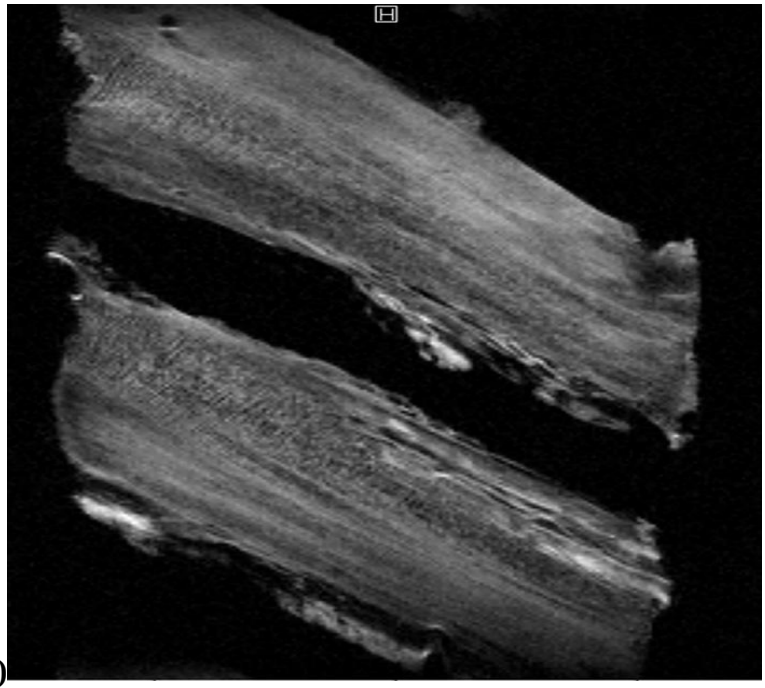

(b)

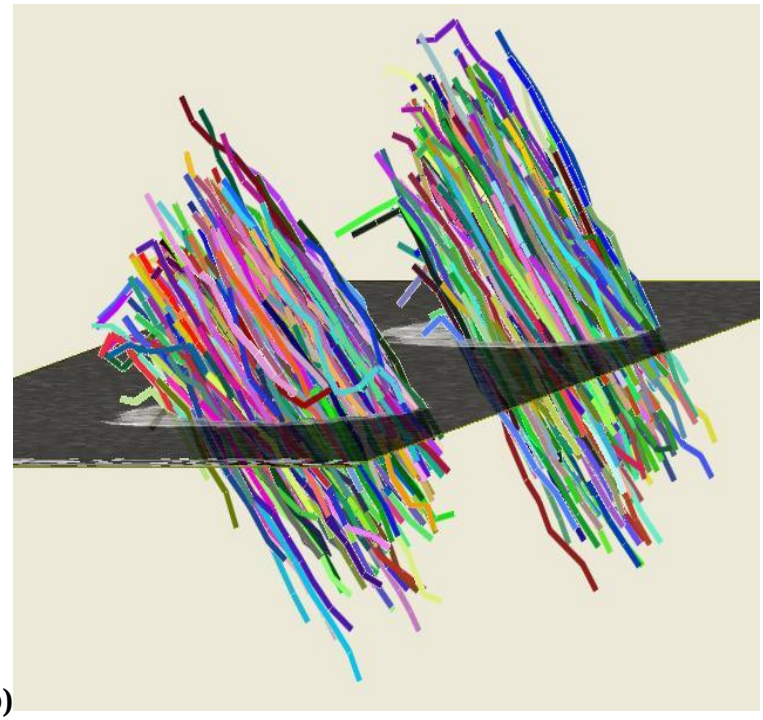

Figure 4.5: (a) DTI image of two rabbit MCLs scanned at magic angle. (b) Tractography showing collagen fiber tracts of two semitendinosus tendons generated using FACT algorithm from DTI Studio.

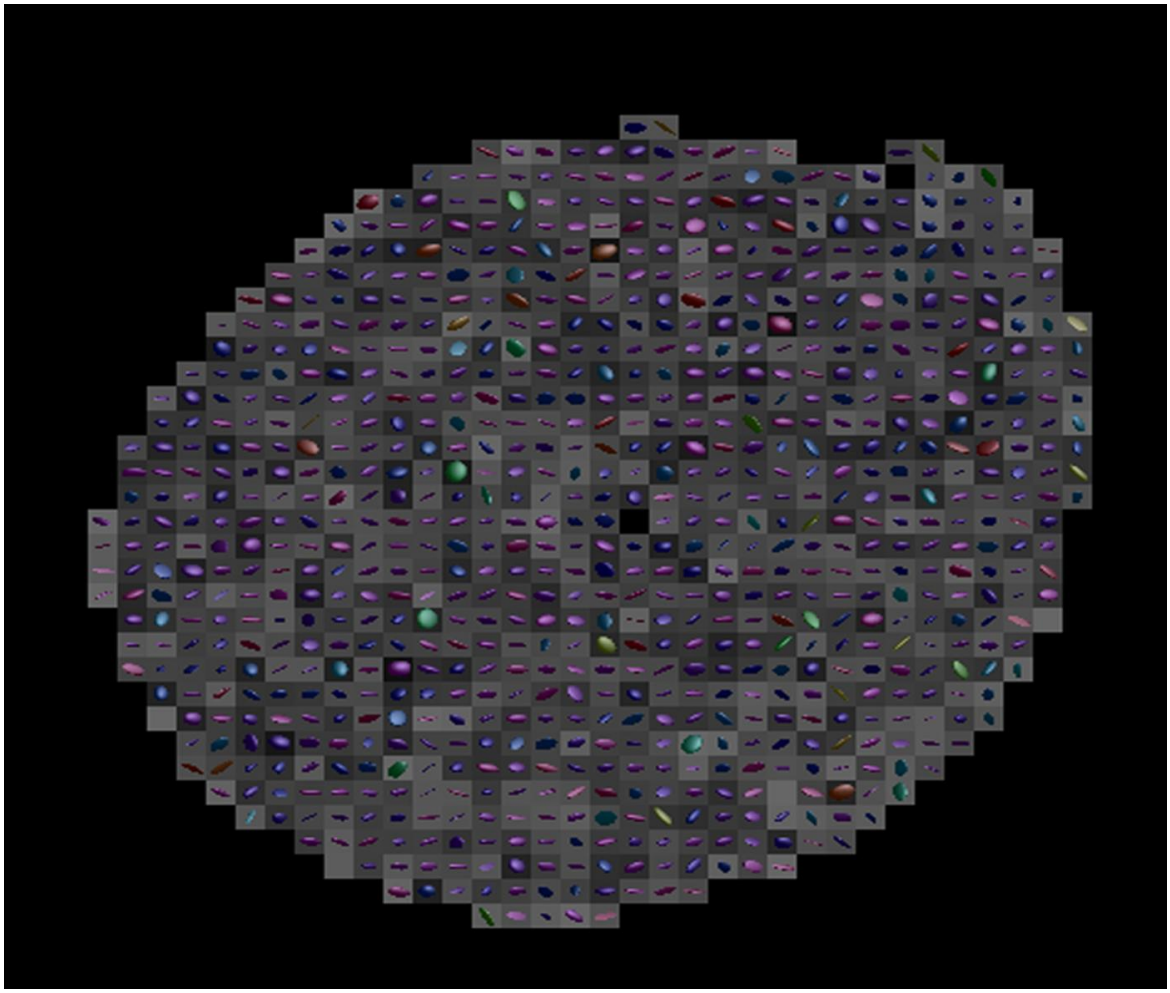

Figure 4.6: Glyph Visualization: Each Voxel in this axial slice of a semitendinosus tendon is overlaid with a diffusion ellipsoid, the shape of which indicates the direction of primary eigenvector for each voxel (Image produced using the MAS software developed by Mareci Research Group, University of Florida, Gainesville, Florida).

(a)

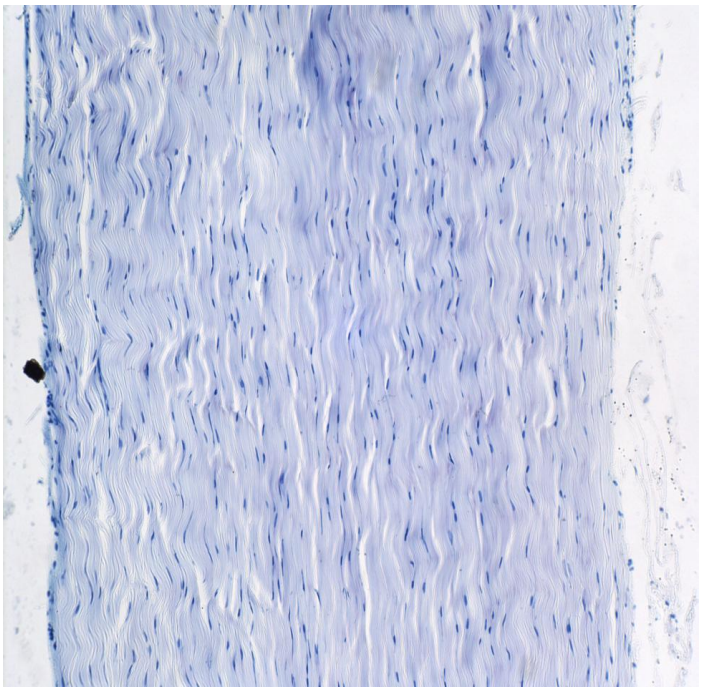

(b)

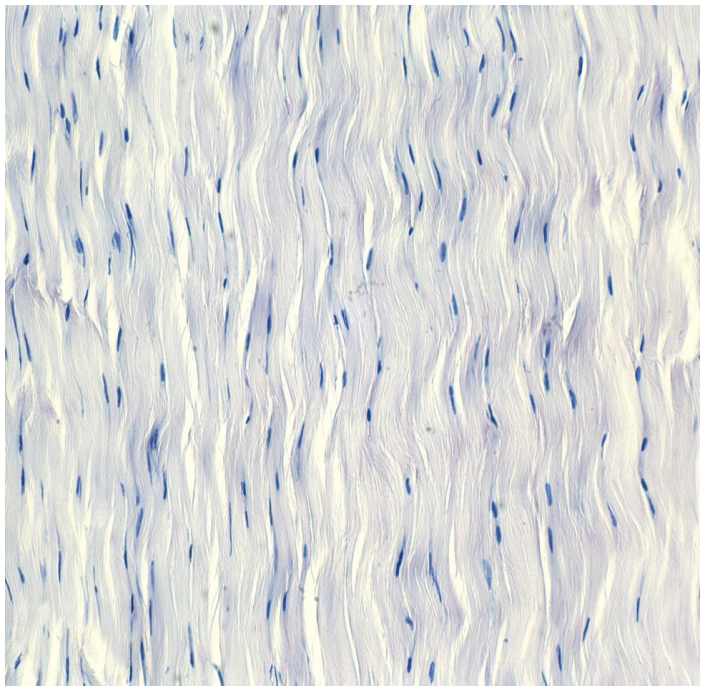

Figure 4.7: Coronal histological section of a Rabbit semitendinosus tendon taken after the DTI scan. (Tol Blue stain) (a) 100x magnification (b) 200x magnification.

4.2 Water content measurements for both MCLs and SemiTs.

As Semitendinosus tendons and Medial collateral ligaments showed similar diffusional anisotropy and mean diffusivity, we studied other physical and mechanical properties of these tissues to look for differences between these two tissues for any of these properties. In particular water content was measured and structural properties for both tissue types were computed by mechanically loading these tissues to failure.

Water content measurements were carried out using a speedvac to remove the water from the tissues. The wet weight and dry weight was measured for 4 semiTs and 4 MCLs. Empty eppendorf tubes were weighed, fresh tissues were then placed in the tubes and weighed again. The tubes with their tops open were then placed in a speed-vac for about an hour. Tubes were weighed, put back into the speedvac for another hour and weighed again. This was continued until consistent values were obtained. Table 4.4a and b show the water content measurements from MCls and SemiTs respectively. Mean water content was 69.5 ± 0.5% for the MCLs and 67± 4.9% for the semiTs.

Sample#	**Wet Weight (g)**	**Dry Weight(g)**	**Wet - Dry**	**% Difference**
1	0.0745	0.0228	0.0517	69.40
2	0.0672	0.0209	0.0463	68.90
3	0.0583	0.0178	0.0405	69.47
4	0.0515	0.0154	0.0361	70.10
Avg.	**0.062875**	**0.019225**	**0.04365**	**69.47**
S.D	**0.0101**	**0.0033**	**0.0068**	**0.49**

Table 4.4(a): Water content measurements from 4 MCLs.

Sample#	Wet Weight (g)	Dry Weight(g)	Wet - Dry	% Difference
1	0.1354	0.0546	0.0808	59.68
2	0.1448	0.0429	0.1019	70.37
3	0.0307	0.0096	0.0211	68.73
4	0.0345	0.0107	0.0238	68.99
Avg.	**0.08635**	**0.02945**	**0.0569**	**66.94**
S.D	**0.0622**	**0.0228**	**0.0407**	**4.90**

Table 4.4(b): Water content measurements from 4 SemiTs.

4.3 Determination of mechanical properties for MCLs and SemiTs.

To study mechanical properties, 7 MCLs and 7 SemiTs were pulled to failure using a electromechanical material testing system (MTS Insight 5). The tendon was secured in custom made grips (with sandpaper gluedinside the clamps to minimize slippage) at both ends; the upper grip attached to a 1000N load cell while lower grip was secured to the MTS base (Figure 5.8). Following an application of a preload of about 5 N, the tendons were loaded to failure at 0.1mm/sec. Maximum load, extension to maxium load and linear stiffness were calculated from the load-deformation curves obtained. Linear stiffness was computed as the steepest slope spanning 40% of the linear region of the load-deformation curve. Table 5.5 (a) and (b) show the maximum load, extension to maximum load and linear stiffness results from the MCLs and SemiTs respectively. The average maximum load to failure for the 7 MCLs was 94.8±26.2 N and 82.5±33.3 N for

the semiTs. Average linear stiffness for the 7 MCLs was 36.8±7.6 N/mm and 32.7±10.4 N/mm for the semiTs.

Sample #	Maximum Load (N)	Extension to maximum load (mm)	Linear Stiffness (N/mm)
1	84.4	3.5	33.7
2	89.2	4.9	27.5
3	111.7	3.5	41.4
4	48.4	2.2	27.3
5	92.9	3	38.1
6	132.5	3.5	46.5
7	104.7	2.9	43.1
Avg.	**94.8**	**3.4**	**36.80**
S.D	**26.2**	**0.82**	**7.6**

Table 4.5 (a): Maximum load, extension to maximum load and linear stiffness results from the 7 MCLs tested to failure.

Sample #	Maximum Load (N)	Extension to maximum load (mm)	Linear Stiffness (N/mm)
1	62.7	3.3	23
2	68.1	3.4	24.5
3	109.6	3.5	37
4	112.2	3.4	45.5
5	57.9	3.7	23.1
6	39.7	1.7	29.4
7	127.2	3.4	46.9
Avg.	**82.5**	**3.2**	**32.7**
S.D	**33.3**	**0.66**	**10.4**

Table 4.5 (b): Maximum load, extension to maximum load and linear stiffness results from the 7 SemiTs tested to failure.

(a)

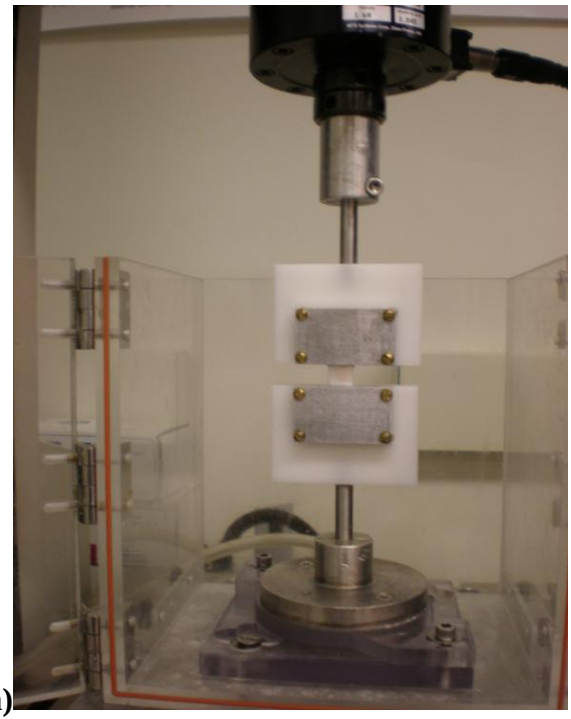

(b)

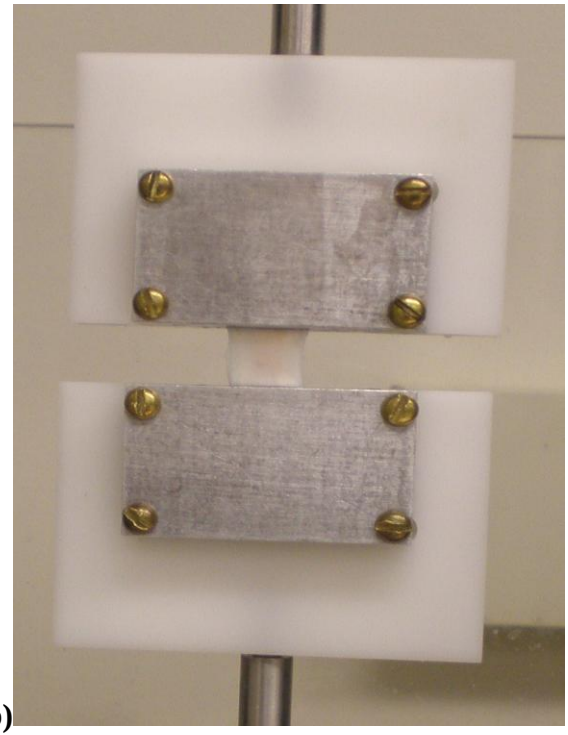

Figure 4.8: Experimental setup for failure tests. (a) Complete setup showing the load-cell and the tissue grips attached to the load cell and secured to the base of the MTS (b) Closeup view of the tendon held in the grips.

4.4 Assessment of Regional variation and determine inter slice variability in FA and MD of the two tissue types.

To further characterize these tissues and investigate potential regional differences in the DTI metrics within each tissue type as well as across the two tissue types, FA, MD, and the three eigenvalues were analyzed across the central nine slices for each of the six semitendinosus tendons and six medial collateral ligaments. First four and the last three slices were excluded from the analysis because of partial volume effects and low SNRs. Frequency distribution graphs (histograms) for 54 slices (6 samples with 9 slices each) for each tissue type are shown in figure 4.9 (a-j). All the analysis were performed using SPSS (SPSS inc., Version 10.0).

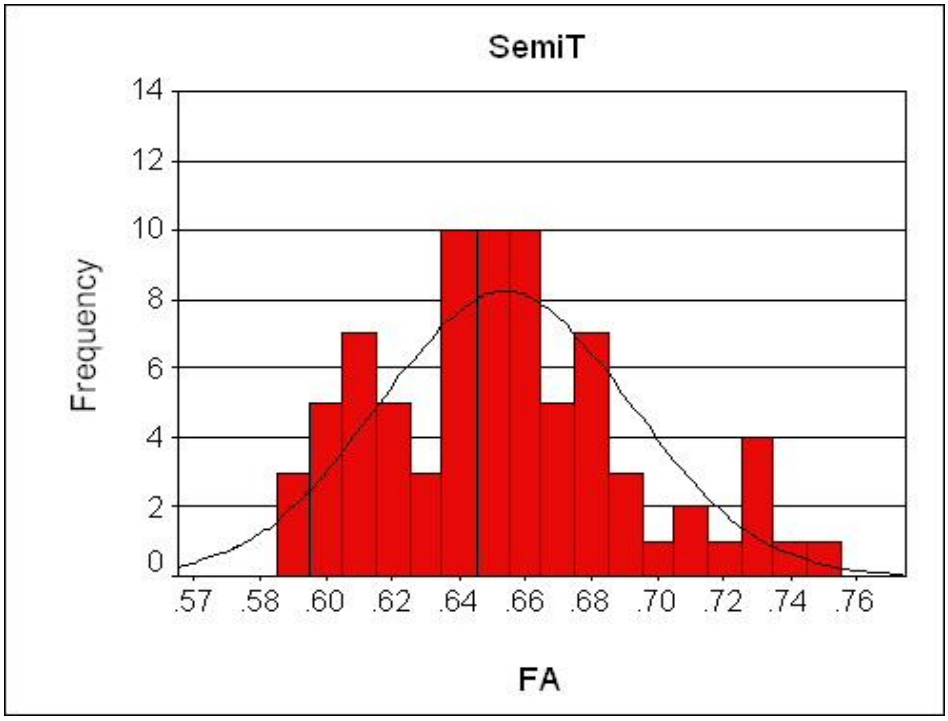

Figure 4.9(a): Frequency distribution of Fractional Anisotropy of six semitendinosus tendons for central nine slices.

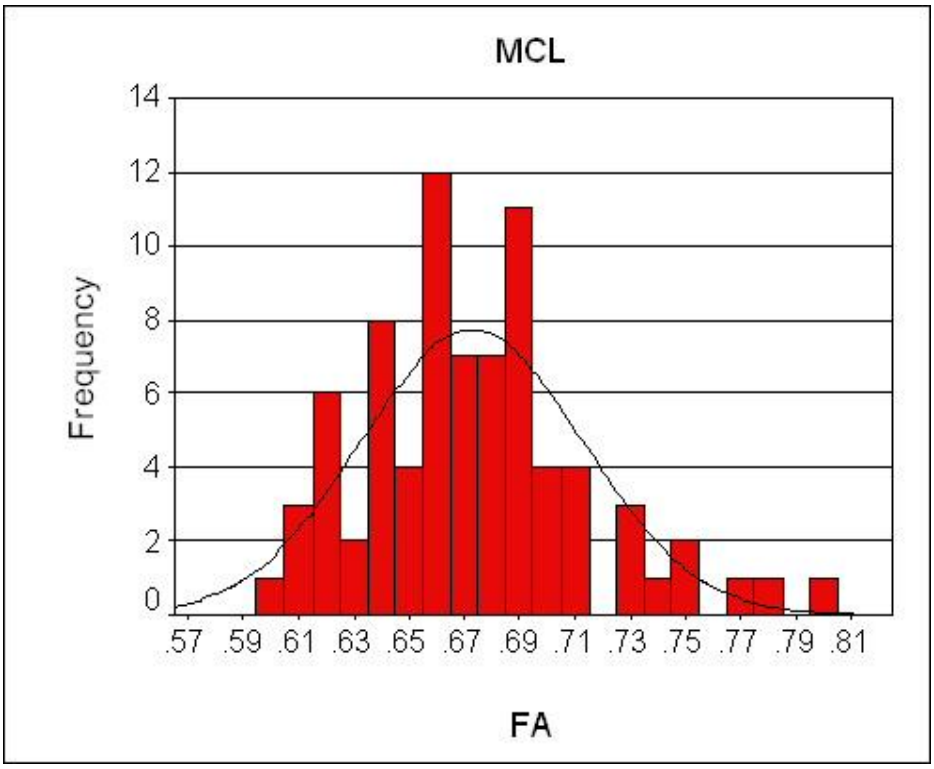

Figure 4.9(b): Frequency distribution of Fractional Anisotropy of six Medial collateral ligaments for central nine slices.

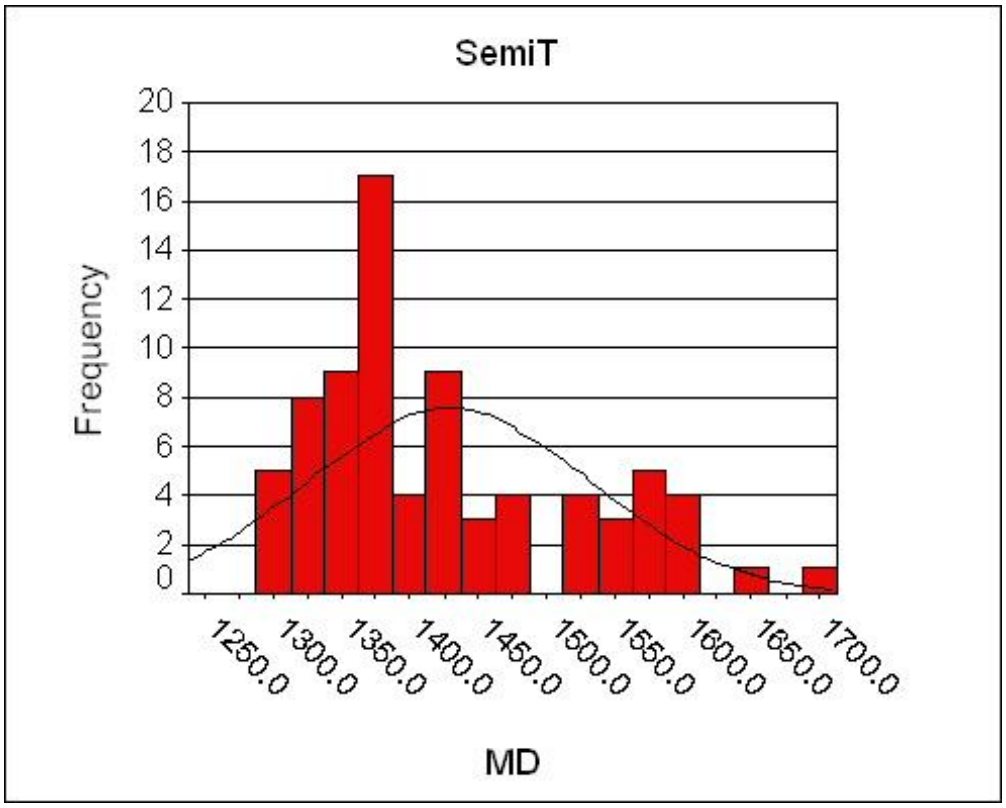

Figure 4.9(c): Frequency distribution of Mean Diffusivity of six semitendinosus tendons for central nine slices.

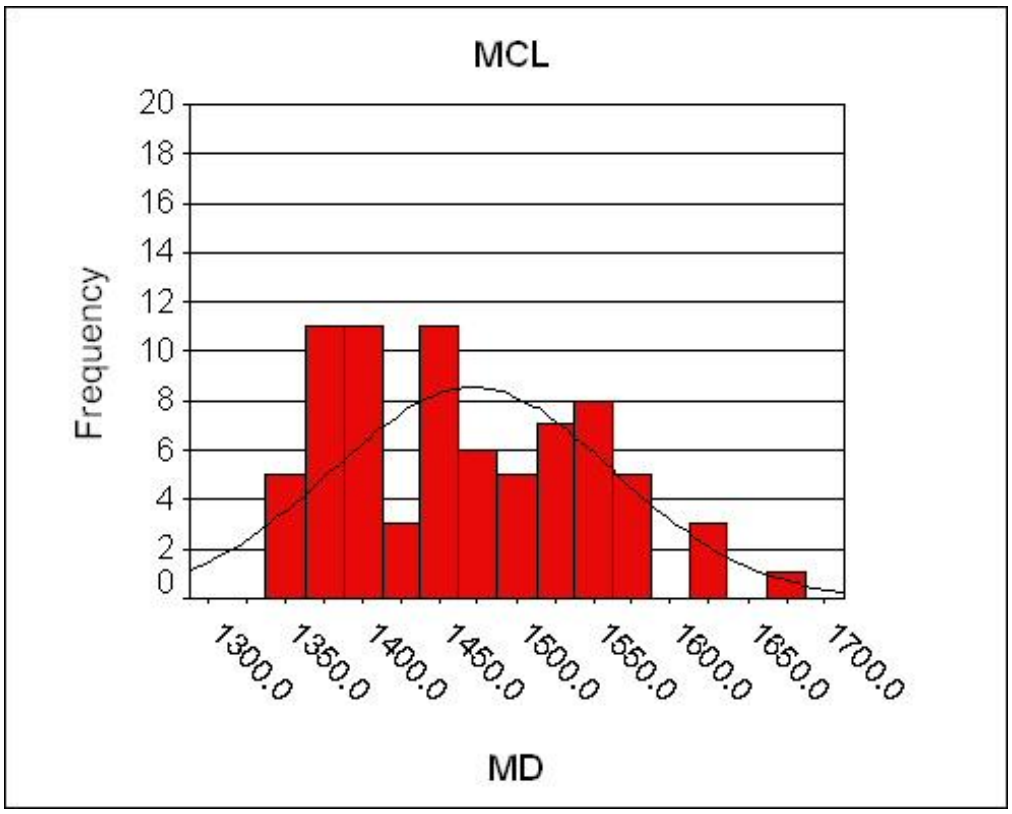

Figure 4.9(d): Frequency distribution of Mean diffusivity of six Medial collateral ligaments for central nine slices

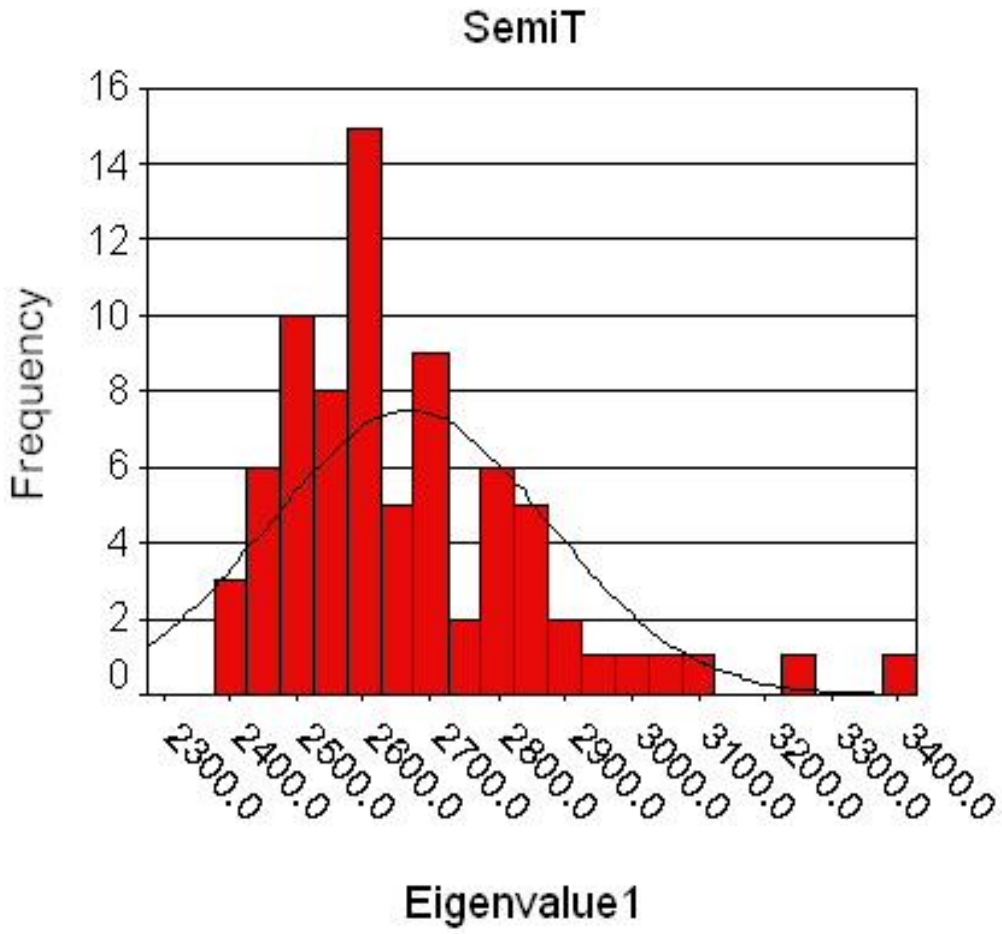

Figure 4.9(e): Frequency distribution of Eigenvalue1 (λ_1) of six semitendinosus tendons for central nine slices.

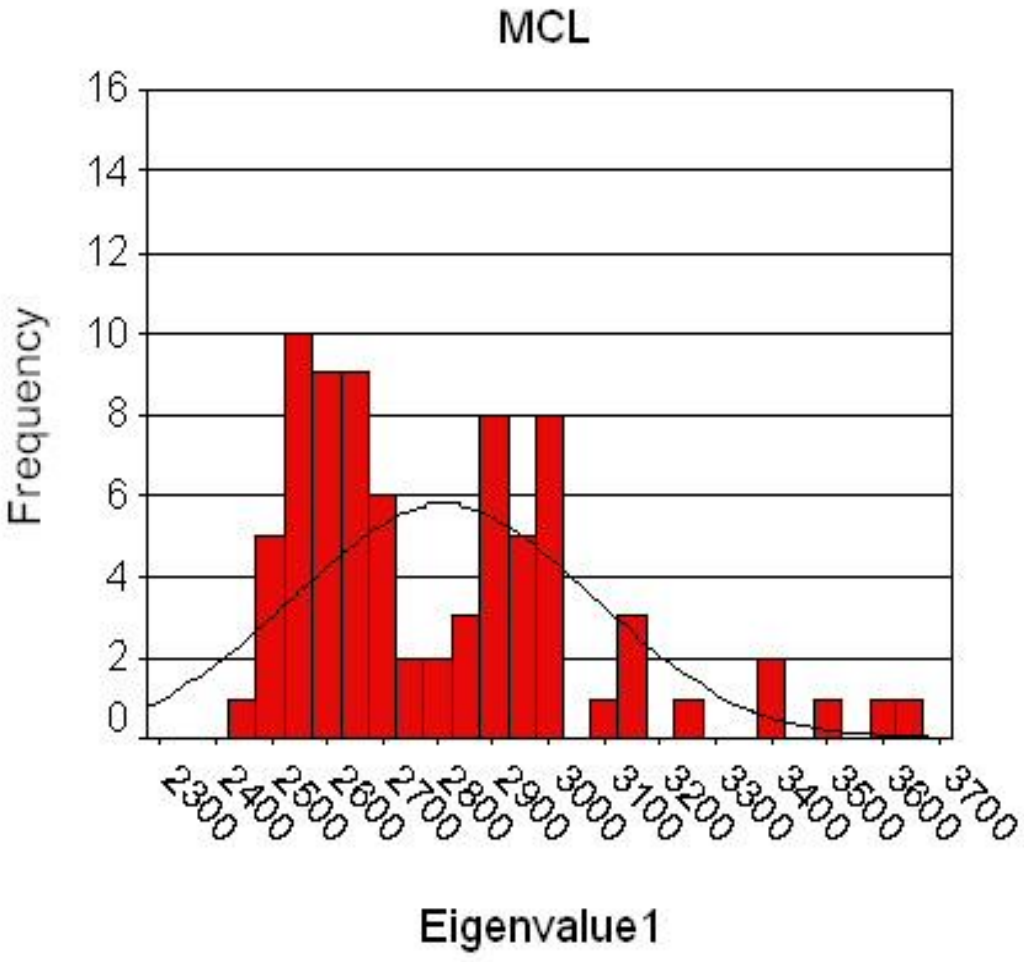

Figure 4.9(f): Frequency distribution of Eigenvalue1 (λ_1) of six Medial collateral ligaments for central nine slices.

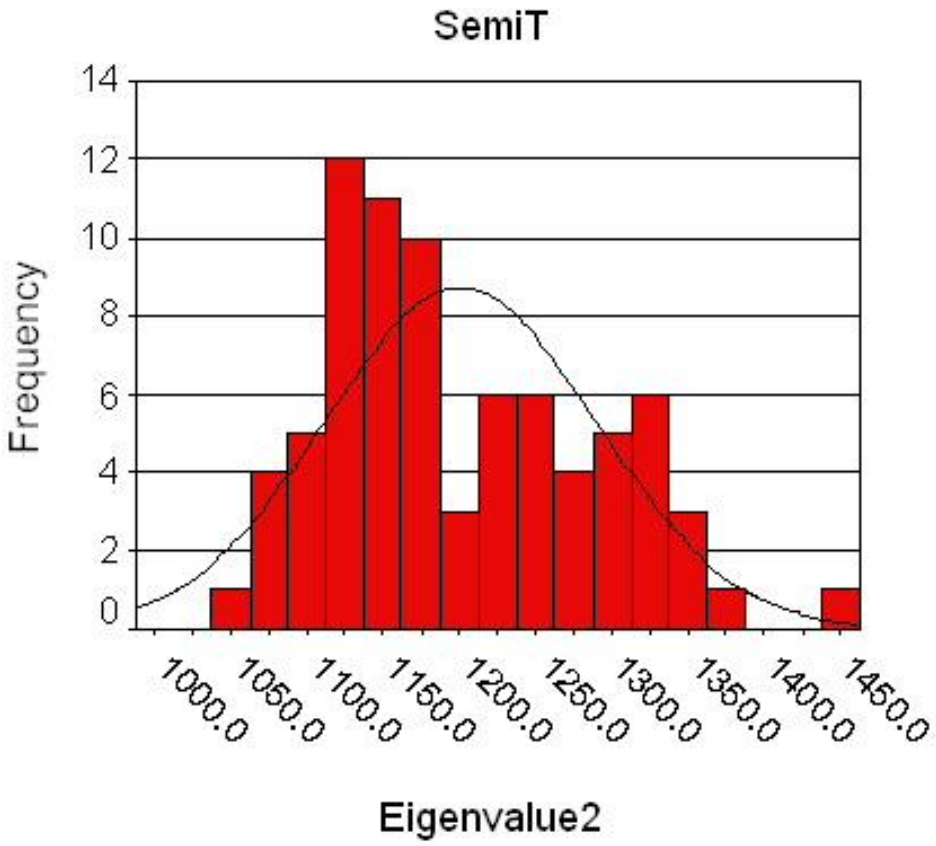

Figure 4.9(g): Frequency distribution of Eigenvalue2 (λ_2) of six semitendinosus tendons for central nine slices.

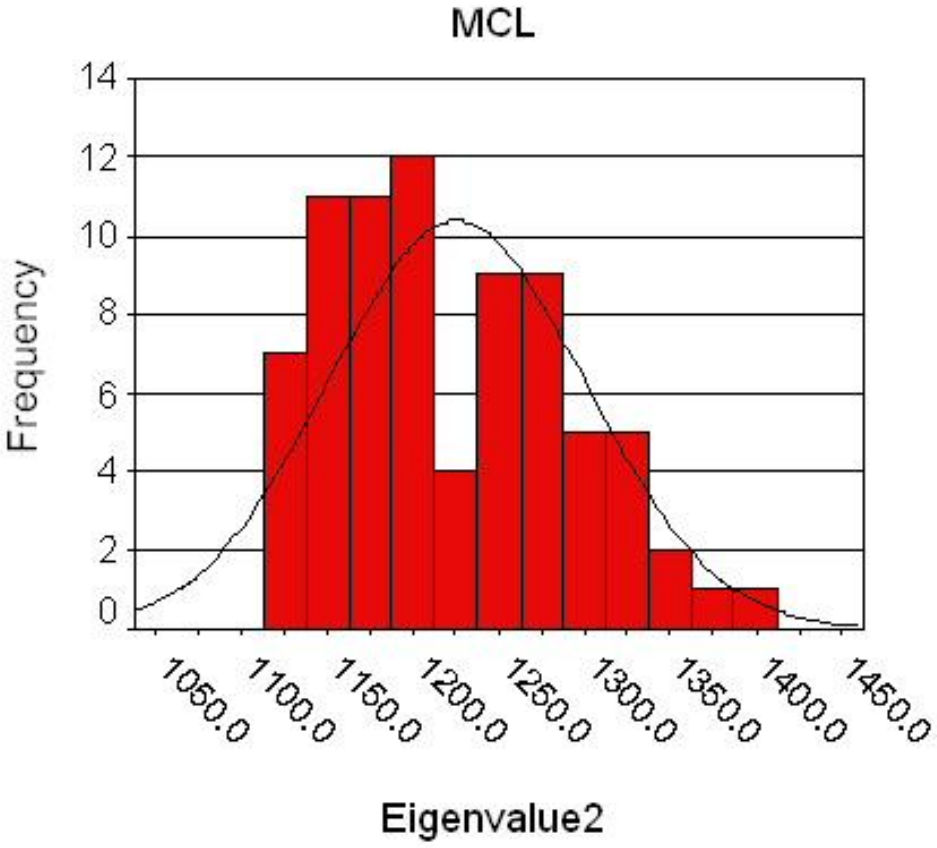

Figure 4.9(h): Frequency distribution of Eigenvalue2 (λ_2) of six Medial collateral ligaments for central nine slices.

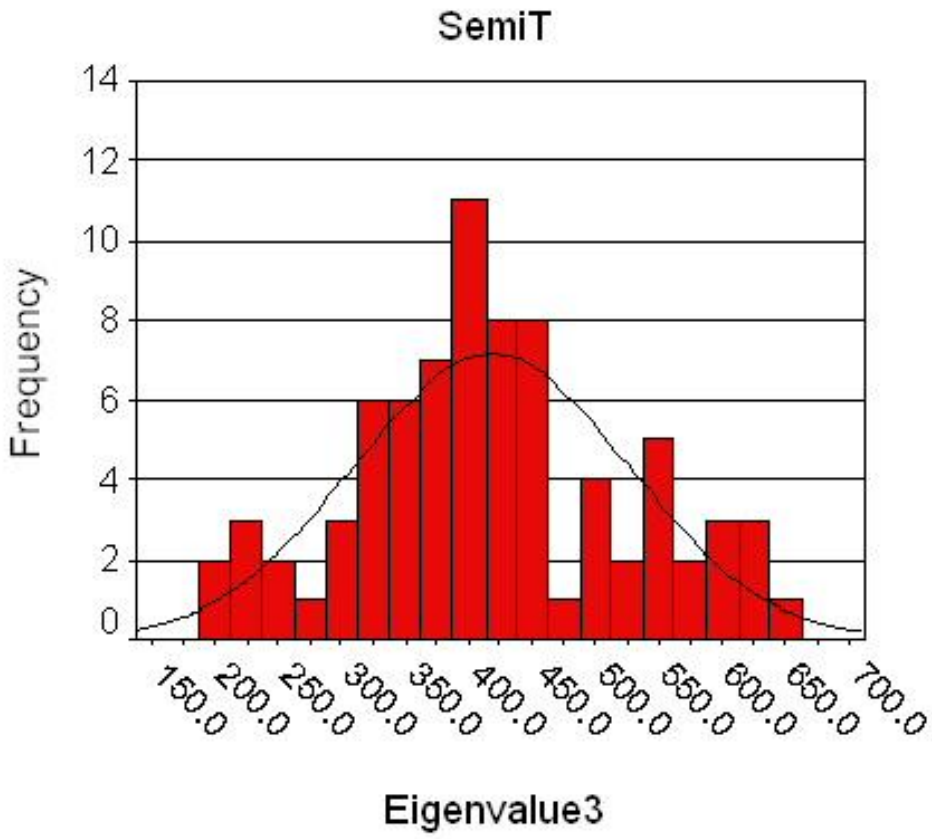

Figure 4.9(i): Frequency distribution of Eigenvalue3 (λ_3) of six semitendinosus tendons for central nine slices.

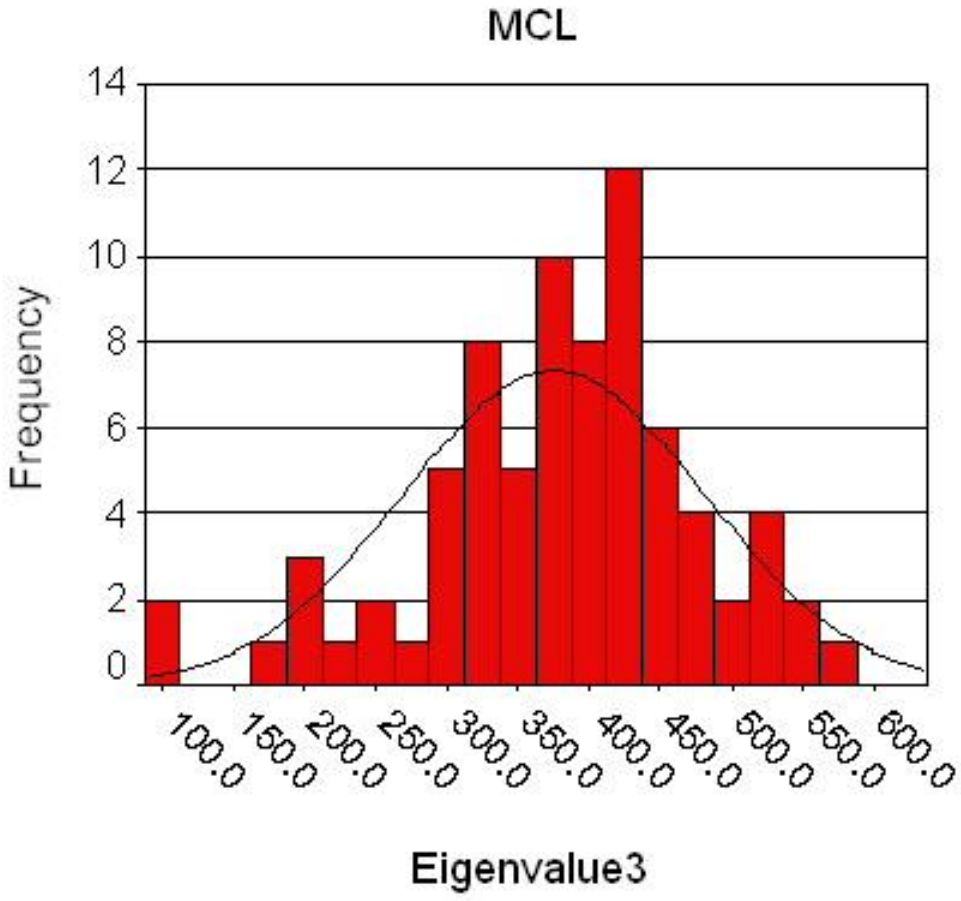

Figure 4.9(j): Frequency distribution of Eigenvalue3 (λ_3) of six Medial collateral ligaments for central nine slices

	DTI Metric	Number of observations	SemiT	MCL	Significance
1	FA	54 each	0.64 ± 0.03	0.66 ± 0.04	P=0.002
2	MD	54 each	1415.8 ± 91.8	1442.2 ± 69.9	P = 0.09
3	λ_1	54 each	2603± 124.8	2707.3 ± 174.2	P = 0.001
4	λ_2	54 each	1192.2 ± 81.7	1201.6± 58.6	P = 0.48
5	λ_3	54 each	452.3 ± 94.5	417.6 ± 66.8	P = 0.03

All MD, λ_1, λ_2, λ_3 values are X $10^{-6}mm^2/s$

Table 4.6: DTI metrics (mean± S.D) from central nine slices for all the six samples from the two tissue types. P-value reflect comparison of tissue types.

Frequency distributions from all the 54 observations for each of the DTI metrics (FA, MD, λ_1, λ_2, λ_3) was normally distributed for both tissue types which was confirmed from normality plots from each of the parameters. F- test (SPSS Inc., v 10.0) was used to compare the two tissue types statistically for all the DTI metrics. Significant differences were observed for FA, λ_1 and λ_3 between the two tissue types as shown in Table 4.6.

Within our design not only did we have tissue type but also slices and samples as independent statistical factors. Interaction of the tissue type with slices and samples was examined to further determine the effect of slices and samples on the tissue type difference finding. Univariate Anova was performed with tissue type as fixed effect and slice as random effect, and another set of univariate ANOVA analysis was performed with tissue type as the fixed effect and sample as random effect. Figure 4.10 (a-e) shows

the interactions of the tissuetypes with slices and figure 4.11(a-e) shows the interactions of the tissuetypes with samples.

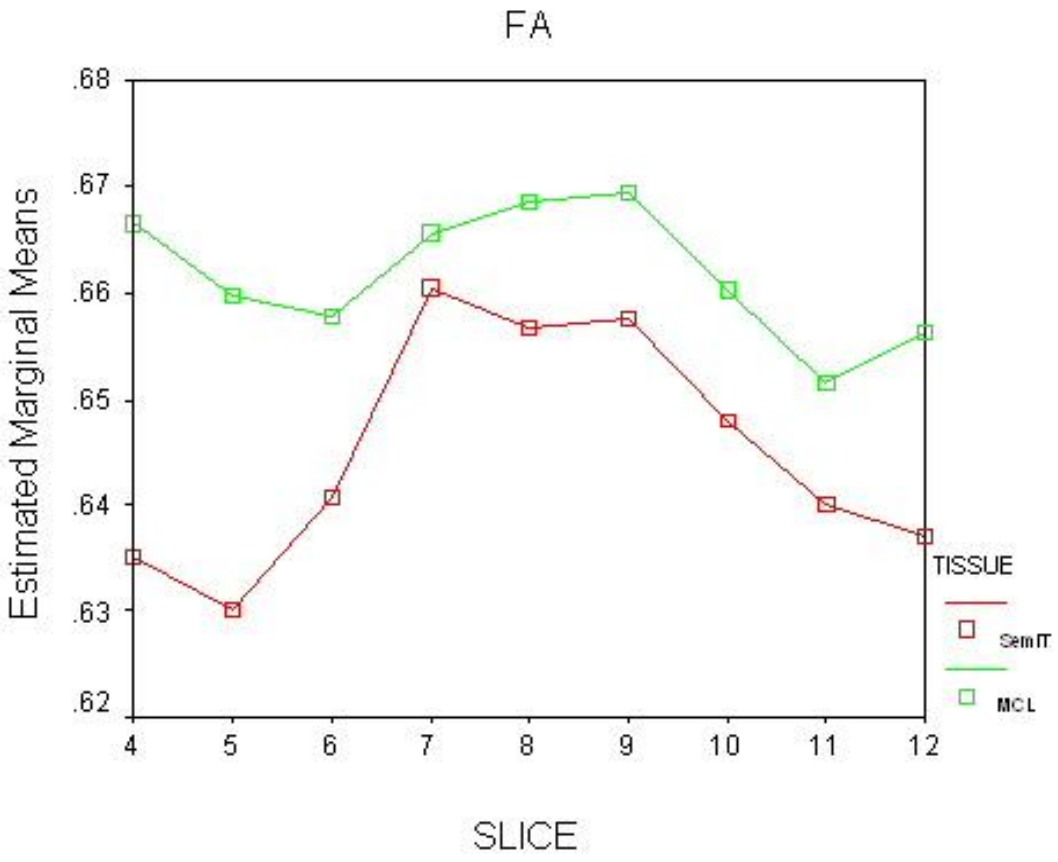

Figure 4.10 (a): Variation of Fractional Aniostropy for the central nine slices for both semitendinosus tendons and medial collateral ligaments. Tissue * slice: F (8,90)= 0.28, p = 0.96

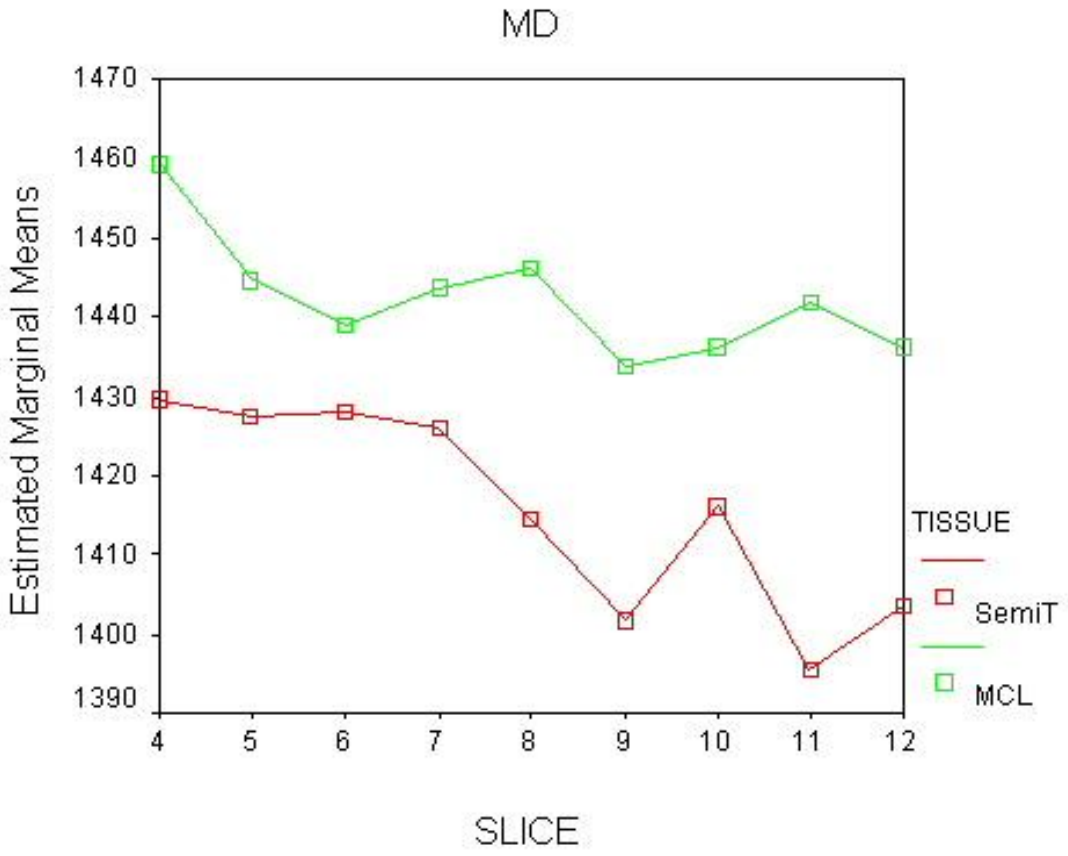

Figure 4.10 (b): Variation of Mean Diffusivity for the central nine slices for both semitendinosus tendons and medial collateral ligaments**.** Tissue * slice : F (8,90)= 0.046, p = 1.00

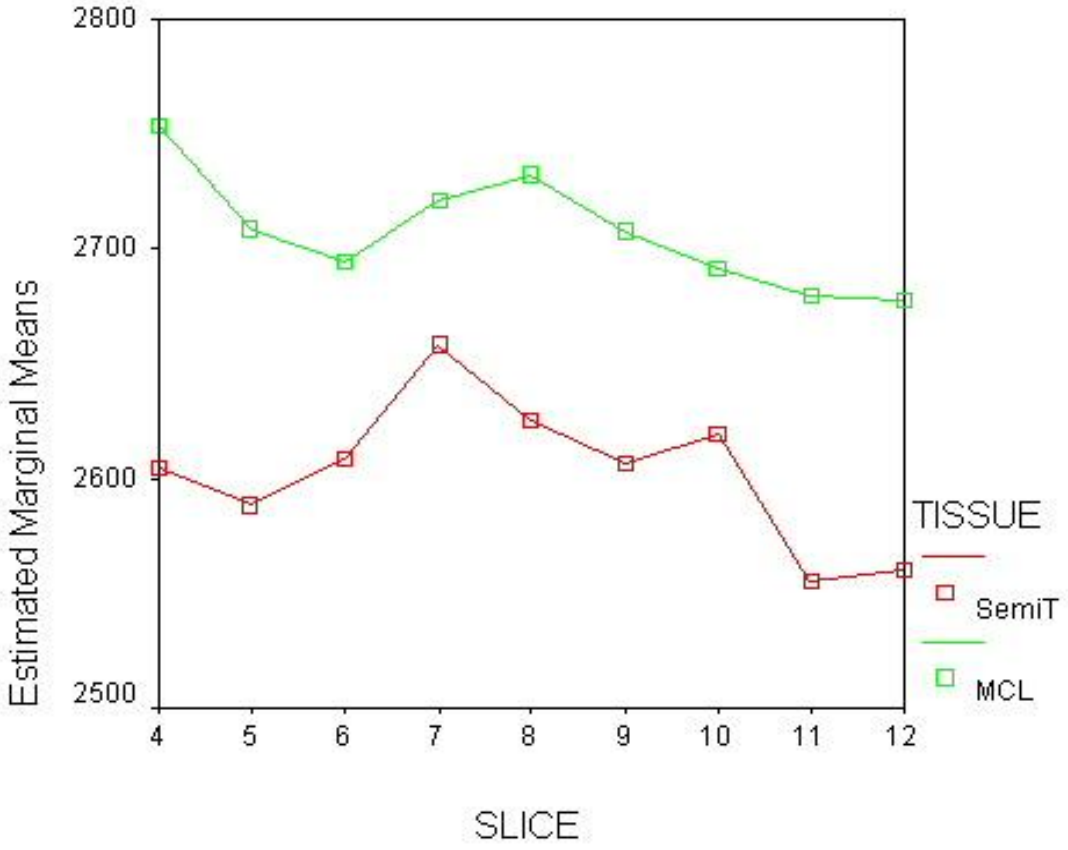

Figure 4.10 (c): Variation of Eigenvalue1 (λ_1) for the central nine slices for both semitendinosus tendons and medial collateral ligaments. Tissue * slice: F (8,90)= 0.087, p = 0.99

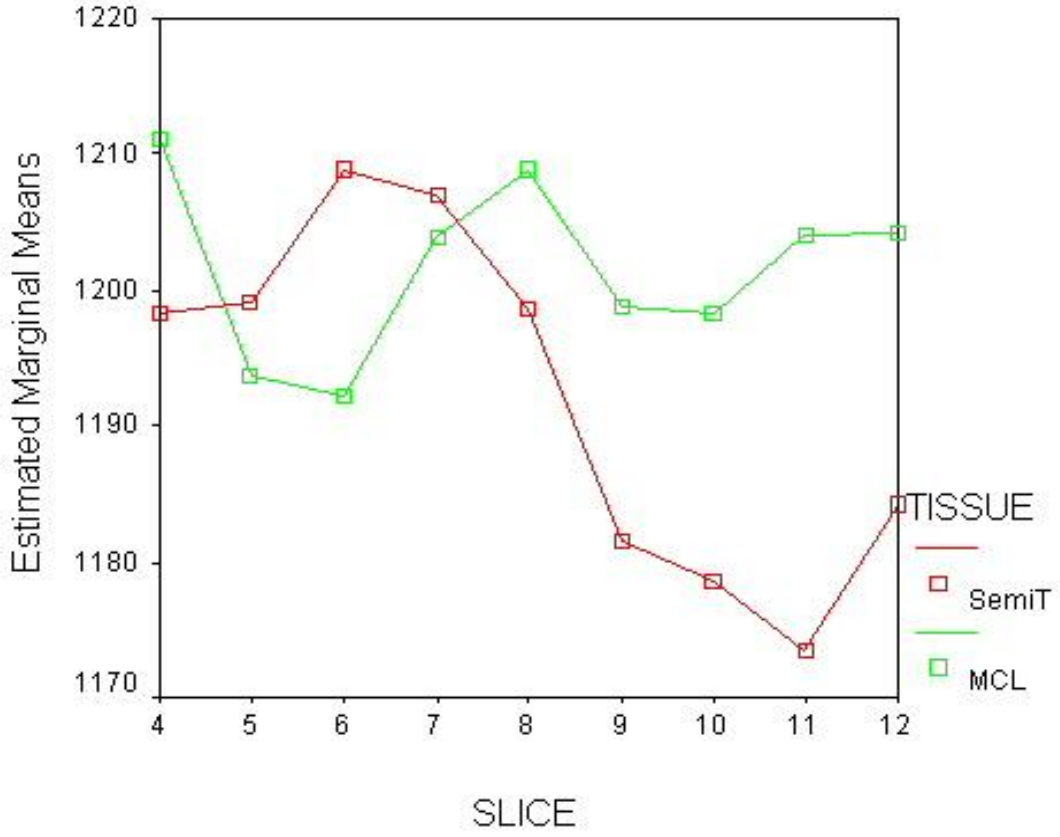

Figure 4.10 (d): Variation of Eigenvalue2 (λ2) for the central nine slices for both semitendinosus tendons and medial collateral ligaments. Tissue * slice : F(8,90)= 0.1, p = 0.99

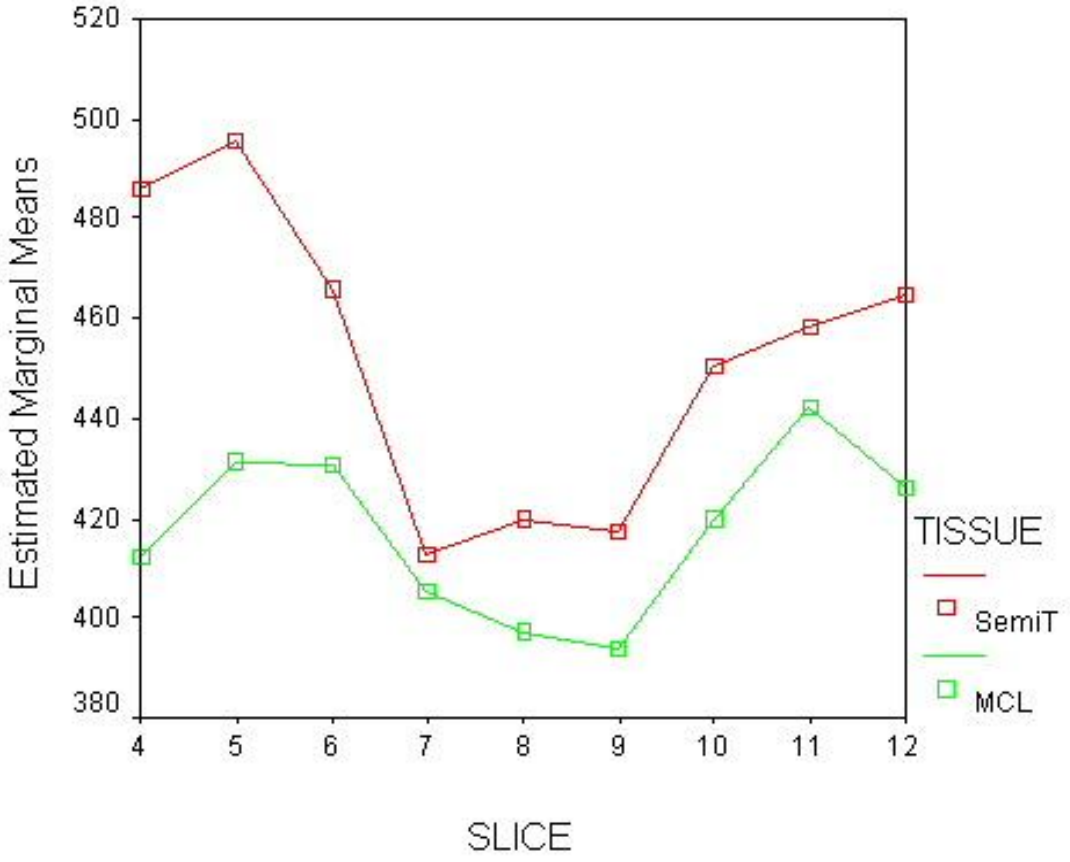

Figure 4.10 (e): Variation of Eigenvalue3 (λ_3) for the central nine slices for both semitendinosus tendons and medial collateral ligaments. Tissue * slice : F (8,90)= 0.19, p = 0.99

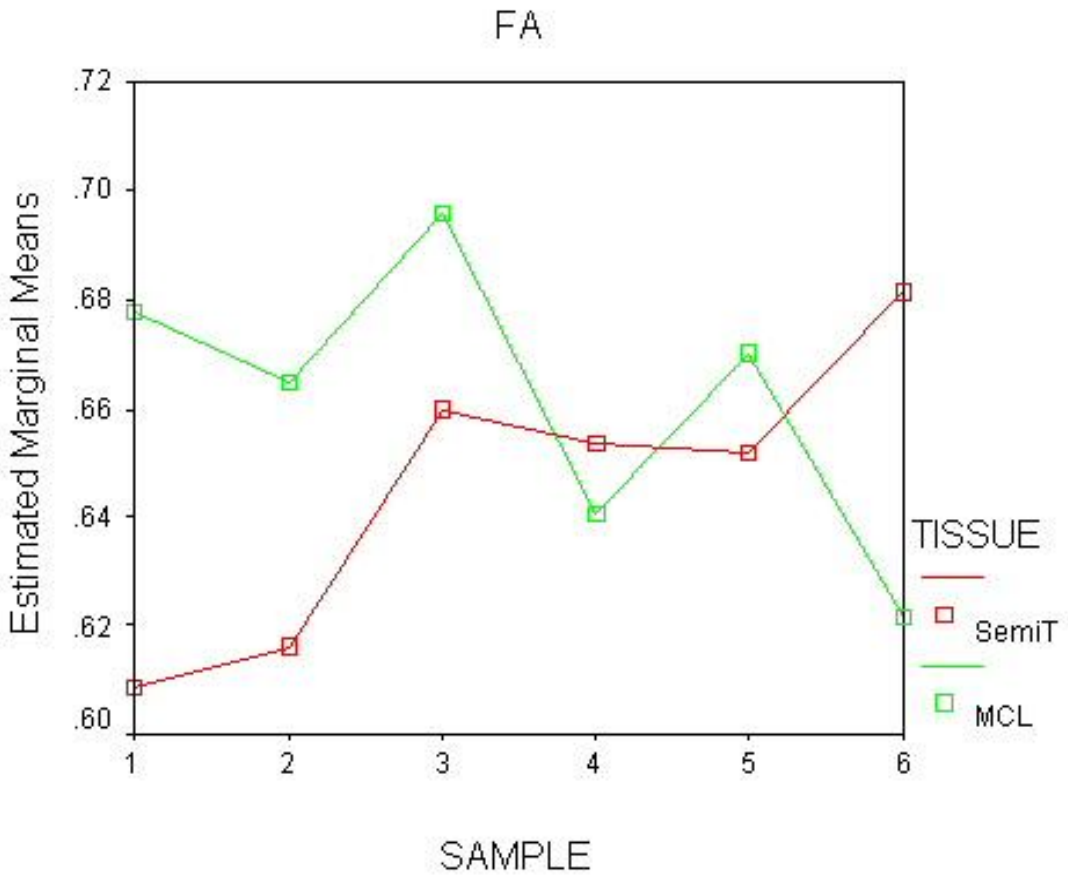

Figure 4.11 (a): Variation of Fractional Anisotropy for the six samples for both semitendinosus tendons and medial collateral ligaments. Tissue * sample: $F(5,96) = 65.9$, $p < 0.005$

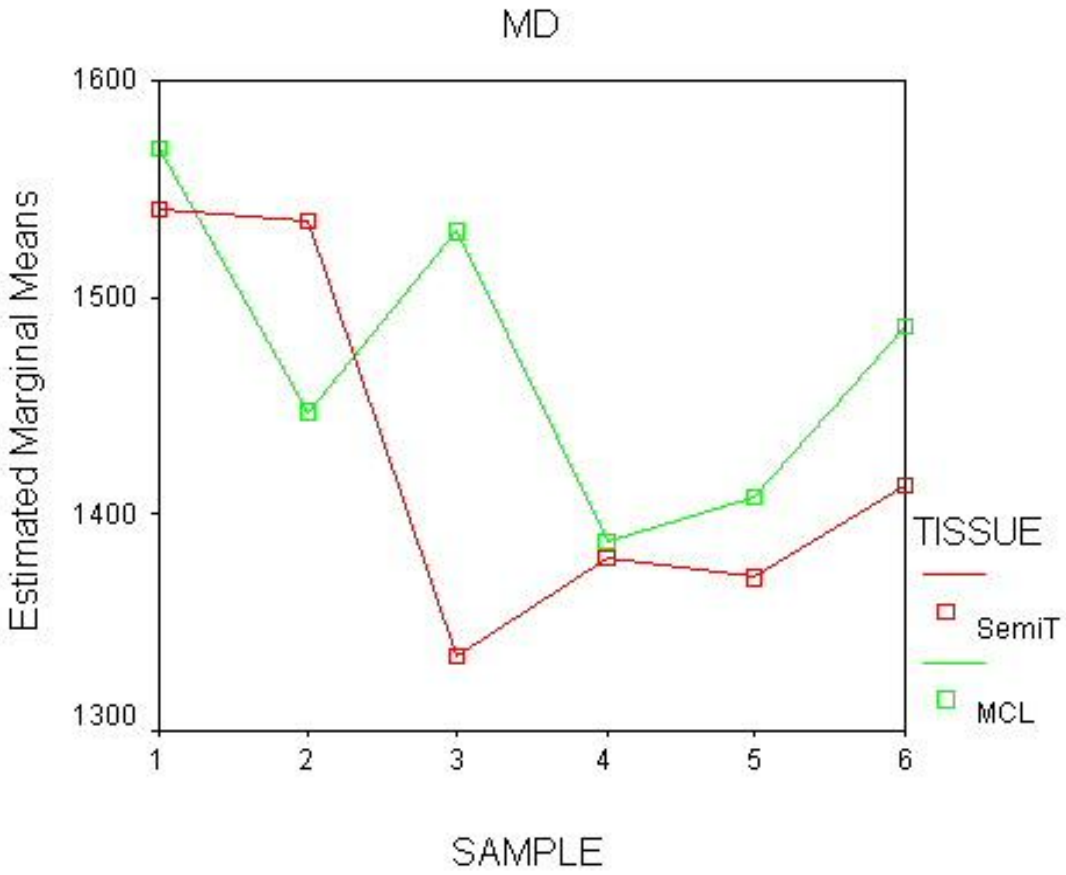

Figure 4.11 (b): Variation of Mean Diffusivity for the six samples for both semitendinosus tendons and medial collateral ligaments. Tissue * sample: $F(5,96)=12.9$, $p < 0.005$

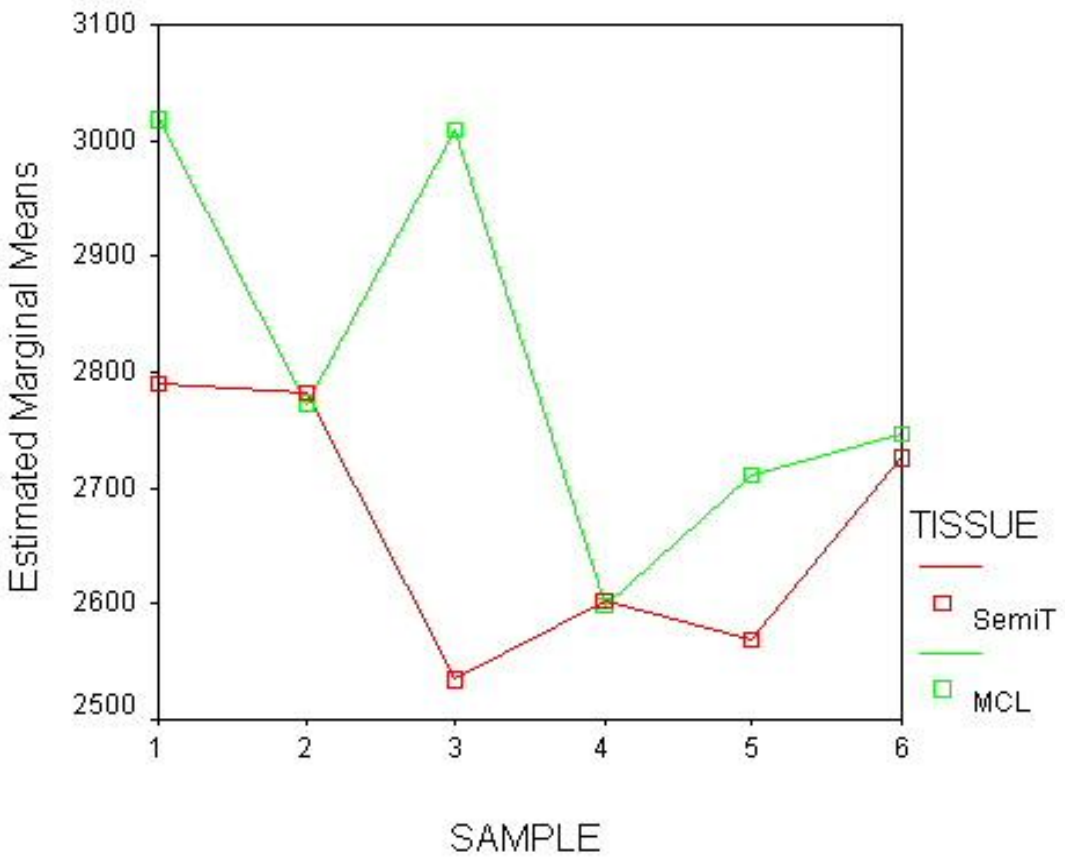

Figure 4.11 (c): Variation of Eigenvalue1 (λ_1) for the six samples for both semitendinosus tendons and medial collateral ligaments. Tissue * sample: $F(5,96)=5.3$, $p < 0.005$

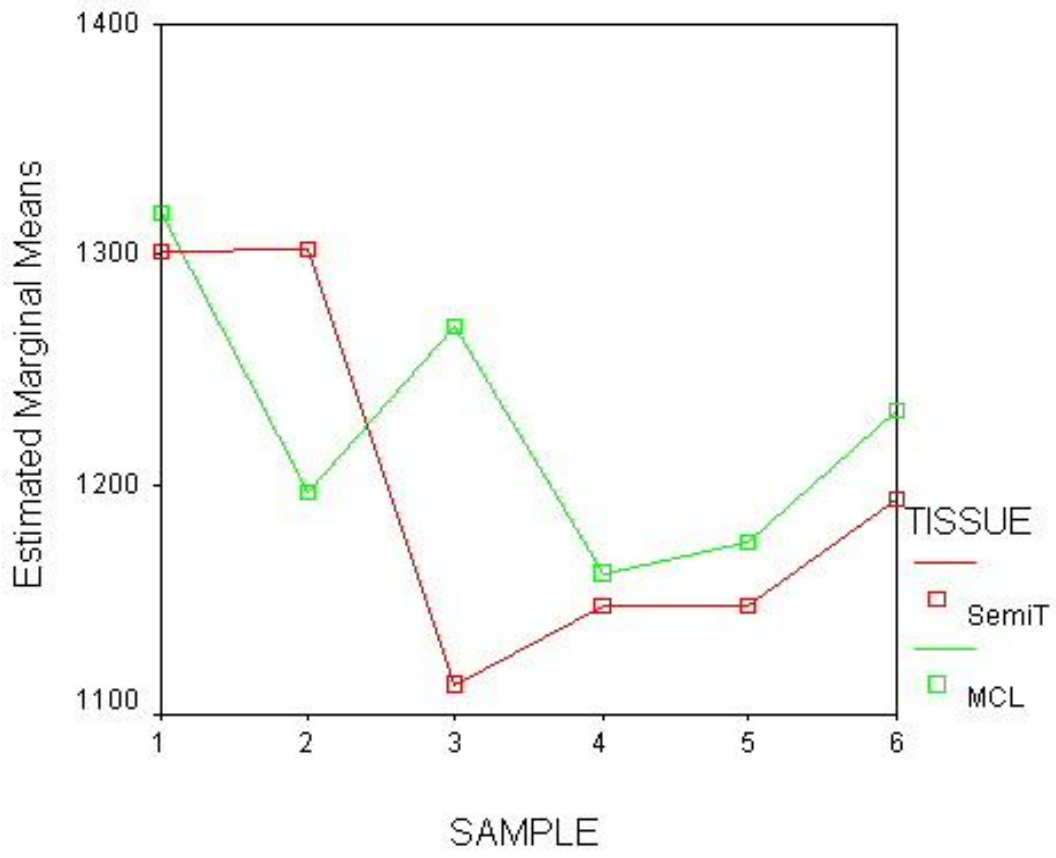

Figure 4.11 (d): Variation of Eigenvalue2 (λ_2) for the six samples for both semitendinosus tendons and medial collateral ligaments. Tissue * sample: F (5,96)=17.3, $p < 0.005$

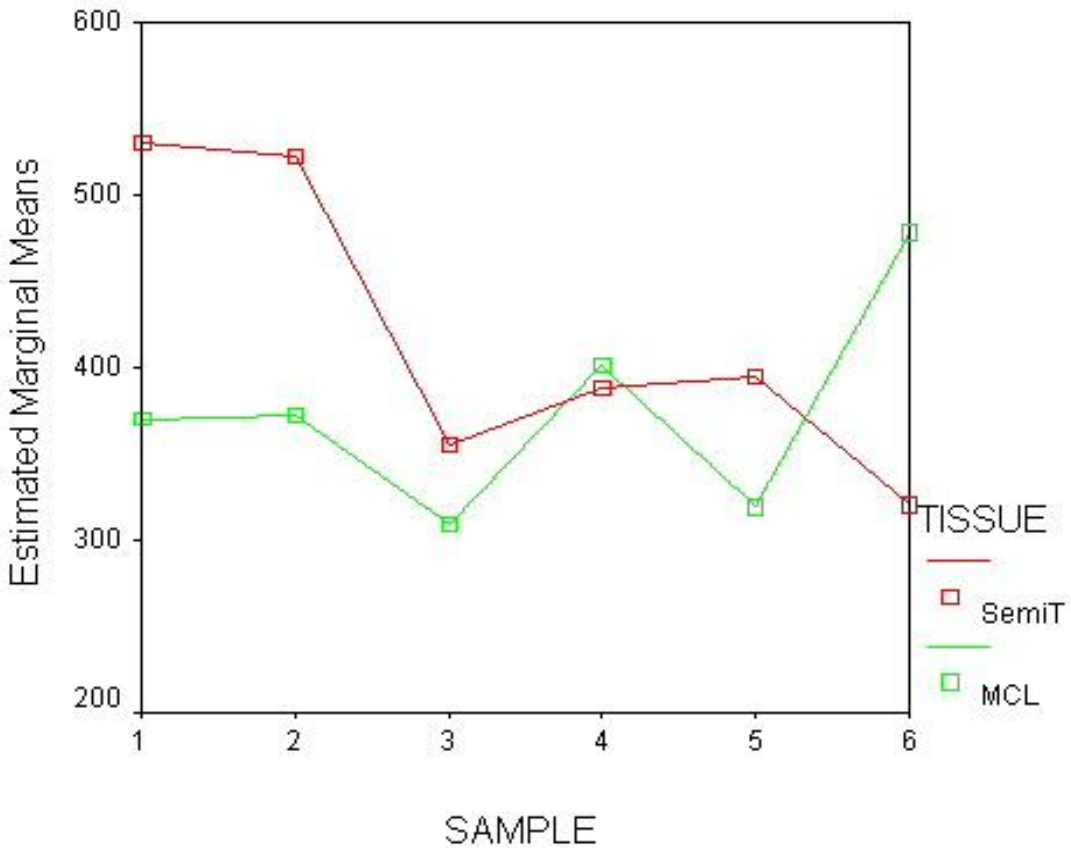

Figure 4.11 (e): Variation of Eigenvalue3 (λ_3) for the six samples for both semitendinosus tendons and medial collateral ligaments. Tissue * sample : $F(5,96)=12.6$, $p < 0.005$

FA by tissue type interaction showed that samples 1,3,5 (which were placed on top of tissue holder) were consistently higher than samples 2,4,6 (which were on bottom of the tissue holder), therefore top vs bottom effect in samples was studied. Figure 4.12 shows the mean Fractional Anisotropy graphs for the samples placed at the top (samples 1,3,5) and samples placed at the bottom (samples 2,4,6). Significant differences were found between the samples placed at the top and bottom for FA ($p = 0.009$), λ_1 ($p= 0.012$) and λ_3 ($p= 0.045$).

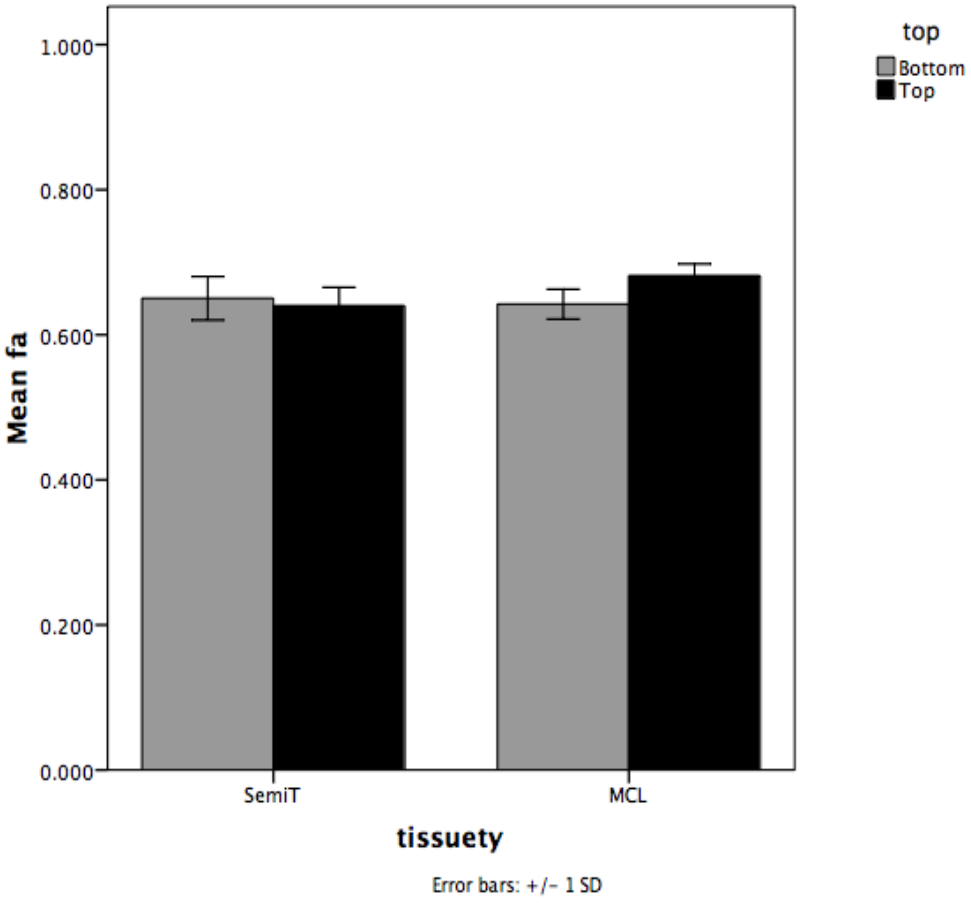

Figure 4.12: Mean Fractional Anisotropy for the samples placed on top (samples 1,3,5) and bottom (samples 2,4,6) of the tissue holder for both semitendinosus tendons and medial collateral ligaments (p=0.009).

Interaction of the tissues with slices showed no significant differences within the semiTs and MCLs for all the DTI metrics. Interaction of the tissues with samples showed significant differences ($p < 0.005$), and when this interaction was further decomposed, significant effect of sample was observed between tissues placed at top and bottom of the

tissue holder but it didn't affect our overall finding that the tissue types are significantly different for the central nine slices analyzed. This finding suggests that maybe we should do only one sample at a time or randomize the samples alternating the positioning of the samples between top and bottom. No significant differences were found between SemiTs and MCLs when considering only the central slice but when more slices were included significant differences were found between the two tissue types for FA, λ_1 and λ_3. Histograms showed normal distribution for all slices and samples for all DTI metrics for both tissue types.

4.5 Discussion

Tendons and ligaments morphologically have similar structure which is represented by a hierarchical composite organization of collagen fibers. Ligaments differ from tendons in the sense that they have more crimp in the fibers compared to tendons which get straightened out during recruitment of the fibers on onset of a mechanical activity represented by the toe region (shorter for tendons) on the stress-strain curve.

Magic angle effect, dreaded by musculoskeletal radiologists as voxels with collagen fibers oriented at this angle might show increased signal intensity which could be misinterpreted as pathology, was used to our advantage in our scans. High density of these tissues makes them extremely difficult to image in natural anatomical position because the water molecules relax quickly after RF excitement, so we imaged these tissues at magic angle, which is at an angle of about 55° to the main magnetic field. When collagen fibers are oriented at 55 degrees to the main magnetic field of the magnet,

dipole-dipole interactions go to zero, resulting in a prolongation of T2 relaxation time and a higher SNR.

Initial feasibility scans performed on these tissues showed that the acquisition time for the coronal plane was considerably longer compared to axial plane for the desired high resolution; hence we performed and reported the results in axial acquisition plane. The decision for scanning the tissues in the axial plane also gave us a flexibility to assess regional variation in these tissues. We were able to divide the tissue in 200 μm thick slices and for a 3.2 mm acquisition slab we were able to get 16 slices from the tissue. Our voxel size was 50x50x200 μm which is similar to a typical fascicle diameter which ranges from 50- 300 μm , suggesting that the molecular diffusion is occurring in between fibrils rather than in between fascicles.

Significant differences were found between the semitendinosus tendons and medial collateral ligaments overall and when analysis was decomposed further, major differences were found due to the slices. We observed that for the central slice there were no differences in the DTI metrics between the two tissue types but when more slices were incorporated in the analysis differences emerged between the two tissues which suggests that the crimp pattern in ligaments plays a role in the diffusional anisotropy of water molecules at the magnetic field strength studied. The crimp banding pattern in ligaments is about 200 μm which is the same as our slice thickness which shows that as more of the tissue volume is analyzed differences begin to emerge between these tissue types. We also observed differences in the samples placed on the top of the tissue holder which could be due to field inhomogeneities and also a possible deviation from the magic angle by a couple of degrees when the tissues are actually placed and glued to the tissue holder.

Also, variability can result from signal acquisition and processing from day to day and session to session. All the tissues were scanned in a taut state which is a limitation as tension to eliminate crimp might yield different results for each tissue type.

Tracking of the fibers was done using the Fiber Assignment by Continuous Tracking (FACT) algorithm using DTI-Studio version 3.0.1. Fiber tractography supplements quantitative data and provides highest level of postprocessing for DTI data. One limitation we faced with this technique was that turning and twisting of the fibers could be observed at the boundaries of the tissue volume because of the noise at the peripheral slices. We tried using different threshold values for FA and different fiber angulations but could still observe the twisting/turning at the edges. Probably using probabilistic tracking methods could provide a different assessment of collagen fiber tracts, but it is expected that different algorithms will give different results and one cannot establish superiority of one algorithm over another. Another inherent limitation associated with DTI metric measurements especially when computing axial and radial diffusivities is that the direction of the primary eigenvector (axial diffusivity) is not always aligned with underlying expected tissue structure. If a voxel contains non-parallel fibers, for example crossing fibers, the diffusion within the voxel will be more uniform in different directions, and it will be hard to distinguish between Axial and Radial diffusivities. This problem calls for assessing of “coherence index” [82, 83]for each of the voxels by measuring the co-alignment of the principal diffusion direction in neighboring voxels with the underlying tissue structure. For this reason, one should be extremely careful

when using the “axial” and “radial” diffusivity terminology as opposed to referring to the eigenvalues of the diffusion tensor.

Another important point to be discussed here is the use of spin-echo pulse sequence which was used for our acquisitions as opposed to a stimulated-echo sequence. A stimulated echo sequence is dependent on T1 relaxation times unlike spin echo which is dependent on T2 relaxation times of the tissues. Considering the short T2 relaxation times of the musculoskeletal tissues one would argue using stimulated-echo sequence because T1 for these tissues are much longer than T2 relaxation times. Aligning the tissues at magic angle, we were able to achieve higher T2’s (about 33 ms) and our diffusion time (Δ) between the two diffusion sensitizing gradient pulses was 8 ms (shorter than the TE of ~14 ms) so use of spin-echo sequence didn’t affect our acquisition, and use of stimulated-echo sequence would have prolonged the acquisition times. However, if one wants to study the effect of longer diffusion times on the DTI metrics, use of stimulated-echo sequence should be preferred over spin-echo sequence.

The scans were conducted on a high-field 11.7 T magnet which, to our knowledge, is probably the highest field strength that has been used to scan these tissues ex-vivo. Using this high field magnet has its advantages and disadvantages. The advantage is that we can achieve a really high resolution which is desirable for the small size of the tissues being studied and can provide an improved signal to noise ratio. On the other hand we have to increase signal averaging to reduce the noise which increases the scan time. High field MRI also exhibits imaging artifacts such B0 and gradient field inhomogeneties and susceptibility artifacts. Also, such high field strength is highly unlikely to be used for human use because of the higher specific absorption rate (SAR). Therefore, additional

work needs to be performed to optimize DTI protocols and standardize this technique at lower field strengths that more closely resembles the current clinical imaging situation.

The fractional anisotropy values obtained in our study are higher than corresponding reported values for articular cartilage, annulus fibrosus and skeletal muscle, consistent with the highly organized collagenous structure of tendons and ligaments. The diffusivity values are similar or lower compared to other musculoskeletal tissues suggesting the dense nature of these tissues. FA, MD, AD and RD show excellent repeatability among tissues, and histological and imaging results including tractography confirm the known microstructural organization of collagen bundles in tendons and ligaments.

5. Sensitivity of b-values on DTI metrics

5.1 Introduction to b-value and its significance.

Diffusion tensor imaging facilitates identification and characterization of tissue structures in the brain, spinal cord, and other tissues with anisotropic microstructures, according to the direction and degree of anisotropic water diffusion. The primary parameter which determines the sensitivity in diffusion sequences is the strength of the b-value. If the b-value is too small, the signal decay by diffusion is too small to be determined. On the other hand, if b-value is too large, signal intensity may reach the level of noise. Therefore, determination of the optimal b-value or b-value range is critical to generating reliable DTI results. The optimum b value differs slightly, depending on the parameter being measured — contrast between tissues in diffusion-weighted images, ADC, anisotropy, eigenvalues, or eigenvectors. Although various optimization strategies have been proposed [84-91], it is still necessary to conduct definitive study for a specific tissue to get the optimization of the DTI scanning parameters, i.e., the optimized b value.

The fiber density index (FDI), which is a recently introduced quantitative index which describes the density of fibers within a bundle passing through a ROI, is one of the parameters that has been used to optimize the b-value for different tissues and at different field strengths. It is calculated by dividing the number of fibers traversing an individual ROI by the area size of the ROI (in pixels).

The highly-organized collagenous structure of tendons makes it possible to use DTI to study the parallel collagen fibers that provide mechanical strength to the tissue. On the

other hand, the relatively short and orientation dependent T2 relaxation values of tendon limits the application of MRI as a reliable approach to assess tendon integrity. Higher SNR at higher magnetic field might make this technique possible. However, to the best of our knowledge, no published study has been found for a specific study of optimizing DTI scanning parameters, especially the optimization of b-value on these tissues. In this study, we systematically assess the optimal b value for DTI and fiber tractography of the rabbit semitendinosus tendon at 11.7 T.

5.2 Methods

Sample Preparation: Contralateral pairs of semitendinosus tendons from three male, skeletally mature New Zealand White rabbits were studied (same tissues as studied in chapter 4). A custom made tissue holder was used to secure the tendon inside the NMR tube. Each specimen was glued on the edges of the holder at an angle of 55 ° to the direction of B0 to take advantage of the magic angle effect. The holder was then fitted and sealed in a 10 mm NMR sample tube (New Era Enterprise Inc) filled with perfluorinated oil (Krytox GPL-102 PFPE oil, DuPont, NJ) to maintain the hydration state of the tendons as well as to minimize proton signals from the bathing medium.

MRI Experiments: All MR experiments were conducted at 11.74 T using a 56 mm vertical bore magnet and a Bruker DRX Avance spectrometer (Bruker BioSpin, Billerica, MA). MR images were acquired using a Bruker Micro 5 imaging probe with triple axis gradients (maximum strength 200 G/cm) and a 10 mm diameter RF saddle coil. DTI acquisition was carried out using a Stejskal — Tanner[16] 3D spin-echo diffusion

weighted sequence with the following acquisition parameters: TR = 1 s, TE = 14 ms, δ/Δ = 2/8 ms, NEX = 1, FOV = 9.6 × 3.2 × 3.2 mm, resolution = 50 × 50 × 200 μm. Six noncollinear directions of diffusion gradients (x,y,z) = (1,1,0), (0,1,1), (1,0,1),(-1,1,0), (0,-1,1), (1,0,-1), plus an image with no diffusion gradients were used. Nine axial DTI scans were performed on each tissue with a range of b-values: 200, 300, 400, 500, 600, 700, 800, 900, and 1000 s/mm^2. The DTI scan time at each b value was 2 hours.

Data Processing: DTI-Studio version 3.0 was used to generate collagen fiber tracts for the tissues using the Fiber Assignment by Continuous Tracking (FACT) algorithm. Fiber density index (FDI) was calculated to describe the density of fibers passing through a ROI. The FDI was calculated by dividing the number of fibers traversing an individual ROI by the area size of the ROI (in pixels) after fiber tracking. Tracking of fibers started when the fractional anisotropy (FA) threshold was above 0.15 or if the fiber angulation exceeded 50 °. The ROIs were chosen carefully inside of each sample to avoid the partial volume effects.

Fractional anisotropy (FA), mean diffusivity (MD), axial diffusivity (AD), radial diffusivity (RD), and color-coded diffusion maps were calculated by applying following equations for each ROI:

$$MD = \langle \lambda \rangle = \frac{\lambda_1 + \lambda_2 + \lambda_3}{3}$$

$$AD = \lambda_1$$

$$RD = \frac{\lambda_2 + \lambda_3}{2}$$

$$FA = \sqrt{\frac{3}{2}} \sqrt{\frac{(\lambda_1 - \langle \lambda \rangle)^2 + (\lambda_2 - \langle \lambda \rangle)^2 + (\lambda_3 - \langle \lambda \rangle)^2}{\lambda_1^2 + \lambda_2^2 + \lambda_3^2}}$$

where λ_1, λ_2, λ_3 are the eigenvalues generated from the diffusion weighted images.

The signal-to-noise ratio (SNR) was calculated as the mean signal intensity of the ROIs divided by the standard deviation (SD) of the background noise.

Statistical Analysis

All quantitative measurements were reported as mean $\pm$ SD. An ANOVA with repeated measurement was used to assess the effect of b-value on FDI, FA and MD. All computations were performed using Excel (Microsoft, Redmond, WA, USA) and SPSS (SPSS Inc., Chicago, IL, USA). Results were considered significant for $p < 0.05$.

5.3 Results

Average fractional anisotropy and mean diffusivity for the six semitendinosus tendons scanned at the nine b-values of 200, 300, 400, 500, 600, 700, 800, 900, and 1000 s/mm^2 are shown in figures 5.1 and 5.2 respectively. FA and MD decrease with increasing b-

values because of the signal loss due to diffusion. Figure 5.3 shows the average Fiber Density Index values calculated for all the nine b-values using DTIstudio. Significant differences were found in the signal to noise ratio for b-values overall and when the analysis was decomposed further, differences were found between b-values of 200 vs 400 and 600, 300 vs 400 and 800, 400 vs 500, 600,700,800,900 and 1000, and 600 vs 800,900 and1000. Significant differences were also found in Fiber Density Indexes and b-values overall and when the analysis was decomposed further, differences were found between b-values of 200 vs 400, 500 and 1000, 300 vs 700, 900 and 1000, 400 vs 700, 800, 900 and 1000, 500 vs 700,800,900 and 1000, 600 vs 900 and 1000, 700 vs 1000 and 800 vs 1000. Figure 5.4 (a-c) shows the qualitative tractography results (fiber tracts) generated using DTIstudio for b-values of 200, 500 and 1000 respectively. At low b-value (b=200) the fiber tracking reconstruction algorithm was not stable, and reconstructed fiber tracts were relatively unorganized and tracking length was short. This likely reflects the limited sensitivity of such low b value acquisitions to molecular diffusion. Fiber tracts were also short at high b values (b= 900, 1000) which may be explained by the fact that with increasing diffusion weighting the SNR decreases due to loss of signal.

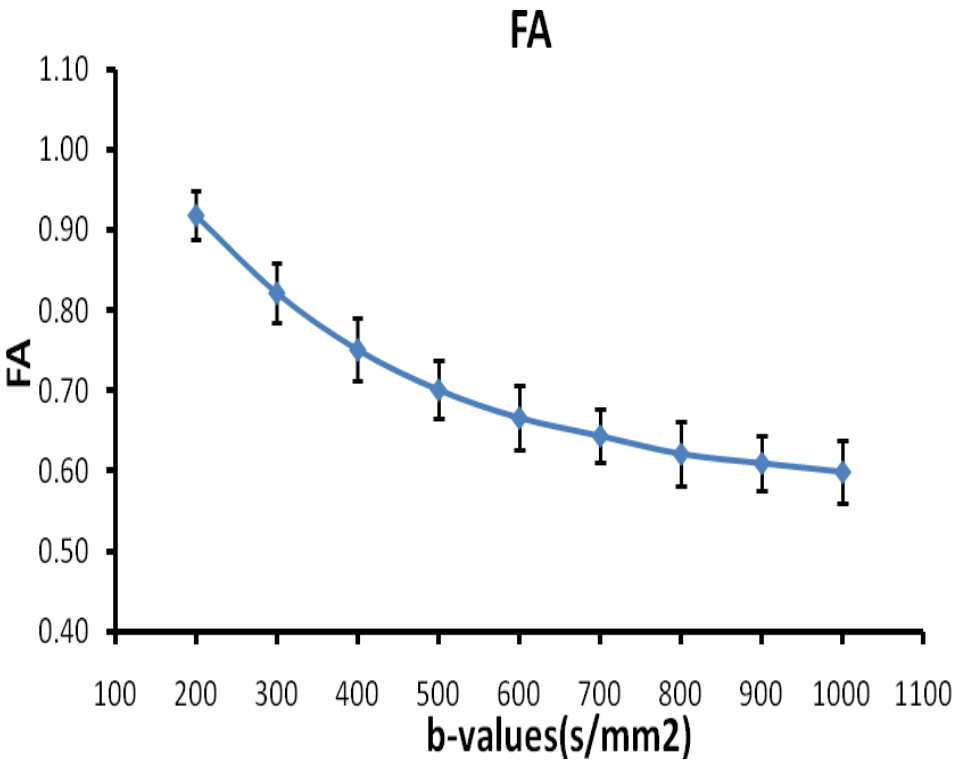

Figure 5.1: Average Fractional Anisotropy values for six rabbit semitendinosus tendons at different b-values.

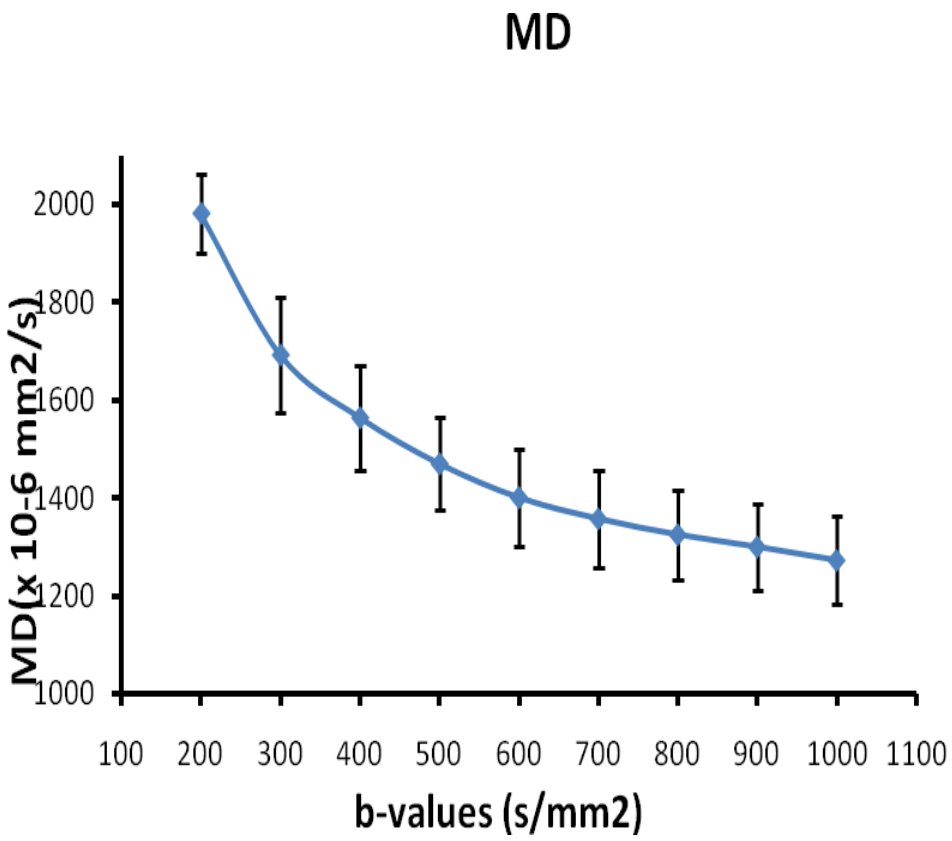

Figure 5.2: Average Mean Diffusivity values for six rabbit semitendinosus tendons at different b-values.

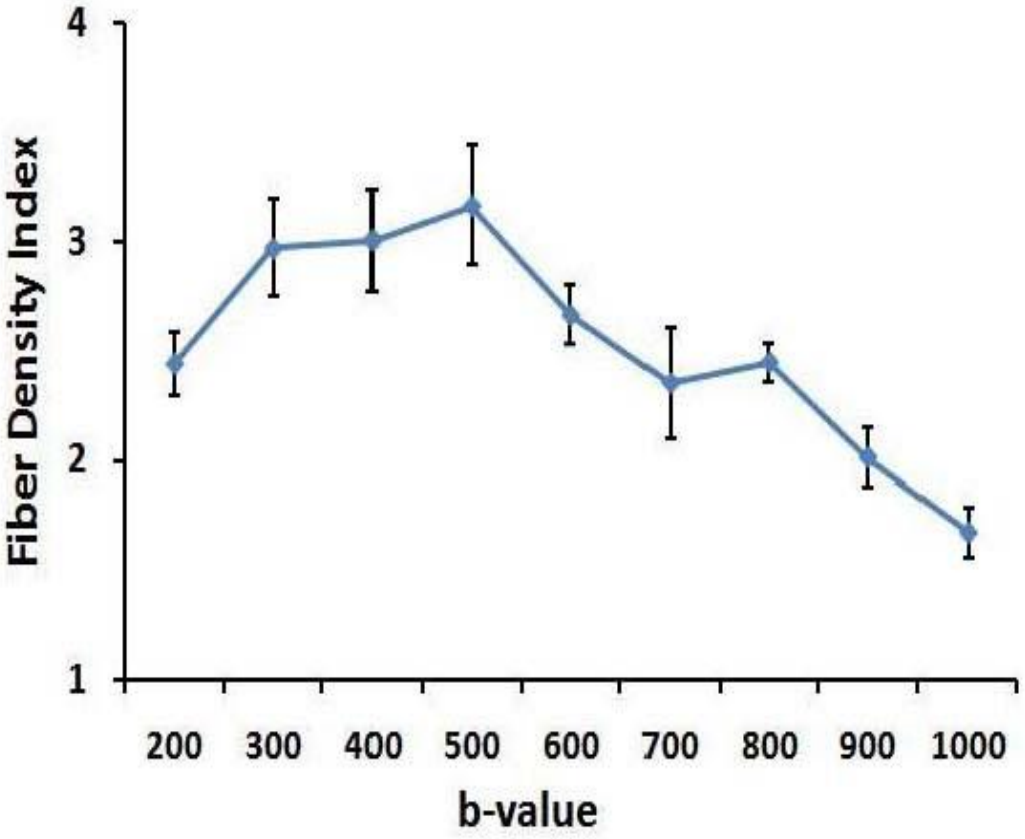

Figure 5.3: Average FDI values for the six semiT samples for different b-values calculated using DTIstudio.

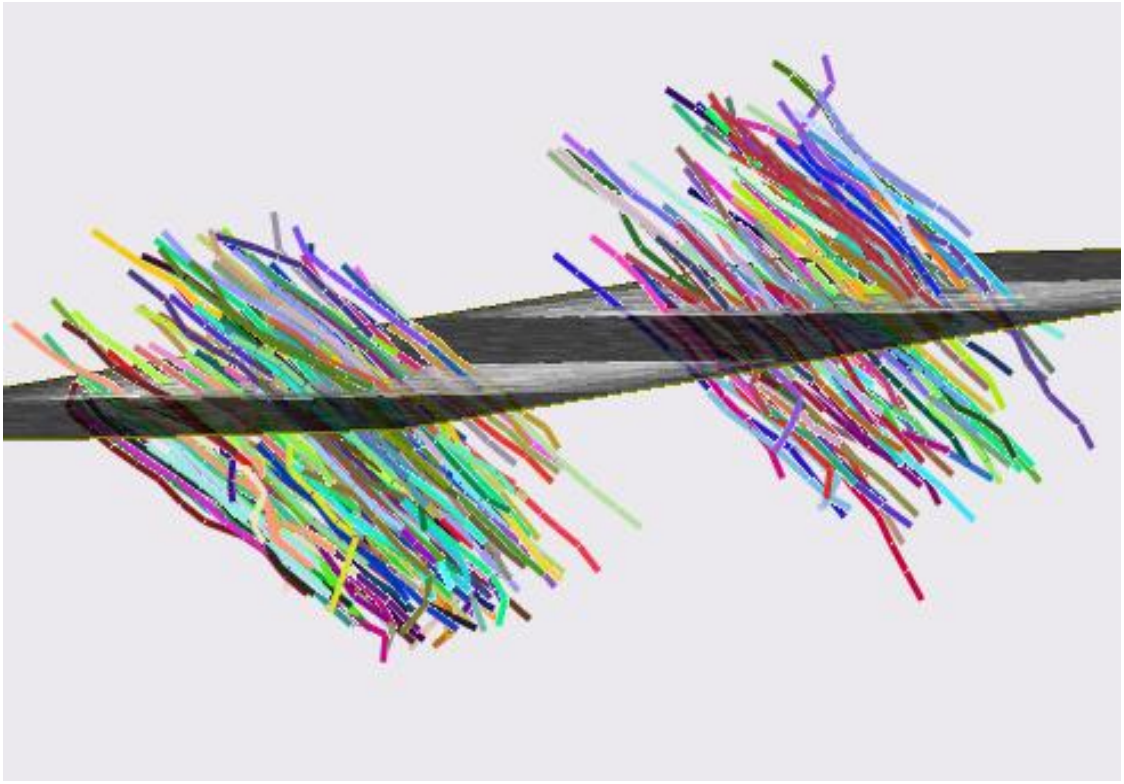

Figure 5.4 (a): Qualitative tractography image showing fiber tracts generated using DTIstudio for two semitendinosus tendons for a b-value of 200. The fiber tracts are shortened and less dense at this b-value indicating limited sensitivity of low b-value acquisition to molecular diffusion.

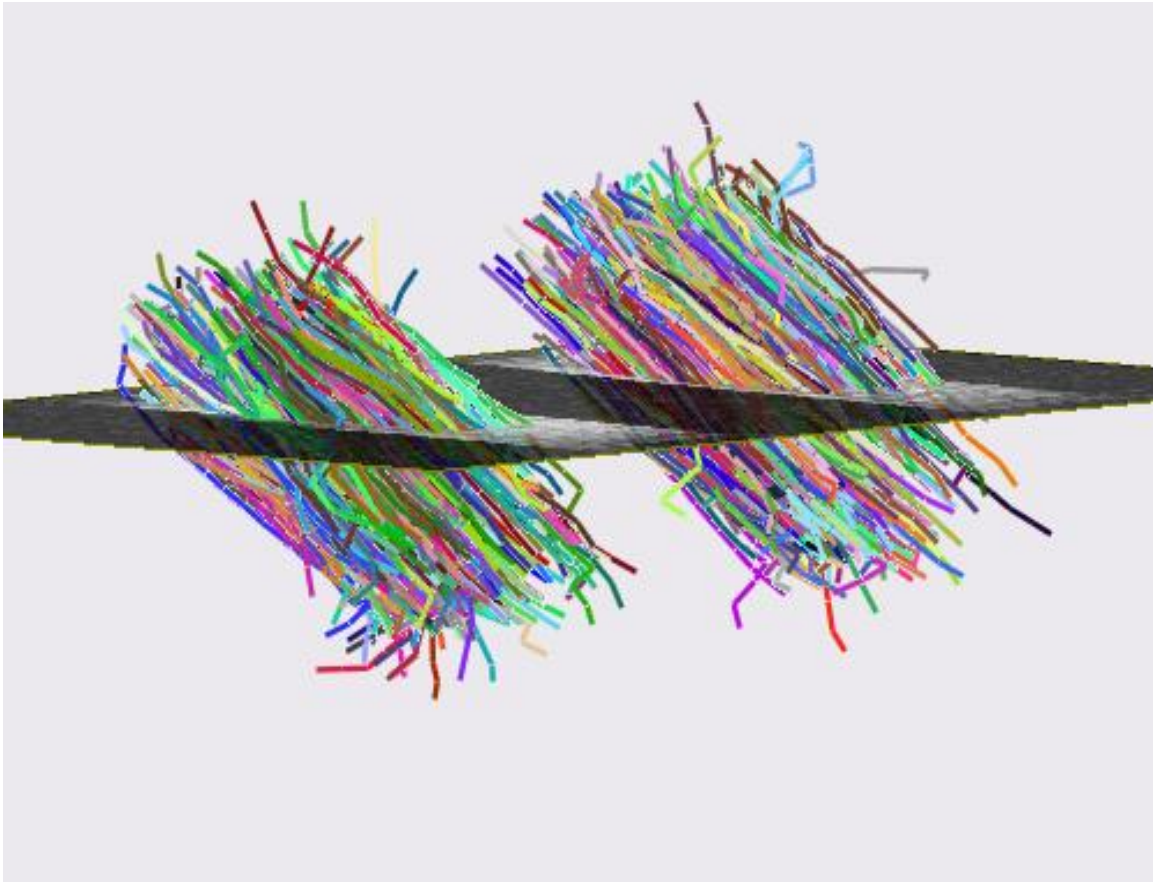

Figure 5.4 (b): Qualitative tractography image showing fiber tracts generated using DTIstudio for two semitendinosus tendons for a b-value of 500. The fiber tracts are long and denser at this b-value.

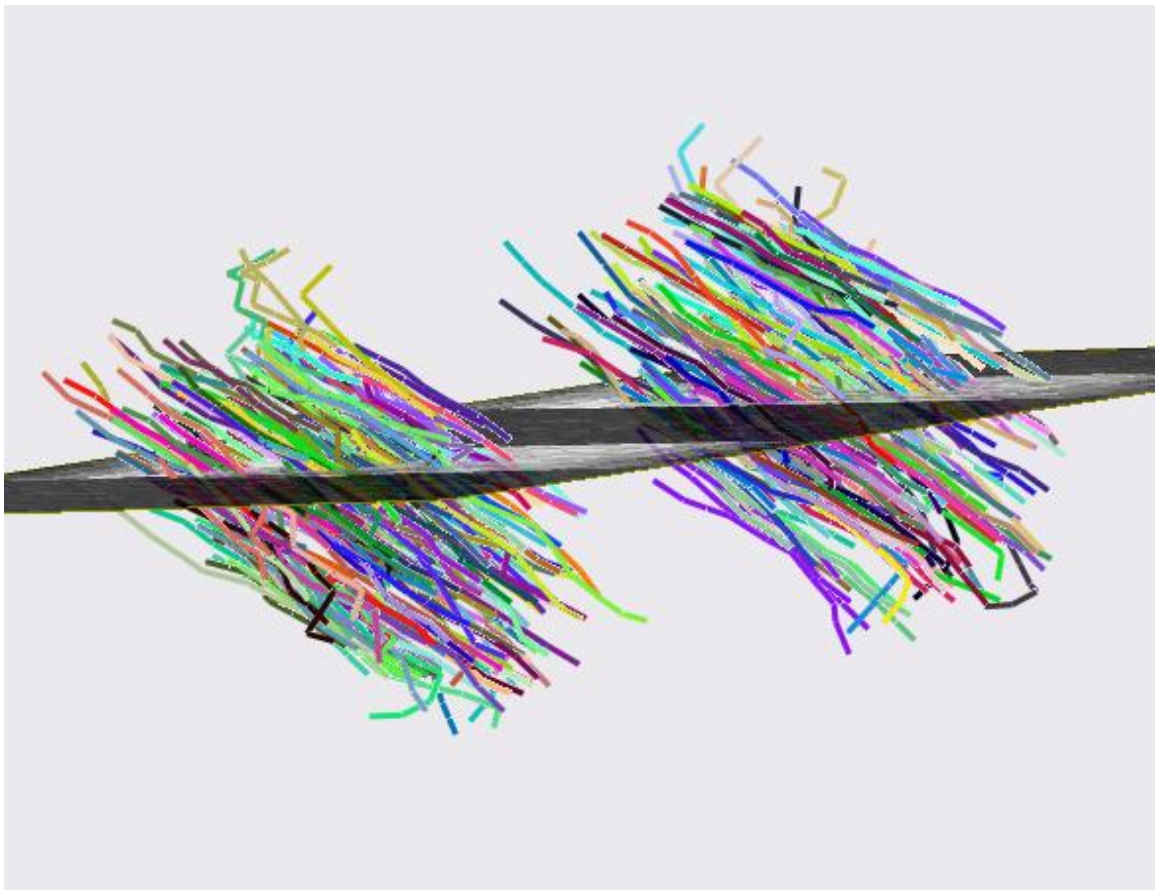

Figure 5.4 (c): Qualitative tractography image showing fiber tracts generated using DTIstudio for two semitendinosus tendons for a b-value of 1000. The fiber tracts are shortened, less dense and appear to be less-organized at this b-value because of signal decay due to molecular diffusion.

5.4 Discussion

The range of b values considered reasonable for DTI measurements is based on the particular tissue being evaluated and the gradient strengths of MRI magnet. Several studies have looked into the optimal b values for different tissues at different magnetic field strengths. For example, a b value of 1,000 s/mm^2 or greater (up to 3,300 s/mm^2) is considered optimal in the assessment of brain tissue at 1.5 T [92, 93], a b-value of 625 s/mm^2 for skeletal muscle (anterior tibialis and lateral gastrocnemius) at 1.5 T, 1,000 s/mm^2 for peripheral nerves at 3.0 T[94], 1025 s/mm^2 for median nerve at 1.5 T and approximately 800 s/mm^2 for rectal cancer at 1.5 T[95].

Fiber density index was calculated to describe the density of continuous fibers tracts passing through a ROI which was placed on the central slice of the semitendinosus tendon. The FDI was originally used in the brain to describe the density of white matter fibers within a bundle passing through a single pixel or a ROI. It depends on imaging parameters and fiber tract reconstruction factors such as spatial resolution, FA cutoff value, and fiber angulation threshold.

Qualitative fiber assessment is another analysis that has been employed by several studies[87, 90] to supplement the quantitative fiber density index data to narrow down to a particular optimum b-value for the tissue being analyzed at the given field strength. For this, several observers (musculoskeletal radiologists) rank the image quality of each tractographic image independently and separately ranking the images from best to worst. Image quality can be assessed on the basis of several factors such as qualitative evaluation of fiber track order and organization, length of continuous fiber bundles observed, appearance of fiber bundles in boundary regions, and apparent density of

muscle fiber bundles. We also made an attempt to assess the fiber tracts qualitatively from tractography images and found that at lower b-values reconstructed fiber tracts were relatively unorganized and tracking length was short. This likely reflects the limited sensitivity of such low b value acquisitions to molecular diffusion. Fiber tracts were also short at high b values which is attributable to the fact that with increasing diffusion weighting the SNR decreases due to loss of signal.

The optimal b value may depend on many factors, including the mean Apparent Diffusion Coefficient's in the regions of interest, the amount of anisotropy, the tensor orientation, and whether TE changes when the b factor changes [89]. Saupe et al. [90] noted that "The optimal b values for diffusion tensor imaging of a particular tissue at a particular magnetic field strength are reflective of a dynamic balance between the sensitivity of diffusion weighted acquisition to diffusion of water molecules, which is maximized at long b-values, and the need for an SNR necessary for accurate fiber tracking and anisotropic fiber characterization, which are maximized at short b-values."

Recently, our group (Weiguo Li et al) introduced a new parameter called *combinatorial SNR difference (CSD)* for optimization of the b-value for DTI of rabbit semitendinosus tendon (unpublished data). The rationale behind using this new parameter for optimization is that FDI is calculated after the DTI maps are extracted and its value depends on the fiber tracking algorithm, the sensitivity of which is affected by many physical and computational variables still poorly understood. Combinatorial SNR difference (CSD) is defined as the summation of the absolute value of SNR difference in the measured DWIs across all the diffusion gradient directions. In contrast to FDI, an advantage of CSD is that the latter parameter is computed from DWI images prior to

reconstruction of DTI (i.e., fractional aniostropy) maps and tractography. Furthermore, CSD can be calculated prior to actual DTI scanning (e.g., at the GSP stage in Bruker ParaVision).

For our DTI measurements, we found a range of b-values from 300-600 s/mm^2 for which the average fiber density index from semitendinosus tendons was the highest. To get down to one particular "optimized" b-value from this range will require more assessments including setting an SNR threshold, detailed qualitative assessments of fiber track order and organization and a combination of FDI and CSD measurements. Looking into the literature, for several years clinicians and researchers have been using b-values perceived appropriate for the particular tissue being studied, until recently when a need for optimization of the b-values was realized for more reliable data. In this study, we proceeded to have not just a thorough characterization of these tissues (which in itself is the first attempt) but also optimized the b-values for these tissues at 11.7 T field strength.

6. Conclusion and suggested future work.

Conventional MRI has been considered as the gold standard in diagnosis of injuries to tendons and ligaments. MRI is a non-invasive *qualitative* tool for detecting large and complete tears in ligaments and tendons, however, low-grade injuries are more challenging to delineate on conventional grayscale MR images. The DTI results offer the unique advantage of providing not only *qualitative* but also *quantitative* microstructural information in a non-invasive manner.

The present work shows that *quantitative* information regarding water diffusion anisotropy, structure and organization of these tissues can be obtained at high spatial resolution using MR diffusion tensor imaging. This dissertation work has several unique contributions to the field of tendon and ligament imaging research.

1) This is the first study to show feasibility an applicability of DTI on Tendons and Ligaments at ultra-high magnetic fields with high resolutions and measure DTI metrics from both tissue types. This demonstrates the capabilities of this technique for determining the diffusion properties of tendons and ligaments and microstructural analysis of the collagen fiber structure and orientation.

2) High Fractional Anisotropy values of 0.67 for semitendinosus tendons and 0.66 for medial collateral ligaments shows the highly anisotropic nature of these soft connective tissues.

3) Axial diffusivity is about 3 times the radial diffusivity which shows diffusion directional anisotropy indicating diffusion preference along the fibers then across them.

4) The present study showed fiber tractography of these tissues at ultra-high magnetic fields with a histological correlation confirming the highly-organized parallel collagen fiber microstructure.

5) Diffusion tensor imaging is sensitive to the diffusional anisotropy differences and can show microstructural differences between tendons and ligaments through DTI metrics at 11. 7 T field strength.

6) The current work found the most feasible range of b-values of 300-600 s/mm^2 which will be best suited for these tissue types at the given magnetic field strength of 11.7T and get more reliable DTI measurements.

Some of the suggestions for future work will involve the following:

1) Perform DTI evaluation on rabbit semitendinosus tendons and medial collateral ligaments ex-vivo with experimentally induced damage.

2) Diffusion tensor imaging of Dyneema fiber phantoms for validation and standardization.

3) DTI evaluation of native and mechanically injured tendons and ligaments in an in-vivo animal model.

Long-term clinical goal is to utilize this advanced MR technique for detection, prevention, and management of Tendinosis/tendinitis, acute injuries/Ligament sprains and assessment of tissue healing following repair.

In conclusion, we were able to successfully demonstrate the feasibility and applicability of this technique for imaging tendons and ligaments. DTI metrics can provide insight into 3D tissue integrity and organization. Fiber tractography graphically supplements the quantitative DTI data. The quantitative and graphical capabilities of DTI provide more rigorous information regarding tendon and ligament structural integrity in comparison to conventional MRI.

REFERENCES

1. Liang Z, Lauterbur PC, IEEE Engineering in Medicine and Biology Society. Principles of magnetic resonance imaging. 2000:416.

2. Gallimore GW,Jr, Harms SE. Knee injuries: high-resolution MR imaging. Radiology 1986;160(2):457-61.

3. Konig H, Sieper J, Wolf KJ. Rheumatoid arthritis: evaluation of hypervascular and fibrous pannus with dynamic MR imaging enhanced with Gd-DTPA. Radiology 1990;176(2):473-7.

4. Benjamin M, Milz S, Bydder GM. Magnetic resonance imaging of entheses. Part 1. Clin Radiol 2008;63(6):691-703.

5. Kassarjian A, Bencardino JT, Palmer WE. MR imaging of the rotator cuff. Radiol Clin North Am 2006;44(4):503,23, vii-viii.

6. Roberts CC, Towers JD, Spangehl MJ et al. Advanced MR imaging of the cruciate ligaments. Radiol Clin North Am 2007;45(6):1003,16, vi-vii.

7. Magee T, Williams D. 3.0-T MRI of the supraspinatus tendon. AJR Am J Roentgenol 2006;187(4):881-6.

8. Magee T. Three-Tesla MR imaging of the knee. Radiol Clin North Am 2007;45(6):1055,62, vii.

9. Muramatsu K, Hachiya Y, Izawa H. Serial evaluation of human anterior cruciate ligament grafts by contrast-enhanced magnetic resonance imaging: comparison of allografts and autografts. Arthroscopy 2008;24(9):1038-44.

10. Khan KM, Bonar F, Desmond PM et al. Patellar tendinosis (jumper's knee): findings at histopathologic examination, US, and MR imaging. Victorian Institute of Sport Tendon Study Group. Radiology 1996;200(3):821-7.

11. Major NM, Helms CA. MR imaging of the knee: findings in asymptomatic collegiate basketball players. AJR Am J Roentgenol 2002;179(3):641-4.

12. Reiff DB, Heenan SD, Heron CW. MRI appearances of the asymptomatic patellar tendon on gradient echo imaging. Skeletal Radiol 1995;24(2):123-6.

13. Bydder M, Rahal A, Fullerton GD et al. The magic angle effect: a source of artifact, determinant of image contrast, and technique for imaging. J Magn Reson Imaging 2007;25(2):290-300.

14. Du J, Pak BC, Znamirowski R et al. Magic angle effect in magnetic resonance imaging of the Achilles tendon and enthesis. Magn Reson Imaging 2009;27(4):557-64.

15. Fullerton GD, Rahal A. Collagen structure: the molecular source of the tendon magic angle effect. J Magn Reson Imaging 2007;25(2):345-61.

16. Filho GH, Du J, Pak BC et al. Quantitative characterization of the Achilles tendon in cadaveric specimens: T1 and T2* measurements using ultrashort-TE MRI at 3 T. AJR Am J Roentgenol 2009;192(3):W117-24.

17. Fullerton GD, Cameron IL, Ord VA. Orientation of tendons in the magnetic field and its effect on T2 relaxation times. Radiology 1985;155(2):433-5.

18. Han S, Gemmell SJ, Helmer KG et al. Changes in ADC caused by tensile loading of rabbit achilles tendon: evidence for water transport. J Magn Reson 2000;144(2):217-27.

19. Helmer KG, Nair G, Cannella M et al. Water movement in tendon in response to a repeated static tensile load using one-dimensional magnetic resonance imaging. J Biomech Eng 2006;128(5):733-41.

20. Helmer KG, Wellen J, Grigg P et al. Measurement of the spatial redistribution of water in rabbit Achilles tendon in response to static tensile loading. J Biomech Eng 2004;126(5):651-6.

21. Wellen J, Helmer KG, Grigg P et al. Spatial characterization of T1 and T2 relaxation times and the water apparent diffusion coefficient in rabbit Achilles tendon subjected to tensile loading. Magn Reson Med 2005;53(3):535-44.

22. Wellen J, Helmer KG, Grigg P et al. Application of porous-media theory to the investigation of water ADC changes in rabbit Achilles tendon caused by tensile loading. J Magn Reson 2004;170(1):49-55.

23. Fechete R, Demco DE, Blumich B et al. Anisotropy of collagen fiber orientation in sheep tendon by 1H double-quantum-filtered NMR signals. J Magn Reson 2003;162(1):166-75.

24. Fechete R, Demco DE, Eliav U et al. Self-diffusion anisotropy of water in sheep Achilles tendon. NMR Biomed 2005;18(8):577-86.

25. Ikoma K, Kusaka Y, Takamiya H et al. Evaluation of collagen fiber maturation and ordering in regenerating tendons employing H-1 double quantum filtered NMR spectroscopy. J Orthop Res 2003;21(1):149-56.

26. Seo Y, Ikoma K, Takamiya H et al. 1H double-quantum-filtered MR imaging as a new tool for assessment of healing of the ruptured Achilles tendon. Magn Reson Med 1999;42(5):884-9.

27. Hannafin JA, Arnoczky SP. Effect of cyclic and static tensile loading on water content and solute diffusion in canine flexor tendons: an in vitro study. J Orthop Res 1994;12(3):350-6.

28. Weiss JA, Maakestad BJ. Permeability of human medial collateral ligament in compression transverse to the collagen fiber direction. J Biomech 2006;39(2):276-83.

29. Henkelman RM, Stanisz GJ, Kim JK et al. Anisotropy of NMR properties of tissues. Magn Reson Med 1994;32(5):592-601.

30. Peto S, Gillis P. Fiber-to-field angle dependence of proton nuclear magnetic relaxation in collagen. Magn Reson Imaging 1990;8(6):705-12.

31. Moseley M. Diffusion tensor imaging and aging - a review. NMR Biomed 2002;15(7-8):553-60.

32. Abe O, Aoki S, Hayashi N et al. Normal aging in the central nervous system: quantitative MR diffusion-tensor analysis. Neurobiol Aging 2002;23(3):433-41.

33. Nusbaum AO, Tang CY, Buchsbaum MS et al. Regional and global changes in cerebral diffusion with normal aging. AJNR Am J Neuroradiol 2001;22(1):136-42.

34. Pfefferbaum A, Sullivan EV, Hedehus M et al. Age-related decline in brain white matter anisotropy measured with spatially corrected echo-planar diffusion tensor imaging. Magn Reson Med 2000;44(2):259-68.

35. Stebbins GT, Smith CA, Bartt RE et al. HIV-associated alterations in normal-appearing white matter: a voxel-wise diffusion tensor imaging study. J Acquir Immune Defic Syndr 2007;46(5):564-73.

36. Bozzali M, Falini A, Franceschi M et al. White matter damage in Alzheimer's disease assessed in vivo using diffusion tensor magnetic resonance imaging. J Neurol Neurosurg Psychiatry 2002;72(6):742-6.

37. Kantarci K, Jack CR,Jr, Xu YC et al. Mild cognitive impairment and Alzheimer disease: regional diffusivity of water. Radiology 2001;219(1):101-7.

38. Medina D, DeToledo-Morrell L, Urresta F et al. White matter changes in mild cognitive impairment and AD: A diffusion tensor imaging study. Neurobiol Aging 2006;27(5):663-72.

39. Wang C, Stebbins GT, Nyenhuis DL et al. Longitudinal changes in white matter following ischemic stroke: a three-year follow-up study. Neurobiol Aging 2006;27(12):1827-33.

40. Rovaris M, Rocca MA, Filippi M. Magnetic resonance-based techniques for the study and management of multiple sclerosis. Br Med Bull 2003;65:133-44.

41. Kanaan RA, Kim JS, Kaufmann WE et al. Diffusion tensor imaging in schizophrenia. Biol Psychiatry 2005;58(12):921-9.

42. Kubicki M, McCarley R, Westin CF et al. A review of diffusion tensor imaging studies in schizophrenia. J Psychiatr Res 2007;41(1-2):15-30.

43. de Visser SK, Bowden JC, Wentrup-Byrne E et al. Anisotropy of collagen fibre alignment in bovine cartilage: comparison of polarised light microscopy and spatially resolved diffusion-tensor measurements. Osteoarthritis Cartilage 2008;16(6):689-97.

44. de Visser SK, Crawford RW, Pope JM. Structural adaptations in compressed articular cartilage measured by diffusion tensor imaging. Osteoarthritis Cartilage 2008;16(1):83-9.

45. Budzik JF, Le Thuc V, Demondion X et al. In vivo MR tractography of thigh muscles using diffusion imaging: initial results. Eur Radiol 2007;17(12):3079-85.

46. Galban CJ, Maderwald S, Stock F et al. Age-related changes in skeletal muscle as detected by diffusion tensor magnetic resonance imaging. J Gerontol A Biol Sci Med Sci 2007;62(4):453-8.

47. Galban CJ, Maderwald S, Uffmann K et al. Diffusive sensitivity to muscle architecture: a magnetic resonance diffusion tensor imaging study of the human calf. Eur J Appl Physiol 2004;93(3):253-62.

48. Galban CJ, Maderwald S, Uffmann K et al. A diffusion tensor imaging analysis of gender differences in water diffusivity within human skeletal muscle. NMR Biomed 2005;18(8):489-98.

49. Zaraiskaya T, Kumbhare D, Noseworthy MD. Diffusion tensor imaging in evaluation of human skeletal muscle injury. J Magn Reson Imaging 2006;24(2):402-8.

50. Benjamin M, Kaiser E, Milz S. Structure-function relationships in tendons: a review. J Anat 2008;212(3):211-28.

51. Blevins FT, Djurasovic M, Flatow EL et al. Biology of the rotator cuff tendon. Orthop Clin North Am 1997;28(1):1-16.

52. Provenzano PP, Vanderby R,Jr. Collagen fibril morphology and organization: implications for force transmission in ligament and tendon. Matrix Biol 2006;25(2):71-84.

53. Kastelic J, Galeski A, Baer E. The multicomposite structure of tendon. Connect Tissue Res 1978;6(1):11-23.

54. Lynch HA, Johannessen W, Wu JP et al. Effect of fiber orientation and strain rate on the nonlinear uniaxial tensile material properties of tendon. J Biomech Eng 2003;125(5):726-31.

55. Quapp KM, Weiss JA. Material characterization of human medial collateral ligament. J Biomech Eng 1998;120(6):757-63.

56. Stabile KJ, Pfaeffle J, Weiss JA et al. Bi-directional mechanical properties of the human forearm interosseous ligament. J Orthop Res 2004;22(3):607-12.

57. Yamamoto E, Hayashi K, Yamamoto N. Effects of stress shielding on the transverse mechanical properties of rabbit patellar tendons. J Biomech Eng 2000;122(6):608-14.

58. Ralphs JR, Benjamin M. The joint capsule: structure, composition, ageing and disease. J Anat 1994;184 (Pt 3)(Pt 3):503-9.

59. Butler DL, Kay MD, Stouffer DC. Comparison of material properties in fascicle-bone units from human patellar tendon and knee ligaments. J Biomech 1986;19(6):425-32.

60. Amiel D, Frank C, Harwood F et al. Tendons and ligaments: a morphological and biochemical comparison. J Orthop Res 1984;1(3):257-65.

61. Kannus P, Jozsa L. Histopathological changes preceding spontaneous rupture of a tendon. A controlled study of 891 patients. J Bone Joint Surg Am 1991;73(10):1507-25.

62. Leadbetter WB. Cell-matrix response in tendon injury. Clin Sports Med 1992;11(3):533-78.

63. Khan KM, Cook JL, Kannus P et al. Time to abandon the "tendinitis" myth. BMJ 2002;324(7338):626-7.

64. Kastelic J, Baer E. Deformation in tendon collagen. Symp Soc Exp Biol 1980;34:397-435.

65. Pollock RG, Wang VM, Bucchieri JS et al. Effects of repetitive subfailure strains on the mechanical behavior of the inferior glenohumeral ligament. J Shoulder Elbow Surg 2000;9(5):427-35.

66. Thornton GM, Shrive NG, Frank CB. Ligament creep recruits fibres at low stresses and can lead to modulus-reducing fibre damage at higher creep stresses: a study in rabbit medial collateral ligament model. J Orthop Res 2002;20(5):967-74.

67. King GJ, Pillon CL, Johnson JA. Effect of in vitro testing over extended periods on the low-load mechanical behaviour of dense connective tissues. J Orthop Res 2000;18(4):678-81.

68. Panjabi MM, Huang RC, Cholewicki J. Equivalence of single and incremental subfailure stretches of rabbit anterior cruciate ligament. J Orthop Res 2000;18(5):841-8.

69. Provenzano PP, Heisey D, Hayashi K et al. Subfailure damage in ligament: a structural and cellular evaluation. J Appl Physiol 2002;92(1):362-71.

70. Schechtman H, Bader DL. Fatigue damage of human tendons. J Biomech 2002;35(3):347-53.

71. Wren TA, Lindsey DP, Beaupre GS et al. Effects of creep and cyclic loading on the mechanical properties and failure of human Achilles tendons. Ann Biomed Eng 2003;31(6):710-7.

72. Fung DT, Wang VM, Laudier DM et al. Subrupture tendon fatigue damage. J Orthop Res 2009;27(2):264-73.

73. Laudier D, Schaffler MB, Flatow EL et al. Novel procedure for high-fidelity tendon histology. J Orthop Res 2007;25(3):390-5.

74. Lin TW, Cardenas L, Soslowsky LJ. Biomechanics of tendon injury and repair. J Biomech 2004;37(6):865-77.

75. Mandelbaum BR, Finerman GA, Reicher MA et al. Magnetic resonance imaging as a tool for evaluation of traumatic knee injuries. Anatomical and pathoanatomical correlations. Am J Sports Med 1986;14(5):361-70.

76. Rose NE, Gold SM. A comparison of accuracy between clinical examination and magnetic resonance imaging in the diagnosis of meniscal and anterior cruciate ligament tears. Arthroscopy 1996;12(4):398-405.

77. Steckel H, Vadala G, Davis D et al. 2D and 3D 3-tesla magnetic resonance imaging of the double bundle structure in anterior cruciate ligament anatomy. Knee Surg Sports Traumatol Arthrosc 2006;14(11):1151-8.

78. Mori S, Barker PB. Diffusion magnetic resonance imaging: its principle and applications. Anat Rec 1999;257(3):102-9.

79. Basser PJ, Mattiello J, LeBihan D. MR diffusion tensor spectroscopy and imaging. Biophys J 1994;66(1):259-67.

80. Othman SF, Li J, Abdullah O et al. High-resolution/high-contrast MRI of human articular cartilage lesions. Acta Orthop 2007;78(4):536-46.

81. Xu H, Othman SF, Magin RL. Monitoring tissue engineering using magnetic resonance imaging. J Biosci Bioeng 2008;106(6):515-27.

82. Klingberg T, Vaidya CJ, Gabrieli JD et al. Myelination and organization of the frontal white matter in children: a diffusion tensor MRI study. Neuroreport 1999;10(13):2817-21.

83. Wheeler-Kingshott CA, Cercignani M. About "axial" and "radial" diffusivities. Magn Reson Med 2009;61(5):1255-60.

84. Jones DK, Horsfield MA, Simmons A. Optimal strategies for measuring diffusion in anisotropic systems by magnetic resonance imaging. Magn Reson Med 1999;42(3):515-25.

85. Gao W, Zhu H, Lin W. A unified optimization approach for diffusion tensor imaging technique. Neuroimage 2009;44(3):729-41.

86. Alexander DC, Barker GJ. Optimal imaging parameters for fiber-orientation estimation in diffusion MRI. Neuroimage 2005;27(2):357-67.

87. Andreisek G, White LM, Kassner A et al. Diffusion tensor imaging and fiber tractography of the median nerve at 1.5T: optimization of b value. Skeletal Radiol 2009;38(1):51-9.

88. Azuma T, Nakai R, Takizawa O et al. In vivo structural analysis of articular cartilage using diffusion tensor magnetic resonance imaging. Magn Reson Imaging 2009;27(9):1242-8.

89. Kingsley PB, Monahan WG. Selection of the optimum b factor for diffusion-weighted magnetic resonance imaging assessment of ischemic stroke. Magn Reson Med 2004;51(5):996-1001.

90. Saupe N, White LM, Stainsby J et al. Diffusion tensor imaging and fiber tractography of skeletal muscle: optimization of B value for imaging at 1.5 T. AJR Am J Roentgenol 2009;192(6):W282-90.

91. White NS, Dale AM. Optimal diffusion MRI acquisition for fiber orientation density estimation: an analytic approach. Hum Brain Mapp 2009;30(11):3696-703.

92. Schwarcz A, Ursprung Z, Berente Z et al. In vivo brain edema classification: New insight offered by large b-value diffusion-weighted MR imaging. J Magn Reson Imaging 2007;25(1):26-31.

93. Toyoda K, Kitai S, Ida M et al. Usefulness of high-b-value diffusion-weighted imaging in acute cerebral infarction. Eur Radiol 2007;17(5):1212-20.

94. Hiltunen J, Suortti T, Arvela S et al. Diffusion tensor imaging and tractography of distal peripheral nerves at 3 T. Clin Neurophysiol 2005;116(10):2315-23.

95. Hosonuma T, Tozaki M, Ichiba N et al. Clinical usefulness of diffusion-weighted imaging using low and high b-values to detect rectal cancer. Magn Reson Med Sci 2006;5(4):173-7.

VITA

EDUCATION

08/2006 – 12/2011 **Doctor of Philosophy in Bioengineering**.

- **Thesis Title:** "Ultra-High Field MR Diffusion Tensor Imaging Characterization of Rabbit Tendons and Ligaments"
- **Advisor/s:** Dr. Vincent M. Wang, Ph.D., Asst. Professor of Orthopedic Surgery, Rush University, Dr. Richard L. Magin, Ph.D., Professor (Former head) at Dept. of Bioengg., UIC
- **Course Highlights**: Biomechanics, Biomaterials, Mechanics of Human spine, Implant Design, Principles of MRI, Imaging systems for tissue.

07/2002- 05/2006 **Bachelor of Engineering in Bioengineering.**
Panjab University, Chandigarh, India.

PROFESSIONAL EXPERIENCE

08/2006 – Present **University of Illinois at Chicago/ Rush University Medical Center, Chicago, IL**
Graduate Research Assistant, Division of Sports Medicine, Department of Orthopedic Surgery

- Designed imaging and biomechanical testing protocols including: pre-clinical, device evaluation studies, and connective tissue characterization.
- Performed extensive analysis of engineering and clinical characteristics of soft tissues such as tendons and ligaments and surgical repair constructs.
- Performed standard biomechanical assessments including statistical assessment, sample size determination and post-hoc power assessment.
- Performed peer reviews and contributed to successful grant proposals.
- Managed several imaging and biomechanics projects simultaneously as a lead testing engineer.
- Worked with interdisciplinary teams including MR physicists, orthopedic surgeons, fellows, residents, and medical students.

Selected Project Highlights:

- **Magnetic Resonance Diffusion Tensor Imaging of Tendons and Ligaments**: Validation of MRI Diffusion Tensor Imaging as a reliable tool for non-invasive, quantitative assessment of tendon and ligament microstructure and integrity.
- **PCL graft reconstruction biomechanics**: Biomechanical Evaluation of Bioabsorbable Versus Metallic Screw for Posterior Cruciate Ligament Inlay Graft Fixation.
- **Evaluation of different surgical procedures for Shoulder Joint biomechanics:** Normalization of glenohumeral articular contact pressures after either Latarjet or Iliac Crest Bone Grafting Procedure.
- **ACL graft reconstruction biomechanics***:* Tibial Fixation of Anterior Cruciate Ligament Allograft Tendons comparing One, Two, and Four Stranded Constructs.
- **Evaluation of selected surgical procedures for Knee Joint biomechanics:** Biomechanical effects of High Tibial Osteotomy (HTO) on a meniscal transplant by comparing intact, absent and transplanted menisci and their corresponding tibial contact pressures.

AWARDS AND HONORS

2010	**UIC Graduate College and Graduate Student Council Travel Award.**
2010	**Finalist for poster award in Musculoskeletal imaging category at ISMRM-ESMRMB Joint annual meeting, Sweden.**
2009	**Western Orthopaedic Association's Lloyd Taylor Award for top paper.**
2008	**Best Poster Presentation Award Winner Rush Sigma Xi.**
2008	**Finalist Rush Surgical Society Research Day Award.**
2008	**Co-Investigator on an Arthroscopy Association of North America (AANA) Grant.**
2006-2011	**UIC Departmental Scholarship and Graduate College Tuition fee waiver.**

SKILLS

Software Operating systems: MS Windows OS system family, Mac OS X, Linux.
Engineering/Productivity: Matlab, Mimics, Labview, SPSS, Statistica, Image J, MS office suite.
Biomechanics: Instron-Bluehill, Materials Testing System-Testworks, Spicatek-DMAS, Tekscan
Imaging: SPM, FSL, Bruker-Paravision, DTIstudio, MRIcro, MAS.

Laboratory Soft tissue Biomechanical testing, Digital motion analysis, ex-vivo joint force evaluation, Ultra high field MRI/DTI (diffusion tensor imaging)of tendons/ligaments/cartilage/IVD, MRI image reconstruction and processing, histological processing, animal handling and tissue dissections.

PUBLICATIONS

1. **Gupta A**, Lattermann C, Busam M, Riff A, Bach BR, Jr.,Wang VM. "Biomechanical Evaluation of Bioabsorbable Versuss Metallic Screw for PCL Inlay Graft Fixation: A Comparative Study." *Am J Sports Med*, 2009.
2. **Gupta A**, Li W, Stebbins GT, Magin RL, Wang VM. "High Resolution Diffusion Tensor MRI of Rabbit Tendons and Ligaments at 11.7T." *Magn Reson Med*, in preparation, 2012.
3. Van Thiel GS, **Gupta A**, Frank RM, Ghodadra N, Shewman EF, Bach BR, Verma N, Cole BJ, Provencher M. "Biomechanical evaluation of a High Tibial Osteotomy with a Meniscal Transplant." *J Knee Surg*, 2010.
4. Park DK, Fogel H, Bhatia S, **Gupta A**, Shewman EF, Wang VM, Bach B, Verma N, Provencher M. "Tibial Fixation of Anterior Cruciate Ligament Allograft Tendons: Comparison of One, Two, and Four Stranded Constructs." *Am J Sports Med*, 2009.
5. Ghodadra N, **Gupta A**, Goldstein JL, Verma N, Bach BR, Romeo AA, Provencher MT. "Normalization of glenohumeral articular contact pressures after either Latarjet or iliac crest bone grafting procedure: impact of graft type, position, and coracoid orientation." *J Bone Joint Surg [Am]*, 2010.
6. Salata MJ, Sherman SL, Lin EC, Sershon RA, **Gupta A**, Shewman E, Mcill KC, Wang V, Romeo AA, Cole BJ, Verma NN. "Biomechanical Evaluation of Trans-Osseous Rotator Cuff Repair: Do Anchors Really Matter?" in preparation, 2012.
7. Garbis N, Romeo AA, Ghodadra N, McGill K, **Gupta A**, Provencher MT, Wang VM, Bach BR, Cole BJ, Verma NN. "Restoration of Glenohumeral Kinematics in Curved vs. Flat Soft Tissue Interposition Graft: Implications of Glenoid Reaming." in preparation, 2012

CONFERENCE PRESENTATIONS

1. **Gupta A,** Li W, Stebbins GT, Magin RL, Wang VM. "Assessment of Rabbit Medial Collateral Ligament and Semitendinosus Tendon Microstructure Using High Resolution MR Diffusion Tensor Imaging and Tractography." **Orthopedic Research Society Annual meeting, Long Beach, 2011**
2. **Gupta A,** Li W, Stebbins GT, Magin RL (presenter), Wang VM. "High Resolution Diffusion Tensor MRI of Rabbit Tendons and Ligaments at 11.7T." **ISMRM-ESMRMB Joint Annual Meeting, Sweden, 2010**.
3. **Gupta A,** Li W, Stebbins GT, Magin RL, Wang VM. "High Resolution Diffusion Tensor MRI of Rabbit Tendons and Ligaments at 11.7T." **Orthopedic Research Society Annual meeting, New Orleans, 2010**.

4. **Gupta A**,Van Thiel GS, Frank RM, Ghodadra N, Shewman EF, Bach BR, Verma N, Cole BJ, Provencher M. "Biomechanical evaluation of a High Tibial Osteotomy with a Meniscal Transplant." **Orthopedic Research Society Annual meeting, New Orleans, 2010**.
5. Van Thiel GS (presenter), **Gupta A**, Frank RM, Ghodadra N, Bach BR, Cole BJ, Verma NN, Provencher MT. "Biomechanical Evaluation of Meniscal Transplantation with a High Tibial Osteotomy." **Podium Presentation International Cartilage Repair Society Annual Meeting 2009,Miami, FL**
6. Ghodadra N (presenter), **Gupta A**, Shewman E, Goldstein J, Verma NN, Bach BR, Romeo AA, Provencher MT. "Normalization of Glenohumeral Articular Contact Pressures after either Latarjet or Iliac Crest Bone Grafting Procedure: Impact of graft type, position, and coracoid orientation." **Meeting of the American Academy of Orthopaedic Surgeons Las Vegas, NV 2009**.
7. Garbis N (presenter), Romeo AA, Ghodadra N, McGill K, **Gupta A**, Provencher MT, Wang VM, Bach BR, Cole BJ, Verma NN. "Restoration of Glenohumeral Kinematics in Curved vs. Flat Soft Tissue Interposition Graft: Implications of Glenoid Reaming." **Poster presentation, European Society for Surgery of the Shoulder and the Elbow Annual Meeting, France. 2011**
8. Salata MJ (presenter), Sherman SL, Lin EC, Sershon RA, **Gupta A**, Shewman E, Mcill KC, Wang V, Romeo AA, Cole BJ, Verma NN. "Biomechanical Evaluation of Trans-Osseous Rotator Cuff Repair: Do Anchors Really Matter?" **Podium presentation, European Society for Surgery of the Shoulder and the Elbow Annual Meeting, France. 2011.**